University of Stavanger

Faculty of Science and Technology

MASTER'S THESIS

Study program/Specialization: Petroleum Geosciences Engineering	Spring, 2018 Open
Writer: Dina Egeland	(Writer's signature)
Faculty supervisor: Chris Townsend	
Title of thesis: Fault Displacement Analysis in the Kalavryta Region of the Corinth Rift System, Greece.	
Credits (ECTS): 30	
Keywords: Structural Geology Fault Displacement Greece Corinth Rift Syn-rift Half-graben Normal Faults Transfer Faults	Pages: 119 +enclosure: 15 Stavanger, 15.06.2018

Fault Displacement Analysis in the Kalavryta Region of the Corinth Rift System, Greece

by

Dina Egeland

MSc Thesis

Presented to the Faculty of Science and Technology

The University of Stavanger

The University of Stavanger

June 2018

Acknowledgements

I would like to express a great thanks to my supervisor Chris Townsend for his continuous support, guidance and helpful discussions. His knowledge of the Corinth Rift and experience in the field proved very helpful. I would also like to thank my co-supervisor Alejandro Escalona for his feedback during the semester, for his constructive comments and discussion related to the thesis. Last, I would like to extend my gratitude to my family and friends for their continued support, patience and encouragement.

Abstract

Fault Displacement Analysis in the Kalavryta Region of the Corinth Rift System, Greece

Dina Egeland

The University of Stavanger, 2018

Supervisor: Chris Townsend

The Corinth Rift of Central Greece is one of the world's most active rifts. Regional N-S extension has resulted in a series of half-grabens within a system of uplifted, rotated and north-dipping normal faults. Extensive footwall uplift has tilted the adjacent hanging walls and created rotated fault blocks, exposed in the Kalavryta-Eliki area.

Previous work in the Kalavryta-Eliki area have identified a number of faults which rapidly terminate, where vertical displacement is lost in a very short lateral distance. There are different views on rift segmentation and lateral fault terminations. Observations in the rift system are that some faults step, and others terminate abruptly along N-S river valleys. Relay structures provides a simple field explanation. However, field evidence of overlapping faults are not clear and 3D models indicate that relays or hard links are very difficult to explain.

Displacement estimations of faults in the Corinth Rift have been quoted in publications, but generally un-clear how these were estimated and what kind of error is associated to them. The main objective of this study is to quantify the fault displacements for each segment and to evaluate the possible interpretations that link the segments. A 3D model has been built to determine fault displacements and their variations across fault surfaces. Lastly, models are proposed to explain present-day fault displacement variations, and compare with previous work.

Through a detailed and robust displacement analysis on the faults in the Kalavryta-Eliki area, it is evident that the sharp change in displacement between fault segments cannot be explained by displacement gradients alone, but rather by something else. The river valleys seem to have an underlying fault control, and the intervals of miscorrelation are therefore interpreted as high-angle transfer faults enclosing individual segments. It is believed that the method of 3D model construction is a good approach to estimating the displacements and highlighting how they vary across single faults and fault segments.

Table of Contents

List of Tables

List of Figures

Chapter 1 – Introduction

The Gulf of Corinth is located in the central part of Greece, north of the Peloponnese Peninsula, separating the peninsula from mainland Greece. The gulf is one of the world's most active rift systems with an average north-south extension rate of 11-16 mm/year (Ford et al., 2013), resulting in the formation of several half-grabens. Extensive footwall uplift, up to 1800 m (Flotté et al., 2005), has tilted the adjacent hanging walls and created rotated fault blocks, nicely exposed on the Peloponnese. Several incised north-trending river valleys provide exposures of these fault blocks, as they cut perpendicular to the strike of the main east-west faults. This allows for detailed studies of normal faulting and its associated syn-rift sedimentation. It also provides an opportunity to assess the structural and stratigraphic evolution of a rift, thus gaining an insight into the basin-forming processes. In addition, this area is interesting for hydrocarbon exploration purposes as it forms an excellent extensional basin analogue to the Norwegian Continental Shelf and other subsurface rift-systems. Within rifts, the interrelationship between fault growth, fault migration and extension rate have been studied using sedimentation patterns and strain partitioning in various rifts such as the North Sea (Cowie et al., 2005).

The study area for this thesis project is located around the Kalavryta-Eliki area, south of the Gulf of Corinth, limited between the Krathis Valley to east and the Finikas Valley to the west (Figure 1.1). The different fault blocks of the area have been studied and mapped in various detail in an effort to understand the structural development and sedimentary infill through time (Doutsos and Piper, 1990; Doutsos and Poulimenos, 1992; Doutsos and Koukouvelas, 1998; Collier and Jones, 2004; Rohais et al., 2007; Finnesand, 2013; Ford et al., 2013; Wood, 2013; Syahrul, 2014; Dahman, 2015; Lopes, 2015; Rhodes, 2015; Rognmo, 2015; Stuvland, 2015; Hadland, 2016; Sigmundstad,

2016; Birkeland, 2017; Oppedal, 2017; Veiteberg, 2017). As a result, several different interpretations of the evolution and current structural and stratigraphic configuration of the rift system have developed. The ongoing debates on rift segmentation and lateral fault terminations, discuss whether this is due to relay zones or pre-existing structures, and how fault displacement is affected (Ford et al., 2013; Wood, 2013; Dahman, 2015; Ford et al., 2016; Hadland, 2016; Oppedal, 2017; Zhong et al., 2018). These abrupt fault terminations have yet to be fully explained. The four alternative explanations include: i) 'natural displacement loss', ii) pre-rift erosion, iii) relay structures or iv) transfer faults (Figure 1.2).

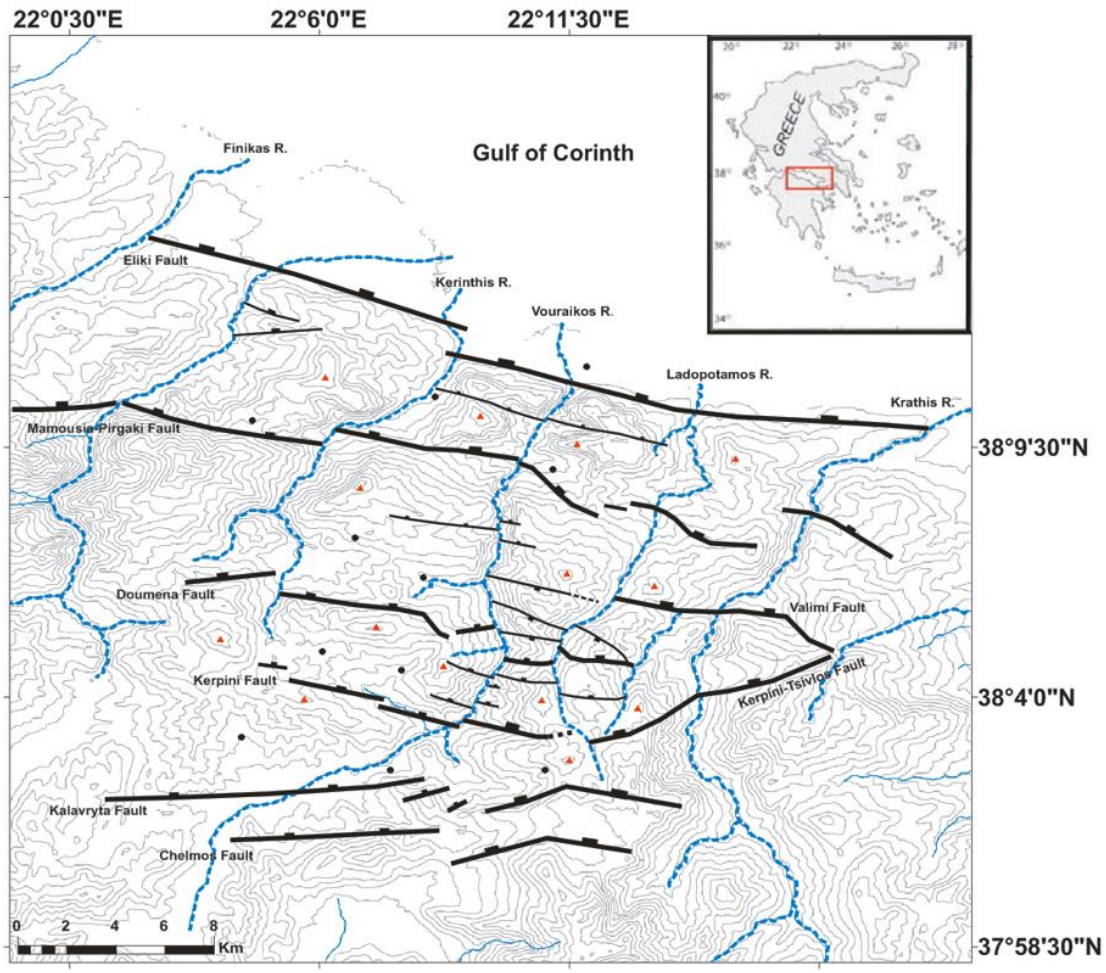

Figure 1.1: Location map showing the study area on the onshore Peloponnese, south of the Gulf of Corinth, enclosed by the Krathis and Finikas Rivers.

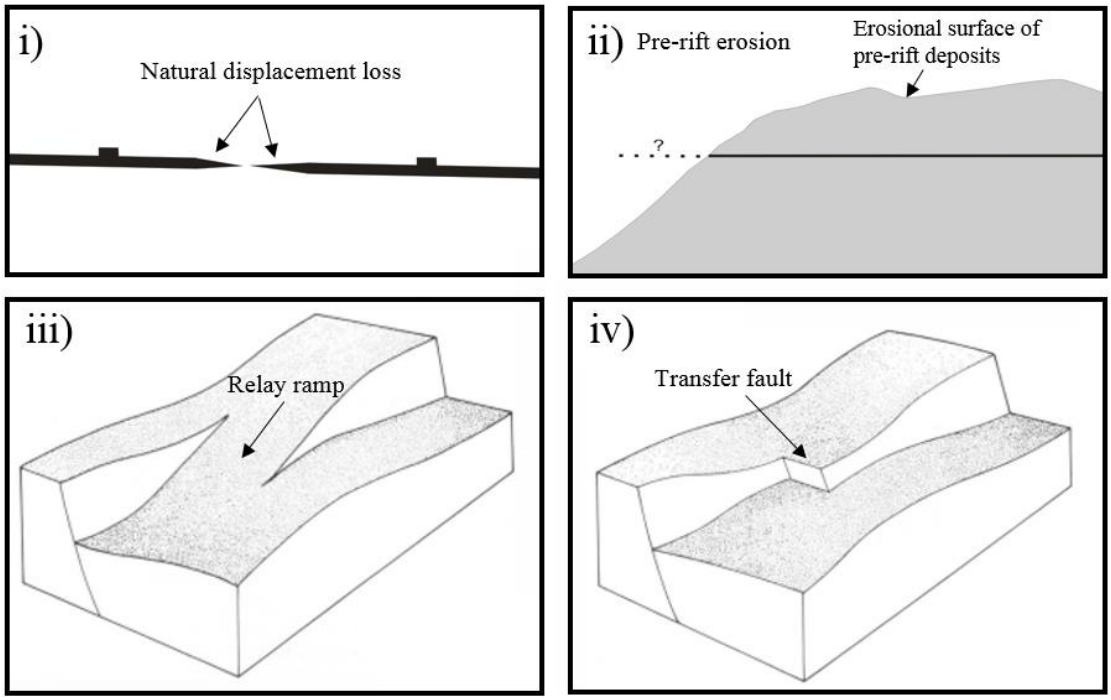

Figure 1.2: Four alternatives causing lateral fault termination, presented as conceptual models: i) Natural displacement loss, ii) Pre-rift erosion, iii) Relay ramp (Modified from Gawthorpe and Hurst, 1993), and iv) Transfer fault (Modified from Gawthorpe and Hurst, 1993).

The focus of this study is to examine fault displacements on the major faults in this rift-system, to determine the rift extension and to document if this varies between the segments. Also, it aims to investigate the discontinuities along the major faults. Several of the major faults cannot be traced directly across river valleys, and there is no wide agreement on whether individual faults simply terminate in the valleys, or are linked to parallel faults by relay or transfer structures. Major faults have recorded displacements up to 2000 m (Doutsos and Poulimenos, 1992; Collier and Jones, 2004; Ford et al., 2013; Wood, 2013). Displacements are often quantified in publications, but it is often unclear how these are estimated, what variations occur along faults and what kind of error is associated with these estimates. Erosion of footwall uplift makes it challenging to calculate the true displacement and changes along the strike. This, in turn, may lead to different interpretations of the fault propagations and the evolution of the basin fill.

1.1 GEOLOGICAL FRAMEWORK

1.1.1 Regional Geology

The eastern Mediterranean has long been recognized as an area of active tectonism (McKenzie, 1972). Various geometries of convergence and interaction of the African, Eurasian, Arabian and Anatolian Plates result in a wide variety of active tectonic processes, such as back-arc extension of the Aegean Plate (Bell et al., 2009; Ford et al., 2013) (Figure 1.3). This crustal extension forming the present-day Gulf of Corinth was initiated within the Early Pliocene and is thought to have formed as a consequence of the north to northeast subduction within the Eastern Mediterranean. The African Plate subducted at the Hellenic Trench (McKenzie, 1972; Doutsos et al., 1988), resulting in back-arc extension in the Aegean Sea (Le Pichon and Angelier, 1979; Jolivet et al., 1994; Gautier et al., 1999), and westward propagation of the North Anatolian Fault (NAF) (Dewey and Şengör, 1979; Jolivet et al., 1994; Armijo, 1999).

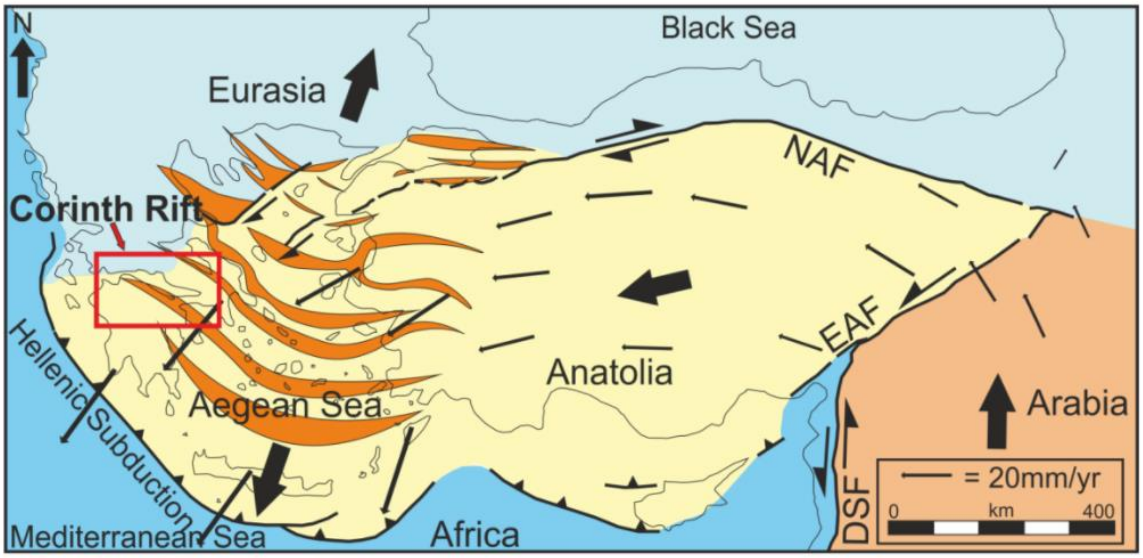

Figure 1.3: Map of the eastern Mediterranean showing the location of the Gulf of Corinth, highlighted by a red square, in a plate tectonic context. (Modified from Armijo et al., 1999; Wood, 2013).

The extension is thought to be due to both gravitational collapse of the thick crust inherited from earlier mountain building (Jolivet et al., 1994) and lithospheric thinning in the Aegean back-arc region (Doutsos et al., 1988). The rifting is estimated to have started in the Pliocene based on micropaleontological dating, around 5 Ma (Ori, 1989; Doutsos and Piper, 1990; Leeder et al., 2008; Ford et al., 2013). Significant recent advances have been made in understanding the Corinth Rift evolution by combining sedimentological and structural analysis. However, improved dating and correlation of individual syn-rift successions and faulting events remains a major challenge (Ford et al., 2013).

1.1.2 Structural and Stratigraphic Overview

The Corinth Graben stretches 115 km from east to west. It spans from the Strait of Rio in the west to the Corinth Canal in the east (Figure 1.4). It forms an elongated asymmetrical graben, oriented N100°E (Moretti et al., 2003), where the major faults offshore and those onshore close to the coastline are still active (Leeder et al., 2008). The major north-dipping faults define the boundaries of the major half-grabens, and dip northwards in the range of 40–60°. The faults generally trend between N080° and N115°. The exposed rotated fault blocks are located between the Chelmos-Kalavryta area in the south, and the Gulf of Corinth in the north. Studies indicate a progressive northwards younging (Collier and Jones, 2004). The Eliki, Mamousia-Pirgaki, Doumena, Kerpini and Kalavryta Faults, which are the major faults on the Peloponnese, segment the five major fault blocks from north to south, respectively. In addition to the major faults, the rift system also contain several minor normal faults, where some of them are antithetic, dipping south, creating minor graben-horst structures within the individual half-grabens.

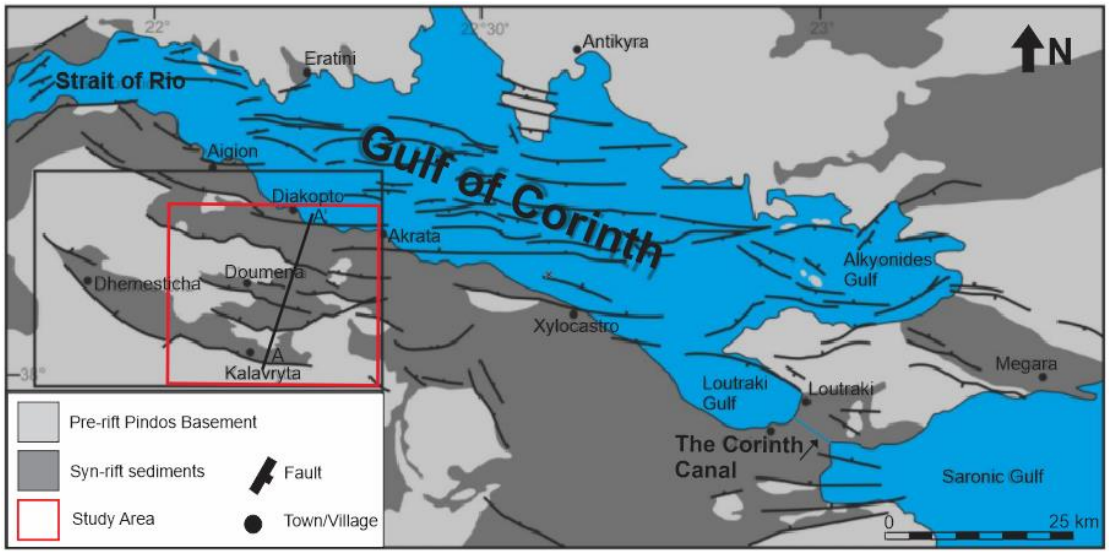

Figure 1.4: Map of the Gulf of Corinth showing the major faults related to the rift system. The study area is highlighted by the red square (Modified from Wood, 2013).

The regional onshore stratigraphic architecture of the study area has been defined as pre-rift Mesozoic low-grade metamorphosed limestone with Pliocene to Quaternary syn-rift sediments, unconformably overlying it. Syn-rift sediments cover extensive parts of the northern Peloponnese, distinctive by its complex architecture with frequent unconformities and lateral changes in facies and thickness. Pliocene to Quaternary sand, marl and conglomeratic sedimentary infill characterize the syn-rift sedimentation (Ford et al., 2013). The stratigraphic lithologies are divided into Pre-rift Pindos carbonate basement deposits, progradational alluvial fan deposits of coarse conglomerates and breccia, upper alluvial and fluvial deposits, and Gilbert-type deltas of modern conglomerate-sandstones. Figure 1.5 shows a cross-section crossing the central part of the study area, showing the distribution of the different lithologies, generally maturing northwards and younging northwards (Ford et al., 2013).

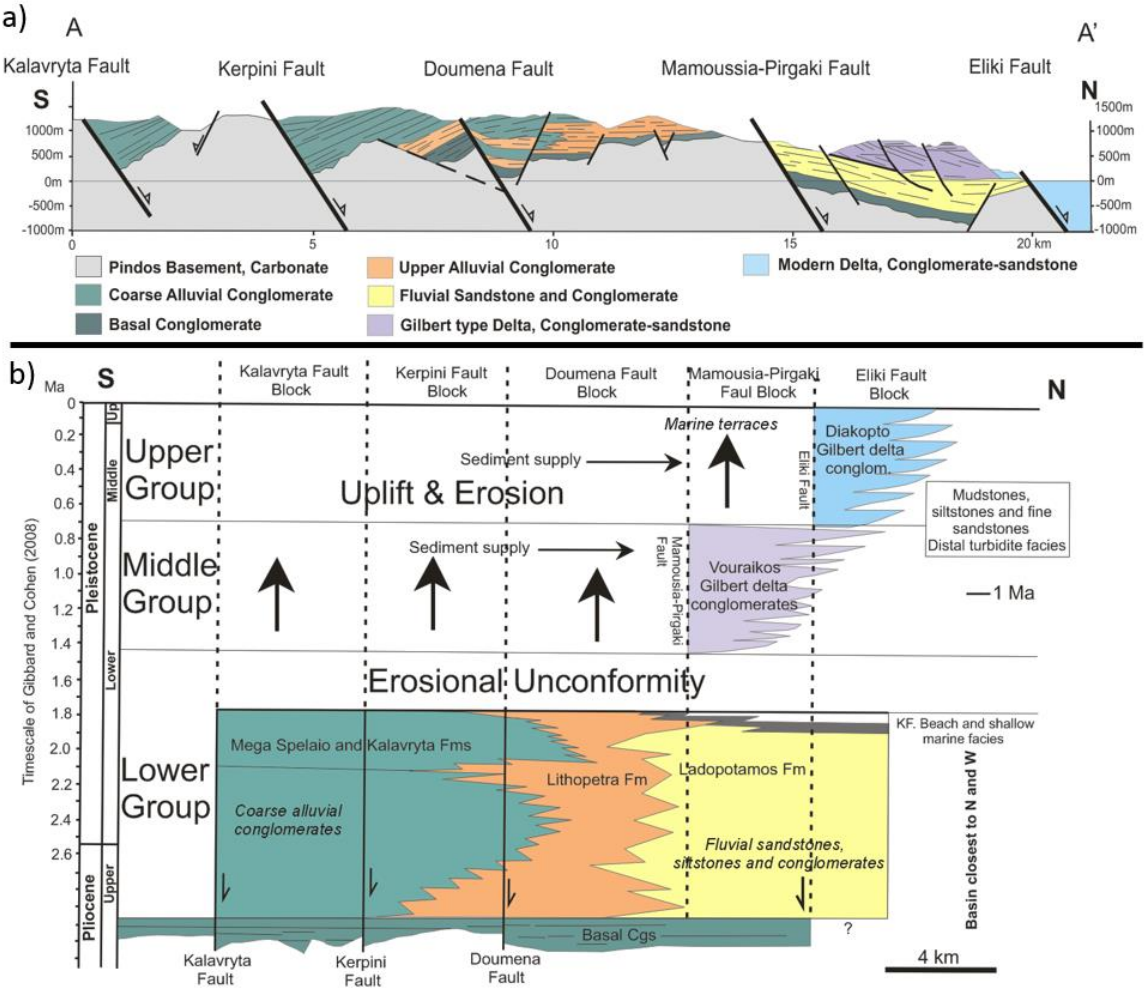

Figure 1.5: a) Cross-section showing the major faults with associated stratigraphic lithologies and b) Chronostratigraphy along cross section A-A' (Modified from Ford et al., 2016).

1.2 Previous Work

For several decades different theories on the structures of the rift and associated fault propagation on the onshore Peloponnese have been proposed. Doutsos and Piper (1990) proposed that the normal faults are of a listric nature, however most researchers disagree and argue that there is not enough evidence and favour a model of planar faults (Westaway, 2002; Moretti et al., 2003; Rohais et al., 2007; Ford et al., 2013). Doutsos and Poulimenos (1992) described the structure of the rift and proposed that the surface

normal faults were linked to a low-angle fault at deeper crustal levels. More recently, Sorel (2000) and Chéry (2001) suggested that the Corinth Rift is underlain by a major north-dipping crustal detachment fault, the "Chelmos detachment", over 100 km long underlying the younger faults, hereby supporting Doutsos and Poulimenos (1992) proposal (Figure 1.6). Following the 1995 Aigon earthquake, interpretation of focal mechanisms (Rietbrock et al., 1996) support a model involving an active low-angle crustal detachment, as recorded micro earthquakes show a north-dipping zone of seismicity below the Gulf of Corinth.

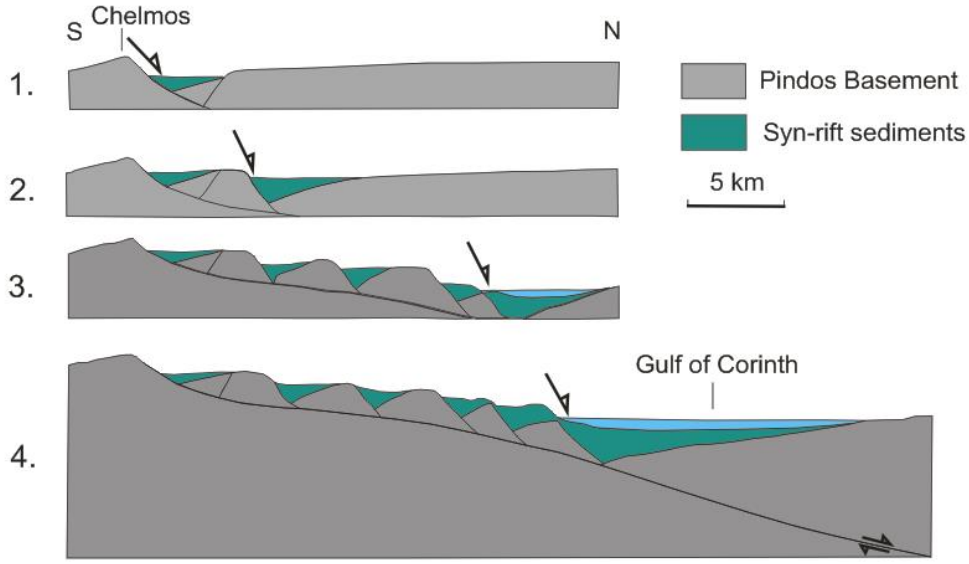

Figure 1.6: Schematic development of the Corinth Rift in four-step sections: 1. Early rift, along active Chelmos Fault, 2. Continued activity of rifting creating another major fault, 3. Progressive rifting creating several new faults and 4. Present-state showing the proposed connection of the Chelmos detachment to the newly formed faults (Modified from Sorel, 2000).

Moving upwards towards the uppermost crust, an ongoing discussion on the rapid fault termination, or fault discontinuities, is still under debate. Previous work has documented a number of faults which rapidly terminate, where vertical displacement is lost in a very short lateral distance, and fault steps occur (Dahman, 2015; Lopes, 2015;

Rhodes, 2015; Oppedal, 2017). The fault steps occur along mostly N-S oriented river valleys indicating some form of alignment. There are different views on rift segmentation and lateral fault terminations. Ford et al. (2013) proposed that each fault step is caused by a short cross fault or relay zone, the latter is supported by Wood (2013). Also, Ford et al. (2016) and Gawthorpe et al. (2003) suggested that there is pre-existing paleotopography prior to the rift, whereas Ghisetti and Vezzani (2005) claimed that the rift segmentation is controlled by pre-existing structures in the underlying pre-rift Pindos Basement.

The fault steps can also suggest that the rift is segmented, and that each segment may have a different total extension. Do the individual faults simply terminate in the valleys, or are they linked to parallel faults by relay or transfer faults? The river valleys are areas of major erosion where from one side of the valley to the other, structural and depositional relations tend to change quite dramatically. Dahman (2015), (Hadland, 2016) and Oppedal (2017) studied the various river valleys in a regional sense and identified an extensive N-S interval of miscorrelation in the Vouraikos Valley. They all preferred a model involving several km long transfer faults to explain the fault steps (Figure 1.7).

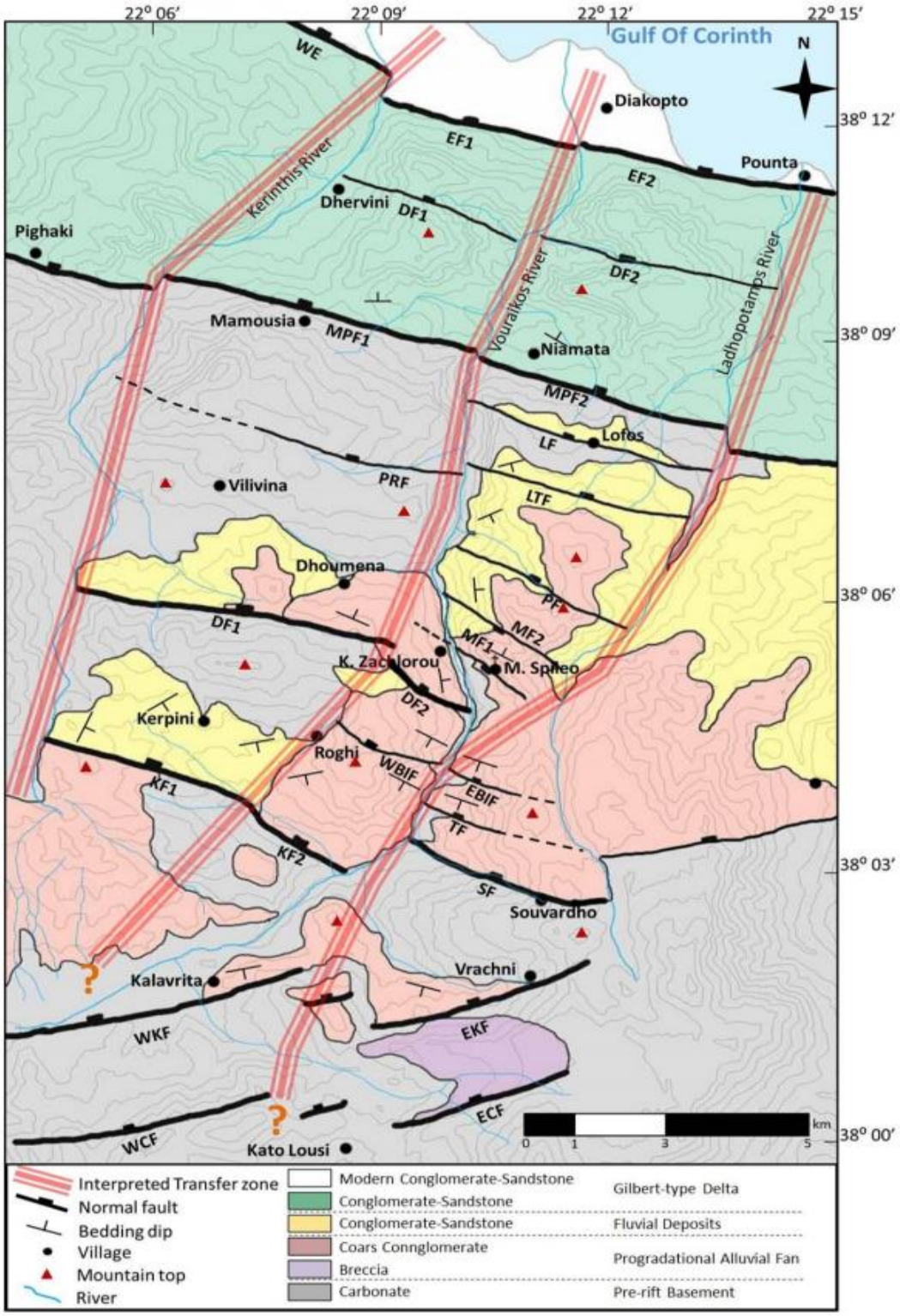

Figure 1.7: Map of the Kalavryta-Eliki area showing the proposed transfer fault scenario that can explain the fault discontinuities (Dahman, 2015).

Fault displacement estimations on the major faults in the Kalavryta-Eliki area are mentioned in papers, but it is generally un-clear on how these were calculated. The methodology and data used are also rarely stated, making it difficult to check and compare results. It is also not stated the locations along strike of the faults where the displacement is estimated. The displacement changes along strike, meaning that it is highly relevant to show the locations of where the displacement estimation was done. There is uncertainty tied to the displacement of the various faults, and calculations vary from study to study. The Kalavryta Fault lacks proper exposure along the strike, and is interpreted to step in several locations. The displacement has been estimated from 800 m (Finnesand, 2013) to 1200 m (Ford et al., 2013). The Kerpini Fault has a better exposure along the entirety of the fault, and several displacement calculations exist for this fault as well. Estimations range from 1500 m (Ford et al., 2013; Syahrul, 2014; Dahman, 2015) to 2500 m (Collier and Jones, 2004). Hadland (2016) concluded that the displacement of the Kerpini Fault is segmented by transfer faults, where Segment I has a displacement ranging between 1500-1700 m, Segment II between 1200-1400m and Segment III around 500 m. The Doumena Fault is obscure, and yields several different calculations which indicate the displacement may change significantly along the fault. The estimations range from 800-2000 m (Collier and Jones, 2004; Ford et al., 2013; Syahrul, 2014; Dahman, 2015). The maximum displacement of the Mamousia-Pirgaki Fault has been estimated to 1500 m (Ford et al., 2013; Dahman, 2015), but Collier and Jones (2004) concluded that the maximum displacement is more close to 2500 m.

1.3 OBJECTIVES

The main objective of this study is to quantify the displacements for each fault segment and evaluate the possible interpretations that link the segments. The focus is summarized in the following points:

- Construct a 3D structural model, using published and unpublished data, to determine fault displacements, their variations and test the repeatability consistency.
- Consider and estimate uncertainty sources related to fault displacement estimates.
- Evaluate the possibility of segmentation in the study area to investigate if there are one single rift-block or several segmented rift blocks.
- Propose models to explain present-day fault displacement variations and compare with previous work.

1.4 DATA

Collected field data from previous Master projects at the University of Stavanger (Finnesand, 2013; Dahman, 2015; Hadland, 2016; Sigmundstad, 2016; Oppedal, 2017; Veiteberg, 2017), along with published work, are the foundation of the study. Also, fieldwork at the end of the study was done to verify previous work, and check on areas of conflict and locations where further classifications were required. Structural measurements, a multitude of photos, recorded facies variabilities and geological mapping make up most of the collected data. In addition, satellite imagery from Google Earth combined with a Digitized Elevation Model (DEM) of the study area in Petrel E&P Software Version 2017, have been important tools. A constructed database in ArcGIS was used to generate maps.

Chapter 2 - Background

2.1 THEORY

It is widely recognized that in rift settings, fault systems develop through a combination of growth, interaction and linkage of individual fault segments across a range of scales (Childs et al., 1995; Cartwright et al., 1996; Cowie et al., 2000; Walsh et al., 2003). Extensional systems are often associated with the creation of half-grabens by normal faulting, where normal faults preferentially form in response to extensional stress fields. The structural features that make up the half-grabens in the Kalavryta-Eliki area can be associated with the *Domino model* where parallel normal faults define blocks that rotate like domino bricks during rifting (Fossen, 2010) (Figure 2.1). However, a rigid model may not convey the natural occurrences that happens during extension, but rather gives an idea of the geometries to expect from such systems. As fault blocks rotate and the footwall side is uplifted, it creates accommodation space for sediments. The syn-rift deposits generally show growth strata, where they are expected to exhibit a change in dip from older to younger as the block rotates.

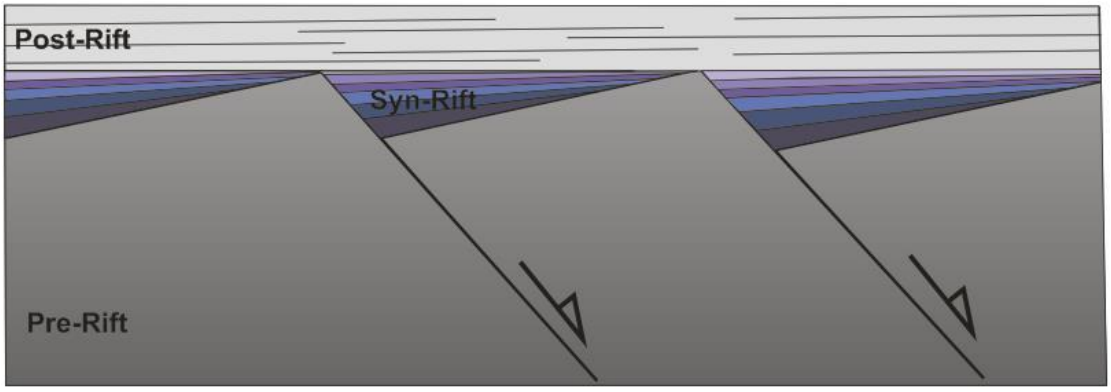

Figure 2.1: Generalized domino structure showing rotated fault blocks with syn-rift and post-rift deposits. The syn-rift sediments show a change in dip angle from older to younger, getting shallower as they become younger (Modified from Faure and Chermette, 1989).

2.1.1 Fault Displacement

The vector connecting two points that were connected prior to faulting indicates the local displacement vector, also called the slip of the fault. Ideally, normal faults have displacement vectors in the dip direction (Fossen, 2010). The distribution of displacement along faults and the scaling relation between displacement and fault length create important constraints on models of fault growth (Watterson, 1986; Walsh and Watterson, 1988; Marrett and Allmendinger, 1991; Cowie and Scholz, 1992; Gillespie et al., 1992; Dawers et al., 1993; Dawers and Anders, 1995). Faults normally tend to show a maximum displacement in the central part of the fault trace, gradually decreasing towards the tips. Two separations related to faulting are commonly referred to as heave (horizontal component) and throw (vertical component). The heave and throw components, along with the total slip of the fault or true displacement, form a right angle triangle (Figure 2.2). In geological field work, stratigraphic markers are often used to constrain the displacement along a fault plane.

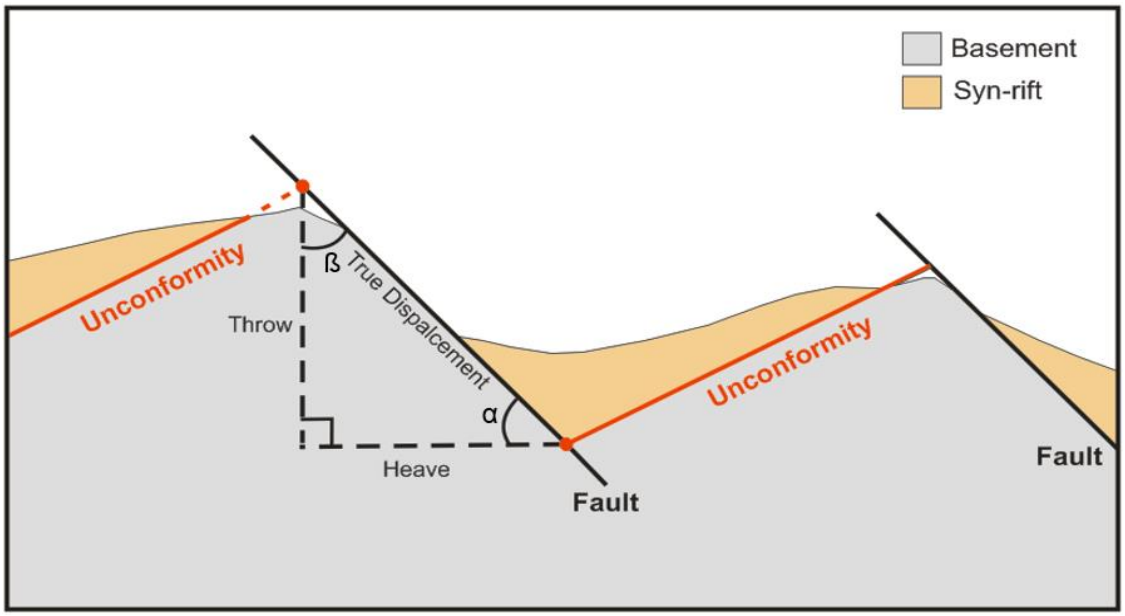

Figure 2.2: Conceptual model showing the fault displacement elements related to the field. Displacement components shown are the true displacement, throw and heave. The α-angle represent the fault dip and the ß-angle represent the hade (the angle that the fault plane make with the vertical.

2.2 FAULT LINKAGE

Faults grow from microfractures or other fundamental weaknesses and accumulate displacement over time as deformation proceeds (Hills, 1972). Faults rarely grow as individual structures over a long period of time. As they grow, they are likely to interfere with nearby faults, forming a fault system. Growth by linkage is a common feature in rift settings, therefore it is important to understand how faults can propagate and interact. The Corinth Rift serves as an important analogue in extensional basins, such as the Norwegian Continental Shelf, for structural development in hydrocarbon exploration. In hanging wall reservoirs, the linkage between faults can impact the facies distribution. The reservoir volumes and the distribution of facies are highly influenced by fault geometry and how this geometry develops with time. As identified in the Kalavryta-Eliki area, several fault discontinuities occur, which would not be easily identified in 2D seismic when mapping prospects. If these structures are not mapped properly, volumes may be incorrectly estimated because relay structures and transfer faults often define migration pathways or structural spill points. Understanding the evolution of rift systems and related timing of sequences of events are essential to predict along-strike discrepancies of faults, and have thus significant implications for the economic aspect of any prospect.

2.2.1 Relay Zones

Faults that approach each other and later overlap, form soft-linked features, as they are not in direct physical contact. With continued fault growth they may eventually link up to form a hard link. The approaching faults “feel” the presence of a neighbouring fault tip, in which case they become kinematically linked. The propagation rate of the fault tips in the area is reduced, which causes the local displacement gradient to increase (Fossen, 2016). This results in asymmetric displacement profiles. This asymmetry becomes more pronounced as the faults overlap, with the layers in the overlap zone are

becoming tilted. The tilting is a result of ductile displacement transfer from one fault to the other and is directly related to the high displacement gradients in the overlapping tip zones. This feature is called a relay ramp and the entire structure is known as a relay structure (Figure 2.3a). More strain leads to one of the faults breaching through the ramp and eventually a single fault is formed. Relay ramps are important structures in a rift system because ramps provide sedimentation pathways which ultimately controls the evolution of the basin fill.

2.2.2 Transfer Faults

Major normal faults in extensional systems commonly terminate at orthogonal strike-slip faults or shear zones, structures similar to that of oceanic transform faults (Bally, 1981). These faults have become known as transfer faults (Gibbs, 1984), where the transfer faults divide the extending terrane into segments (Figure 2.3b). However, the definition of transfer faults have become somewhat ambiguous in some cases. Transfer faults may be confined to the upper plate, affecting only the tilt-block geometry. The structures are a general feature of extended terrenes; therefore, they should be expected to occur commonly in passive continental margins (Lister et al., 1986). Transfer faults are also important in accommodating oblique extension.

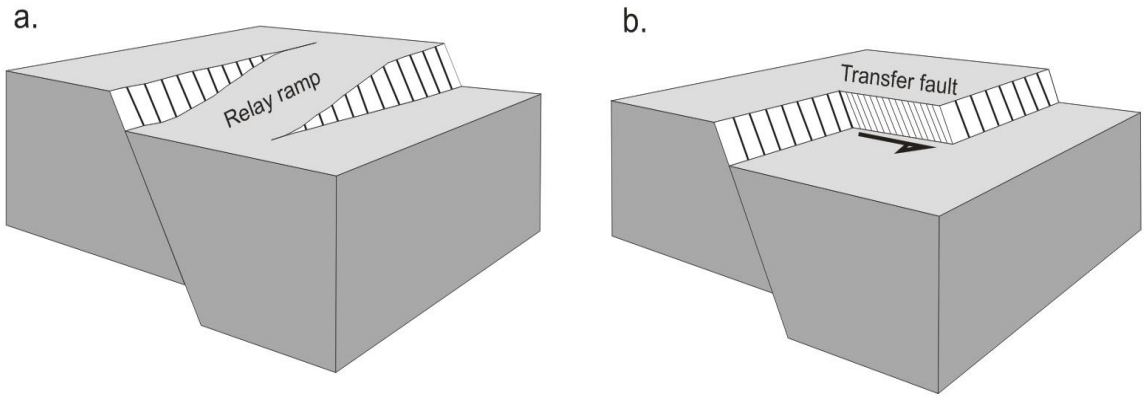

Figure 2.3: Conceptual models of a) Relay ramp and b) Transfer fault. Modified from Gawthorpe and Hurst, 1993.

Segments are the transient features in fault evolution, as faults grow and interact, eventually forming larger structures (Gawthorpe and Leeder, 2000) (Figure 2.4). Transfer faults cause abrupt terminations of the fault displacement, creating a step in the fault. In general, transfer faults occur in all scales and they connect a range of structures. Transfer faults in rift systems may provide breaches that can create pathways for the sediments to travel due to underlying weaknesses and deformation in the lithology along these faults.

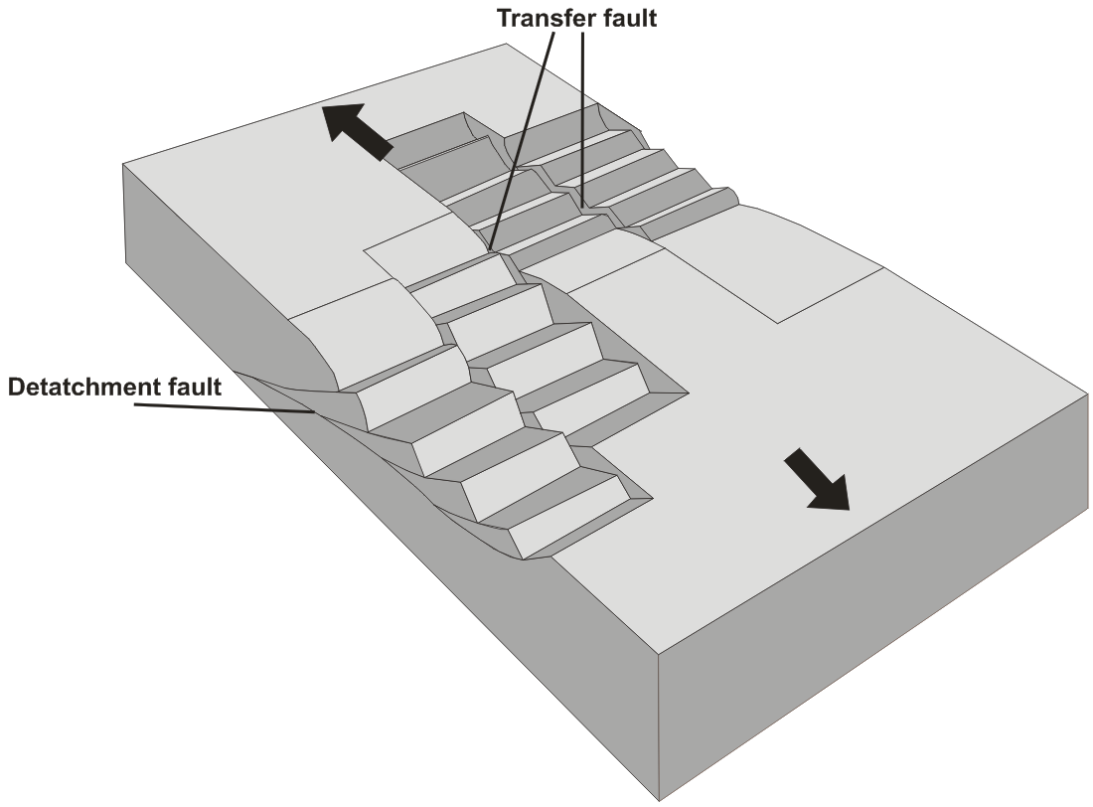

Figure 2.4: Half-graben complex showing transfer faults created in a rifting system, dividing blocks into segments (Modified from Lister et. al., 1986).

2.3 GEOLOGICAL CHALLENGES

Faults in the Kalavryta-Eliki region are mapped based on high-angle contacts (more than 20°) between pre-rift Pindos basement rocks and overlying clastic syn-rift infill. In contrast, unconformities are mapped by low-angle contacts which typically dip towards the fault surfaces.

Wood (2013) presented three approaches to determine displacement on faults using dip projection for syn-rift hanging wall and footwall, respectively (Figure 2.5). This figure also show restrictions associated to the methods where one may get under- or over estimates of fault displacement. Cartwright and Mansfield (1998) measured the displacement by correlating bedrock stratigraphy in the hanging wall with the footwall, and observing the vertical offset in a correlative marker horizon. However, in the Corinth Rift, footwall uplift and its subsequent erosion makes displacement estimates and along-strike analysis challenging (Figure 2.6). Defining accurate and repeatable methods for estimating fault displacement with minor associated uncertainty sources have not yet been appropriately documented in this area. It is important to understand the interaction between sedimentation and faulting, and the tectonic evolution of such extensional rift systems.

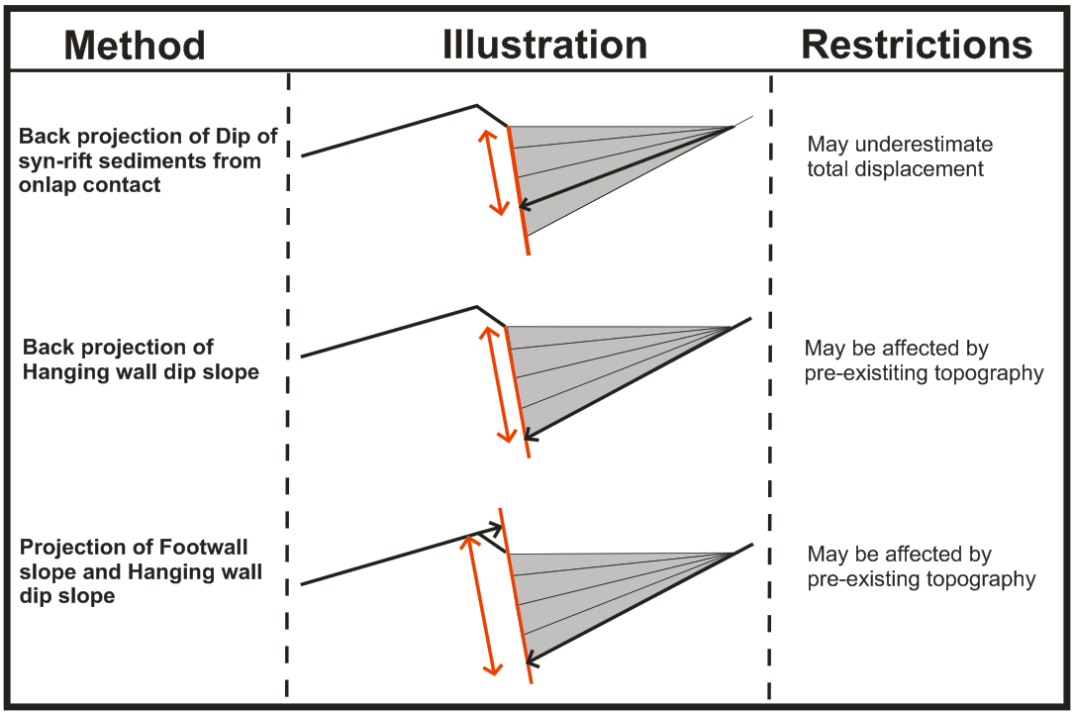

Figure 2.5: Schematic illustration showing the different approaches on estimating fault displacement, including their restrictions (Modified from Wood, 2013).

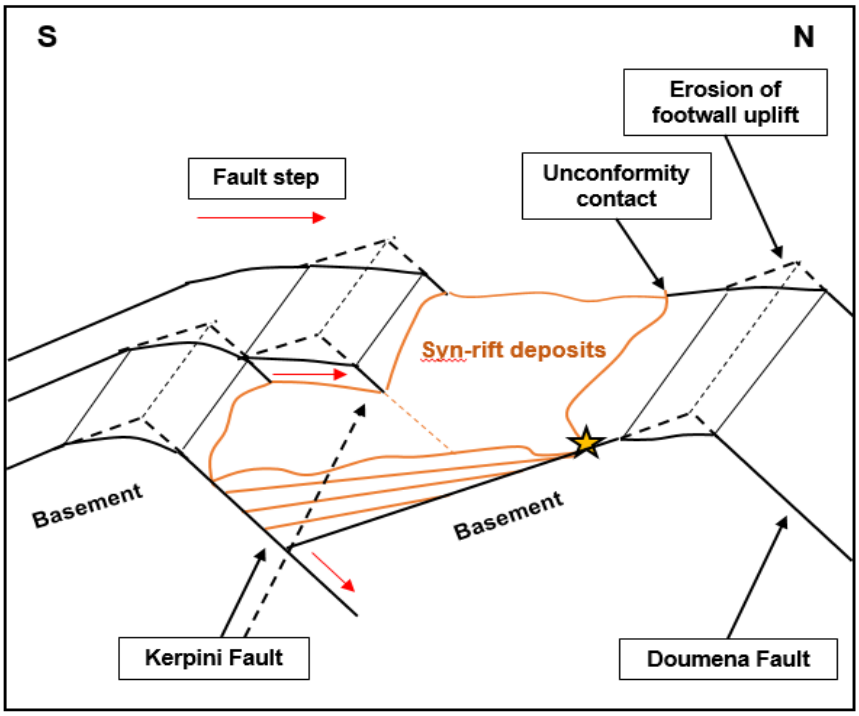

Figure 2.6: Example from the Kerpini Fault Block showing some of the geological challenges related to fault displacement estimations. The yellow star indicating the unconformity contact.

Chapter 3 – Methodology

3.1 MODELLING

A collection of field data from published work and from several Masters theses from the University of Stavanger have been used to construct 3D structural models of the study area. These models have been used to analyse and investigate the possible geometries that can explain the rapid changes in fault displacement and changes in facies. The 3D geological model representing the study area was built using Petrel E&P Software Version 2017 (Petrel). Within Petrel, a Digitized Elevation Model (DEM), representing the topography of the entire Peloponnesus, was used to form a basis for the model construction (Figure 3.1). The surfaces defining the 3D model are the DEM, constructed faults and unconformity surfaces, and a base surface that limit the model. The DEM used in Petrel has a grid size of 90 x 90 m, which is adequate to resolve the main topographic features of the study area. Chapter 4.3 explains the workflow used to build the 3D model in greater detail.

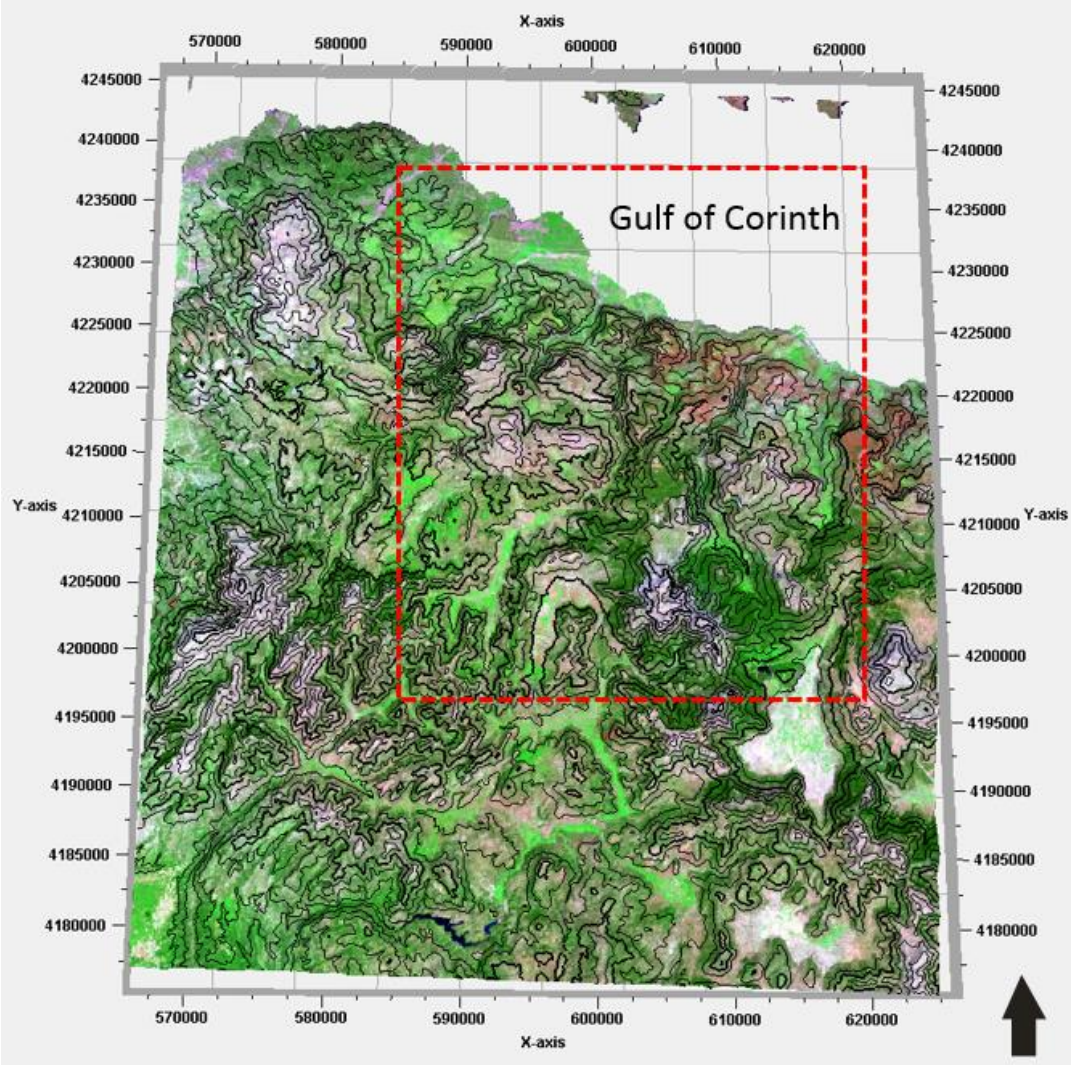

Figure 3.1: Digitized Elevation Model (DEM) surface in Petrel, representing the topography. The red square represent the study area.

3.1.1 Displacement Estimation

The fault displacement was estimated by creating vertical cross sections and measuring the slip on each section using a 3D model in Petrel (Figure 3.2). The point of intersections between the fault plane and unconformity surfaces was used with basic trigonometry to calculate the displacement. This was done by inserting the x and y values of the footwall and hanging wall cut-offs in Excel 2016, were the displacement

calculation was executed. The displacement estimates are presented as strike projection displacement plots using 200 m increments.

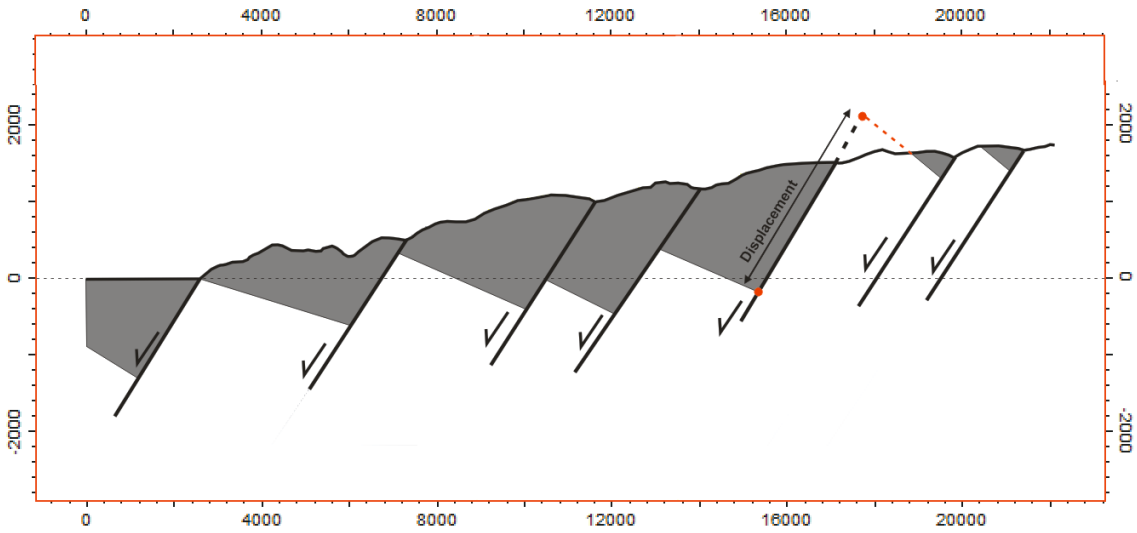

Figure 3.2: An example showing displacement estimation using vertical cross sections in Petrel by measuring the slip. The grey area represent the syn-rift deposits overlying the basement (white colour). The displacement (slip) is highlighted by a black arrow and two red circles, where the unconformity surfaces hit the fault plane. The unconformity plane has been projected in areas where erosion has occurred, as shown by the stippled red line.

Displacements in the Corinth Rift are often quoted in publications (Doutsos and Poulimenos, 1992; Ghisetti and Vezzani, 2005; Ford et al., 2013; Wood, 2013), but it is unclear how these were estimated and what kind of error is associated to them. Ghisetti and Vezzani (2005) estimated a range of displacements calculated from offset of geological markers and along-strike variations of throw are bracketed by the extreme values. Ford et al. (2013) calculated the displacement along multiple cross-sections using the basal unconformity as reference, where the faults are extrapolated as planar structures to a depth of 1 km below sea level (bsl). Although not explicitly stated, it is generally assumed that offset of the unconformities are used. Variations that occur along faults and what kind of error associated with these displacement estimations are hardly mentioned and not properly considered.

In addition to estimating displacements along the faults, analyses of the sensitivity related to the fault displacement was done by adjusting the dip of the faults and the strike and dip angles of the unconformity surface (Chapter 5.4). The results are presented in displacement plots.

3.2 FIELD WORK

The fieldwork consisted of a two-week excursion towards the end of the study. This focused on i) investigating less explored areas or areas with limited data, ii) verifying previous work, iii) checking on areas of conflict and iv) checking locations where further classifications were required. Data collected were mainly fault strike and dip measurements, dip directions and displacement estimations, and collecting a variety of photographs and facies descriptions. The syn-rift sediments were differentiated based on sedimentological characteristics such as grain size, roundness, sorting, grading, orientation and bed thickness.

A geological Silva Compass was used for all the structural measurements. To reduce the uncertainty related to dip measurements, a repeated series of dip angles were measured at every contact. The positions of fault and unconformity contacts were mapped, and extrapolated in challenging areas where the exposure was poorly exposed or missing entirely. The major faults can typically be identified by a significant topographic high, for example a mountain, representing the uplifted footwall, often dominated by the Pindos carbonate basement. An incised valley or other drainage feature, which can be classified as topographic lows, often represents the hanging wall. These were important guidelines working in the field, in particular when mapping the major faults.

The post-field work mainly concerned data processing, further interpretation of the gathered data and integrating them to the previous analysis done. Field measurements were organized and plotted into ArcGIS and Petrel Software to compare with the data used from previous work.

Chapter 4 – Structural Analysis

4.1 INTRODUCTION

This chapter will present the structural configuration of the study area, including field observations, 3D model building and structural cross-sections. The study area is characterized by major normal north-dipping faults that are particularly well-exposed in the river valleys (Figure 4.1). The major normal faults of interest, from south to north, are the Chelmos, Kalavryta, Kerpini, Doumena, Mamousia-Pirgaki and Eliki Faults. They all form discontinuous features, meaning that they clearly step along their lengths. Minor faults, including antithetic faults, are also present, and some of them are supplemented into the analysis. The colour legend from Figure 4.1 is consistently used for the lithologies throughout this thesis.

The structural map, which forms the basis of the analysis, is compiled from various Masters Projects from the University of Stavanger (Figure 4.2). The map for the southern part (Chelmos and Kalavryta Fault Blocks) has been compiled from Finnesand (2013), and the Kerpini Fault Block from Hadland (2016). The Doumena Fault Block, west of the Vouraikos Valley, has been compiled from Veiteberg (2017), and the central part, east of the Vouraikos Valley, from Oppedal (2017), including the eastern segments of the Mamousia-Pirgaki Fault. The Mamousia-Prigaki Fault Block and the Eliki Fault is based on the studies of Dahman (2015) and Ford et al. (2016). Faults mapped and described in previous studies, have each been given specific names. The same fault names are used in this study.

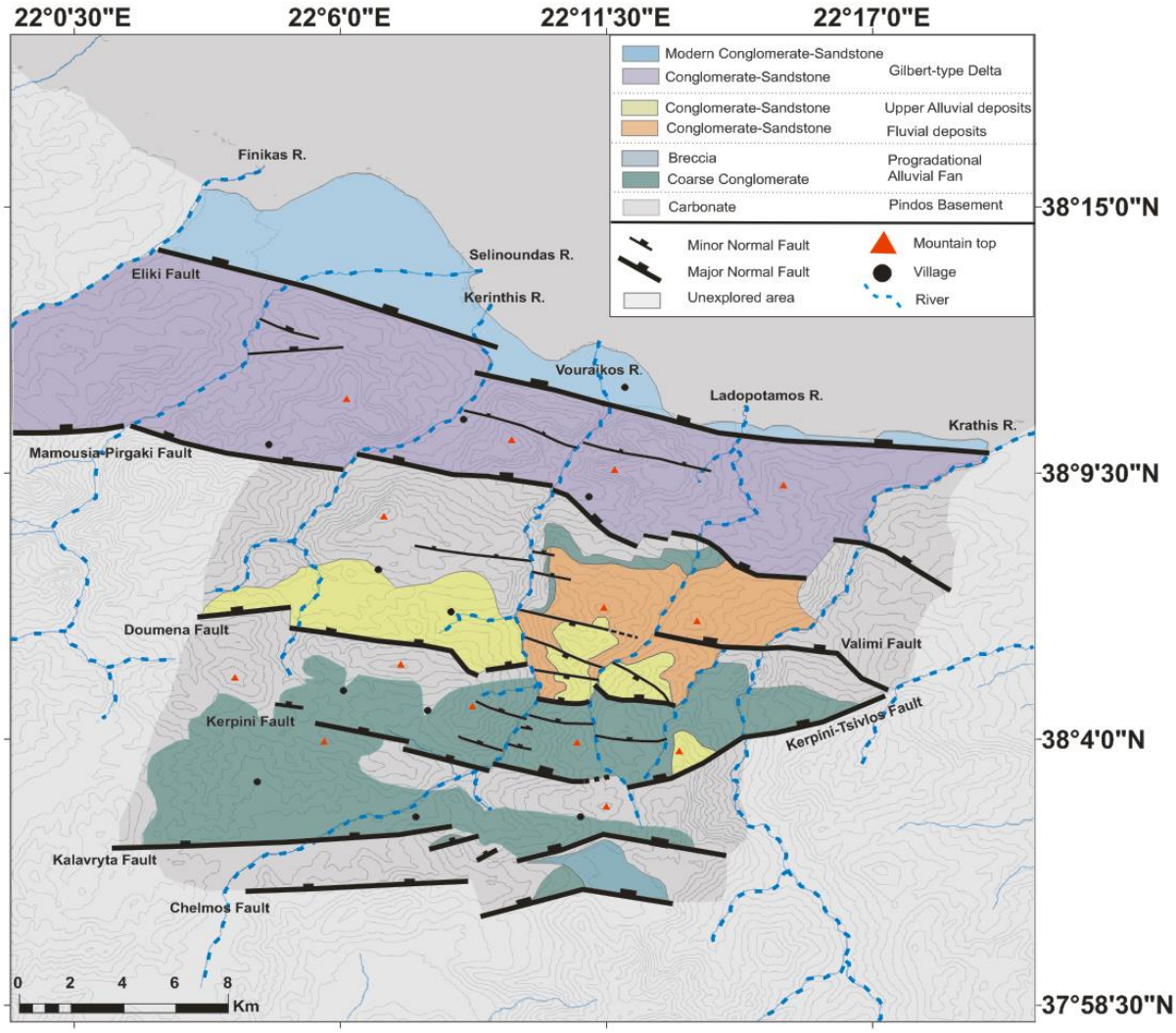

Figure 4.1: Structural map of the study area, including stratigraphic facies.

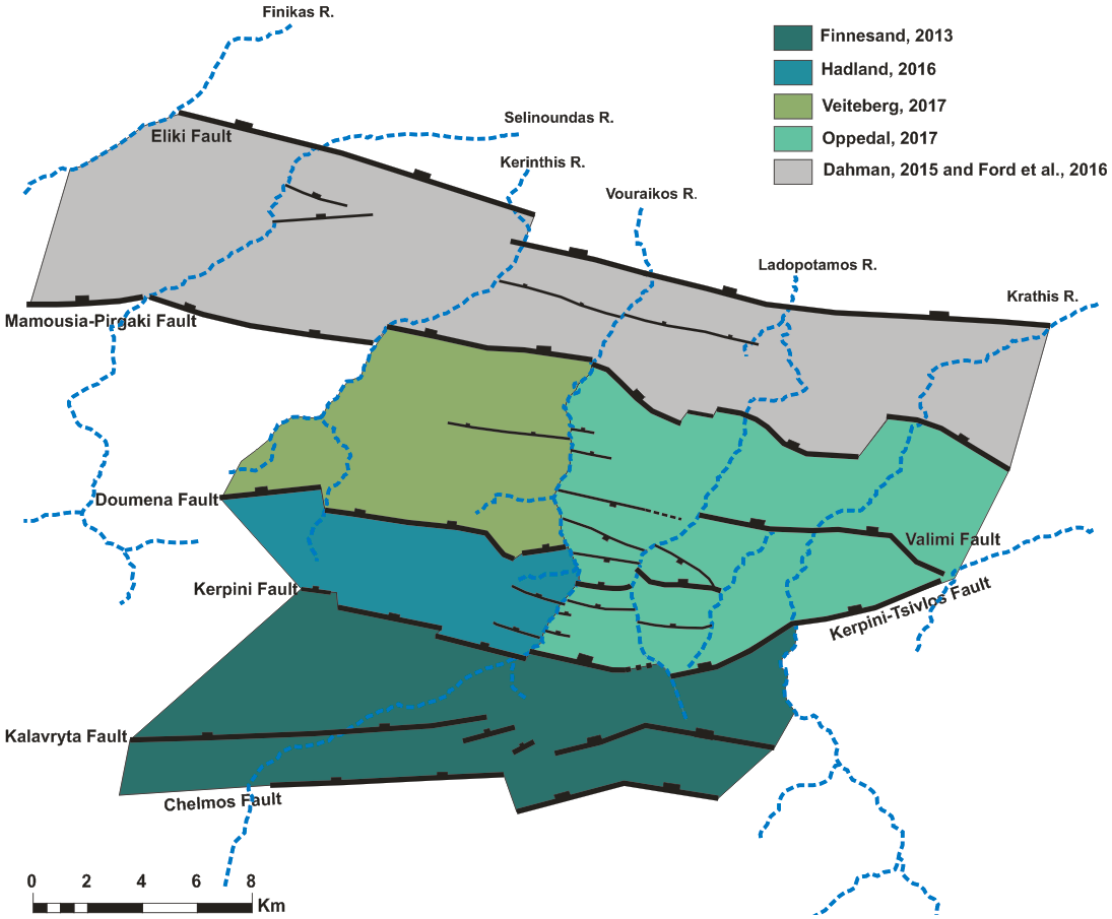

Figure 4.2: Structural map of the study area, highlighting the areas mapped in previous studies and have been used to compile the map in Figure 4.1.

4.2 Field Observations

This sub-chapter will present a short overview of field observations done at the end of the study to check areas of conflict and locations where further classifications were required, and to verify previous work. Figure 4.3 shows the main locations visited.

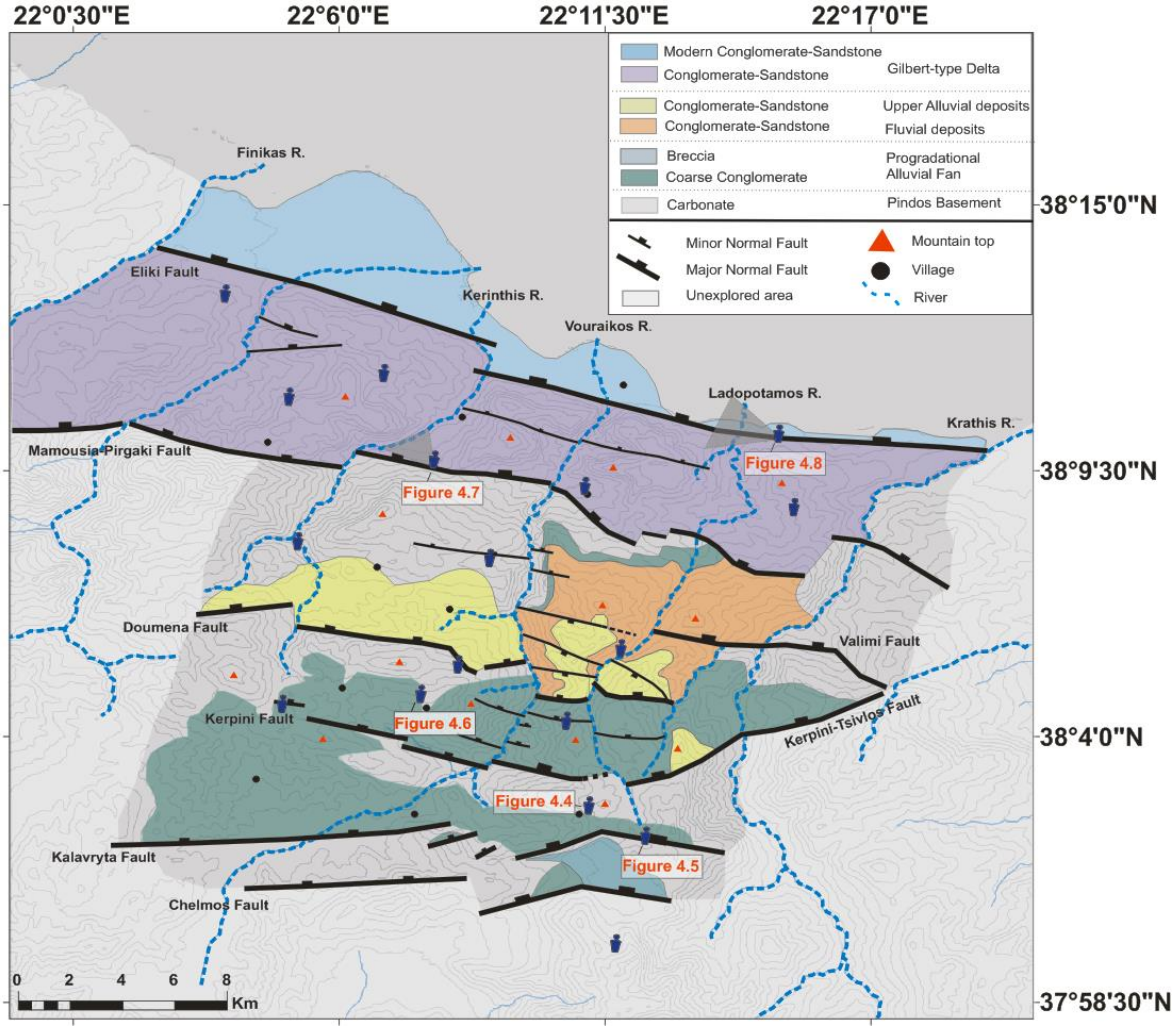

Figure 4.3: Structural map showing important locations and viewpoints visited, highlighted by dark blue-coloured statues.

The stratigraphic lithologies identified can primarily be divided into deformed basement carbonates of Triassic to Cretaceous age (Figure 4.4) overlain by a variety of Pliocene to Pleistocene syn-rift deposits (Figure 4.5-4.7), predominantly conglomerate-sandstones. Also, present-day deltas are building out into the Gulf of Corinth (Figure

4.8). Exposures in this area are variable but numerous road cuts, deeply incised river valleys, and cliffs allow the characterisation of the main outcrop pattern. Contacts exposed in the field are generally high-angle faults and low-angle syn-rift on basement unconformities.

Figure 4.4: Pindos Basement of deformed carbonate deposits. The outcrop location is marked on Figure 4.3.

Figure 4.5: Breccia deposits from the Chelmos Fault Block. The outcrop location is marked on Figure 4.3.

Figure 4.6: Progradational alluvial fan deposits from the Kerpini Fault Block, dipping approximately 25° south (Coarse conglomerates). The outcrop location is marked on Figure 4.3.

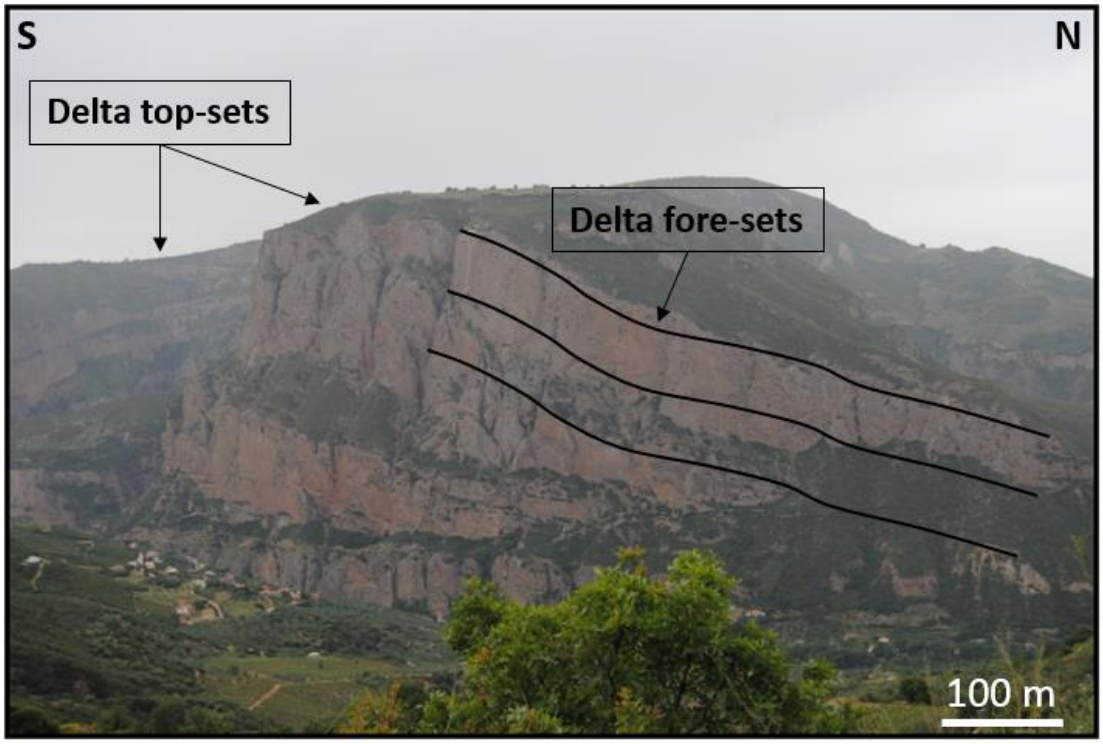

Figure 4.7: The Kerinthis Delta, view from the east. Example of the ancient Gilbert fan type delta deposit (Upper Pliocene). The top-sets and fore-sets are highlighted by block arrows. The development of the delta is contemporaneous of the Mamousia-Pirgaki Fault activity and the delta is cut by the Eliki Fault to the north. The outcrop location is marked on Figure 4.3.

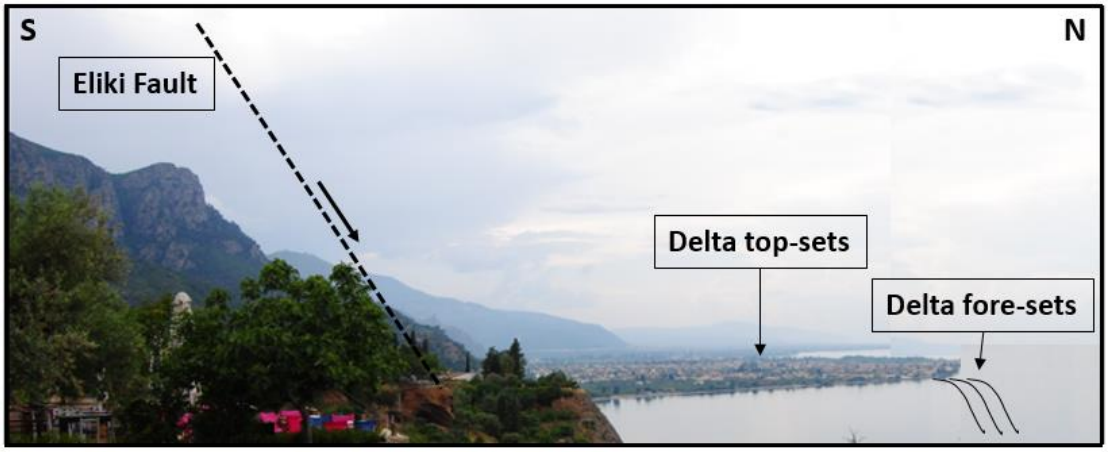

Figure 4.8: Modern delta building out into the gulf in the hanging wall of the Eliki Fault. Delta top-sets and fore-sets are highlighted by black arrows. The outcrop location is marked on Figure 4.3.

The main objective of the field work was to check locations of faults and unconformities and verify their strike and dip measurements from previous work as they are the main parameters for the displacement analysis. Additional observations contributing to the study were:

- Syn-rift sediments identified south of the Chelmos Fault, which help to estimate the displacement on this fault. Previously, the topography was used to estimate the minimum displacement.
- The Mamousia-Pirgaki Fault might be tipping to zero displacement to the west due to dramatic loss in topography, but field observations suggest a rapid termination.

4.3 3D MODEL BUILDING

The following sub-chapter presents a workflow of the 3D structural model-building. The modelling process can be divided into three main steps: Fault modelling, unconformity surface modelling and 3D structural modelling.

4.3.1 Model Input Preparation

Step 1. Fault Modelling

Faults mapped during fieldwork, along with faults compiled from previous Masters Projects (Finnesand, 2013; Dahman, 2015; Hadland, 2016; Oppedal, 2017; Veiteberg, 2017) are digitized into the Petrel model. Faults are digitized by drawing polygon lines on the DEM in 2D-view (Figure 4.9). It is important to draw the polygon lines on the DEM to get the correct elevation on the z-axis. A variation of different dip angles were tested to see which best fit with the DEM surface and the basic fault mapping. Furthermore it allows the documentation of the possible ranges of fault dips and strikes. Through many years of field work in the Kalavryta area, different strike and dip measurements has been published on the very same faults. Dip angles of the major faults tend to be in the range between 45-55°, getting steeper from south to north (Collier and Jones, 2004; Ford et al., 2013).

Google Earth, in combination with a 3D structural model, was used to extrapolate faults mapped in the field wherever challenging terrain prevented tracing them throughout. It is also helpful to follow the strike of the faults on satellite images where the higher topography may indicate an uplifted footwall of a fault. Several faults tend to be located on boundaries between sparsely and densely vegetated areas or simply on small groove in the topography.

During modelling in Petrel, surfaces were created for each fault. These were quality checked by testing how planar fault surfaces intersect with the DEM. These were further checked by comparing them to features observed in Google Earth. If miscorrelations occurred, corrections were applied by adjusting the polygons to get an improved fit.

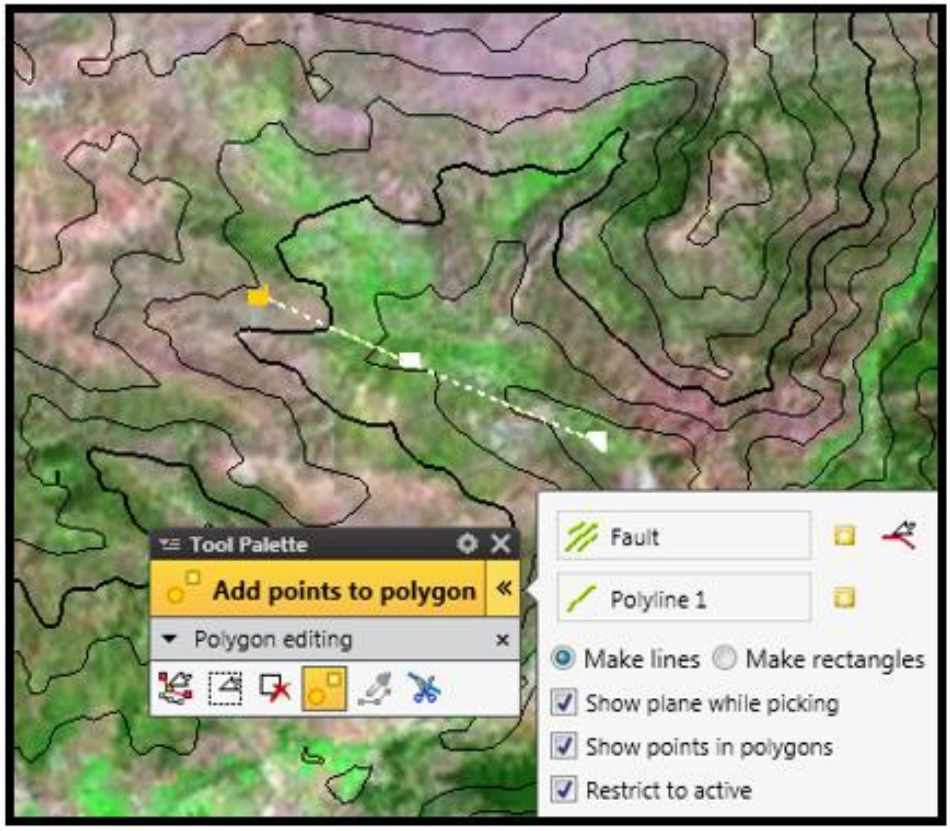

Figure 4.9: Digitalisation of faults by drawing polygon lines on the DEM in Petrel.

After tracing the polygon line to the correct position, a copy of the polygon was made and this was translated using the appropriate strike and dip angles (Figure 4.10). In this process, the strike direction of the polygon line is projected 1000 m in the z-direction from the original polygon line, with a dip angle of 45° between them. The two polygon lines were appended in preparation of the input for the fault surface modelling.

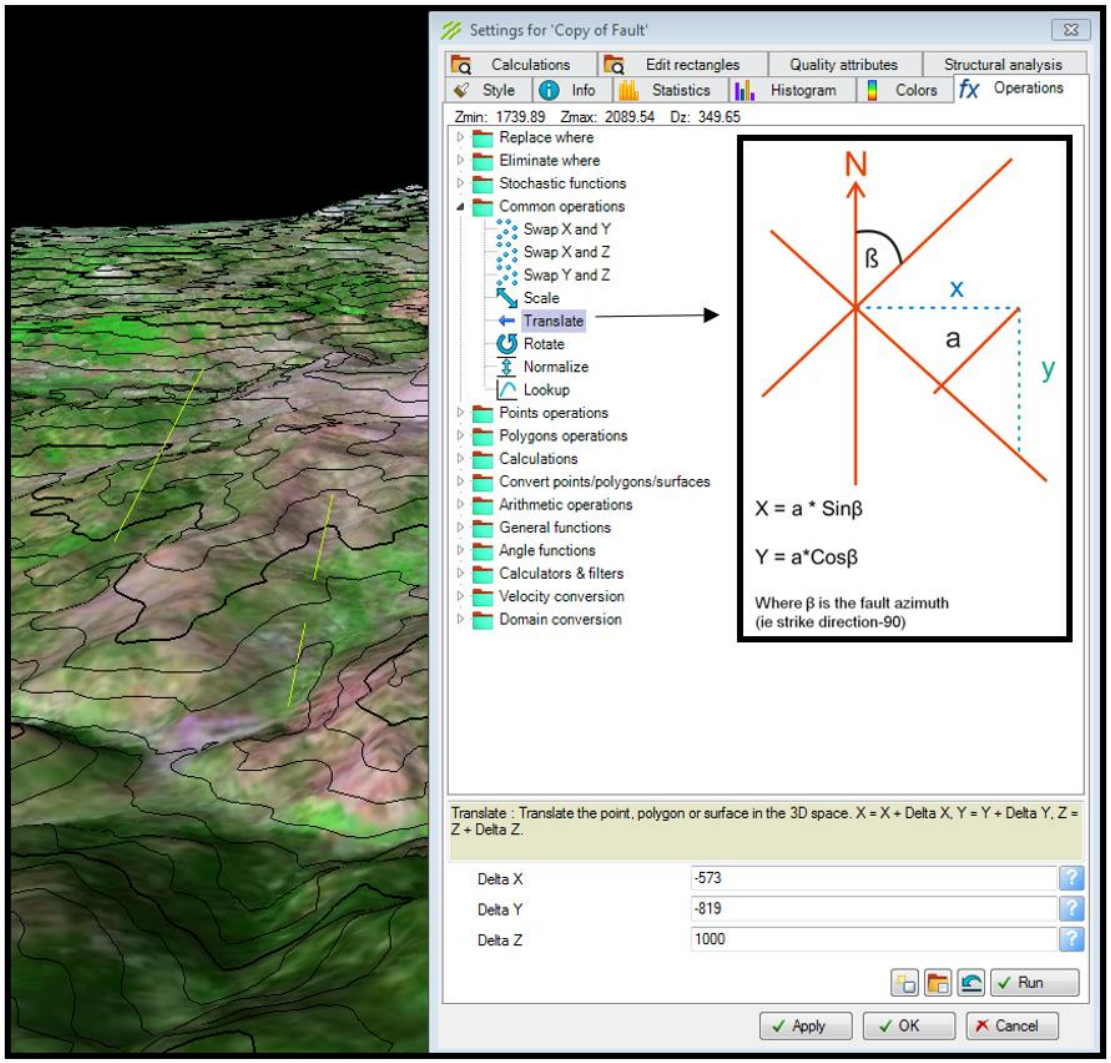

Figure 4.10: Translation of polygon lines of the Kerpini Fault West I in Petrel.

Fault surfaces were generated and projected between the appended polygon lines (Figure 4.11). In this process the main input is the appended polygon lines and an input boundary. Methods used are convergent interpolation which is a control point orientated algorithm (rather than grid point) which will converge upon the solution by adding more and more resolution with each iteration. This means that general trends are retained in areas with little data while detail is honored in areas where the data exists. The extrapolation method used is trend. The plane will extrapolate beyond the polygon lines, but is confined by the input boundary.

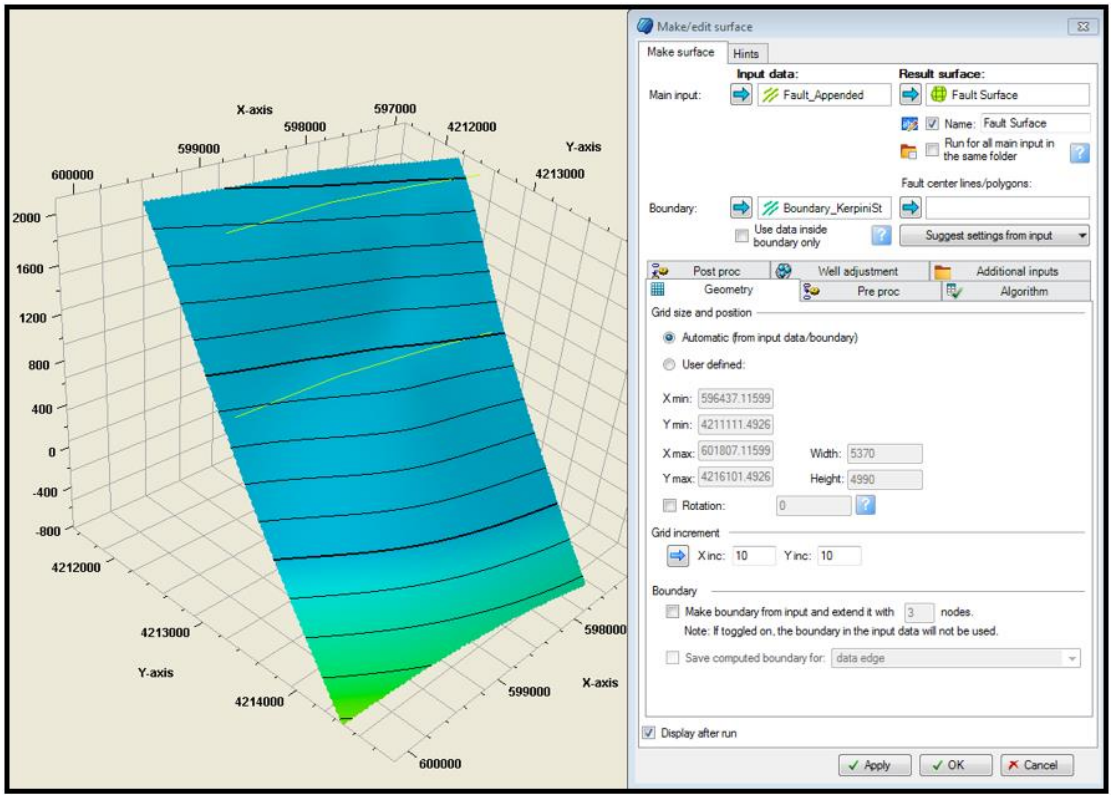

Figure 4.11: "Make/edit Surface" in Petrel. Showing how a plane is projected between the two polygon lines. The fault plane is limited by a polygon boundary.

Challenges related to fault modelling may be artifacts on the fault plane. It is not uncommon to generate curved or "wavy"-fault surfaces. This problem usually occurs some distance from the input data (polygon lines) and is likely due to the extrapolation method, where the surface is extrapolating far from the data until the boundary confines it. A good solution is to make a smaller boundary which limits the data extrapolation to correct for this problem (Figure 4.12).

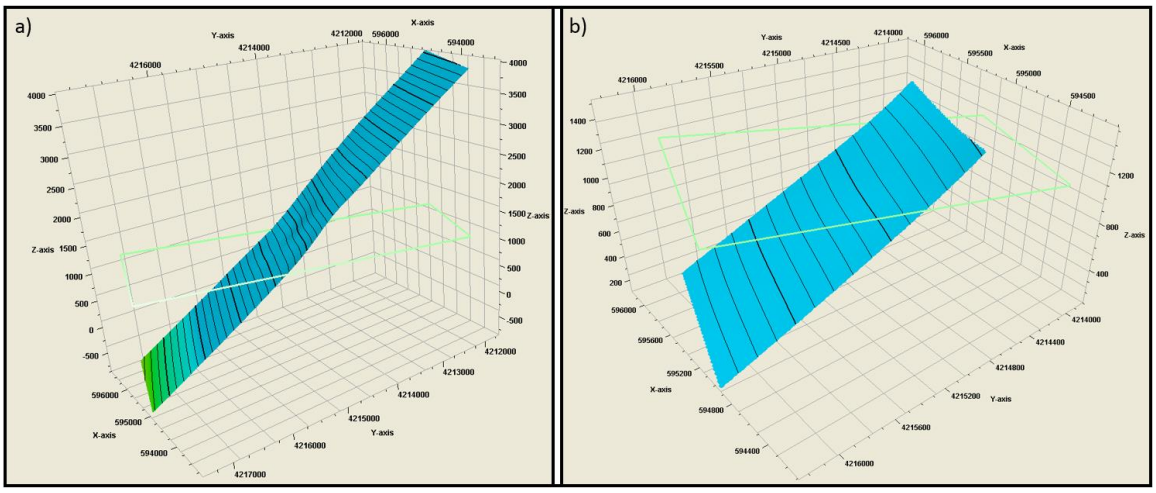

Figure 4.12: Petrel image of a) Modelled fault plane with a large boundary and b) Modelled fault plane with a more confined boundary.

Step 2. Unconformity Modelling

Unconformity surfaces can be digitized in a similar process as the fault surfaces. The first step is to find a point on the DEM where the unconformity surface should be located according to field observations. The x, y and z-values of this point is put into "Make Surface". The method used is artificial algorithm-plane. This takes a single point as input, plus a surface dip and strike value, and generates a planar surface (Figure 4.13). This method assumes that the unconformity surfaces are planar and suffered little or no erosion prior to the onset of extension.

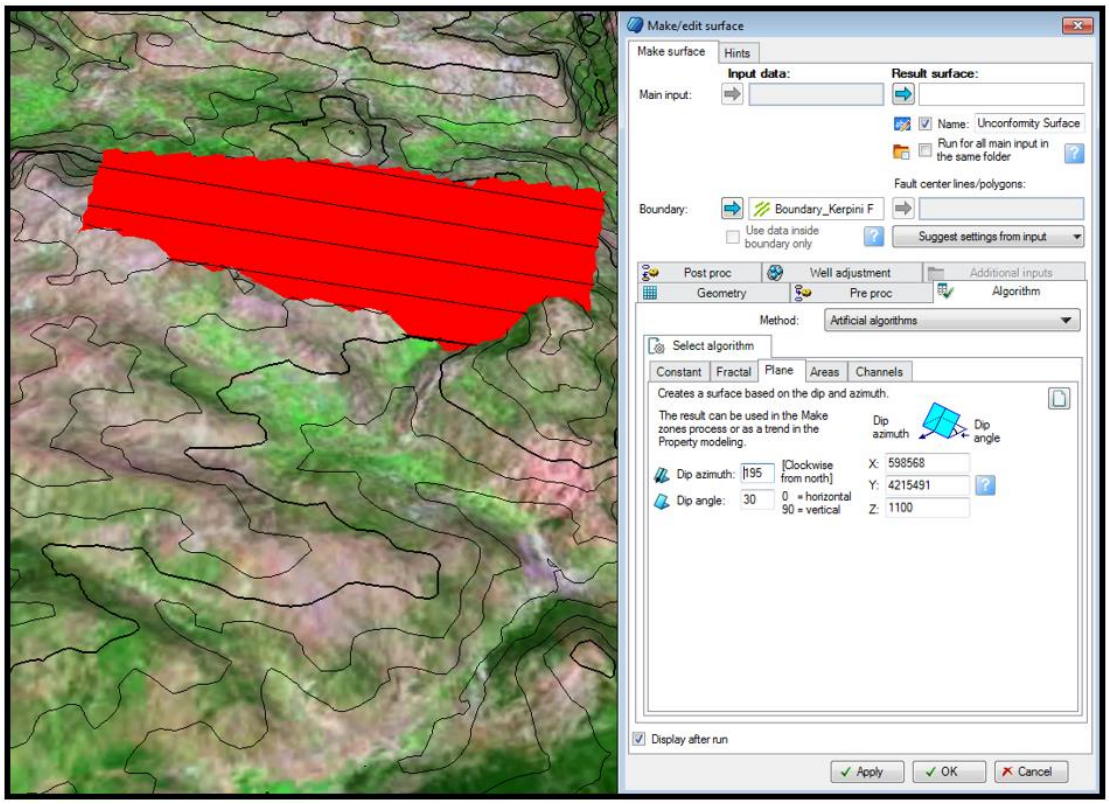

Figure 4.13: Unconformity modelling in Petrel. The box to the right show the assigned values for the modelled plane, here using the method of artificial algorithms.

A challenge related to unconformity modelling is to get the same pattern on the DEM, as the one traced in the field. In most cases the trace was optimized by adjusting the dip and strike parameters of the surface to get the best fit with the topography. Satellite imagery from Google Earth have good resolution and is used to help trace and control the contacts. In order to optimize the surface with the mapped traces, both for faults and unconformities, adjustments of 0-5° were required.

Modelling Example - The Doumena Fault West

An example of the modelling process using the Doumena Fault Block will now be presented, both modelling the fault surface and the unconformity surface. Figure 4.14 shows where the observation of the fault plane has been traced and how the fault

plane in Petrel was modelled. When correlating faults across the river valleys, this was a tool to check that the present-day topography does not yield misleading indications.

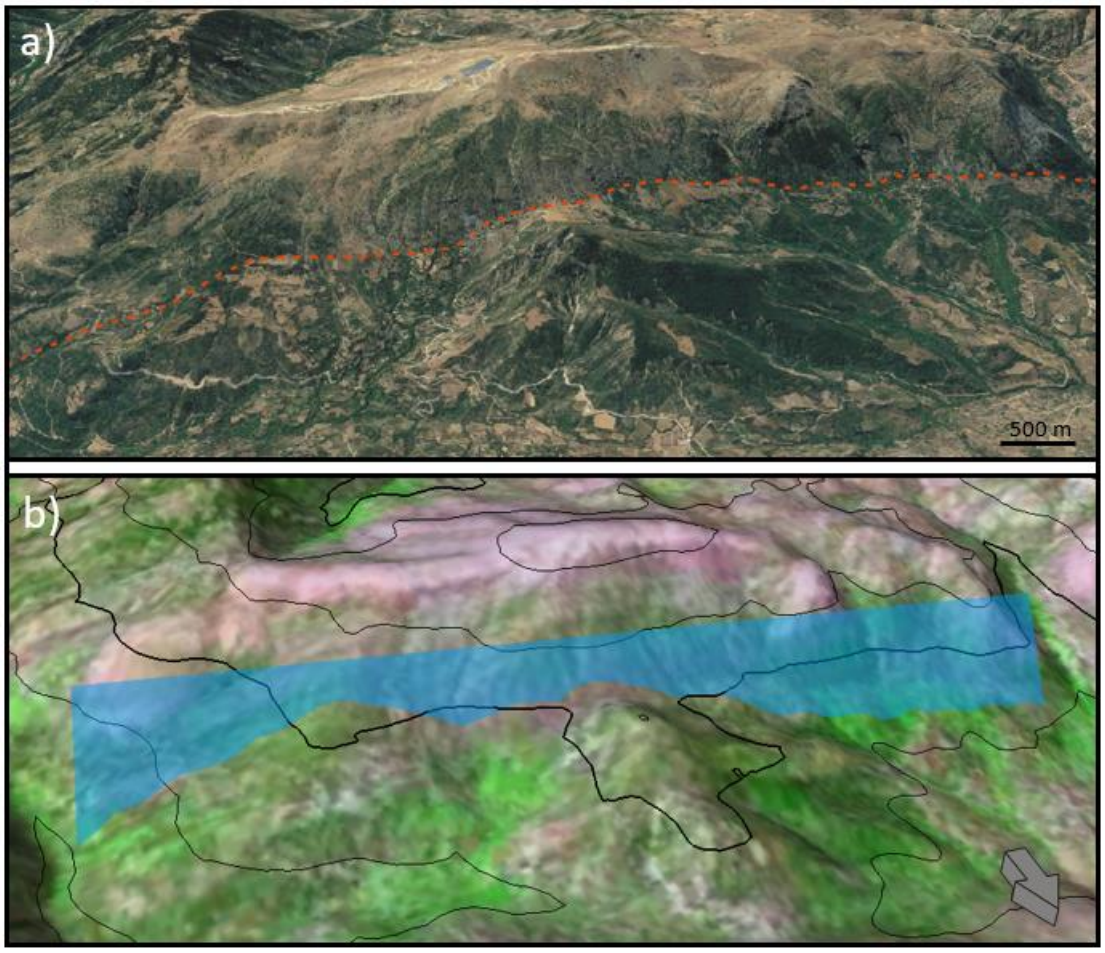

Figure 4.14: Comparison of a) the observed Doumena F. West traced in Google Earth to b) the model fault traced in Petrel. The modelled plane dip 45°N.

The traced position of the Doumena unconformity surface was also marked on Google Earth and compared to the modelled plane in Petrel (Figure 4.15). Minor discrepancies differ from the observed contact to the modelled contact, however, it is a fairly good match. When modelling the unconformity surfaces, the same strike and dip values are assigned to the whole plane. But in reality, the strike and dip may change along the fault surface. This may be a reason why it can be challenging to model the same fault trace as mapped in field, but the results usually show a fairly good match.

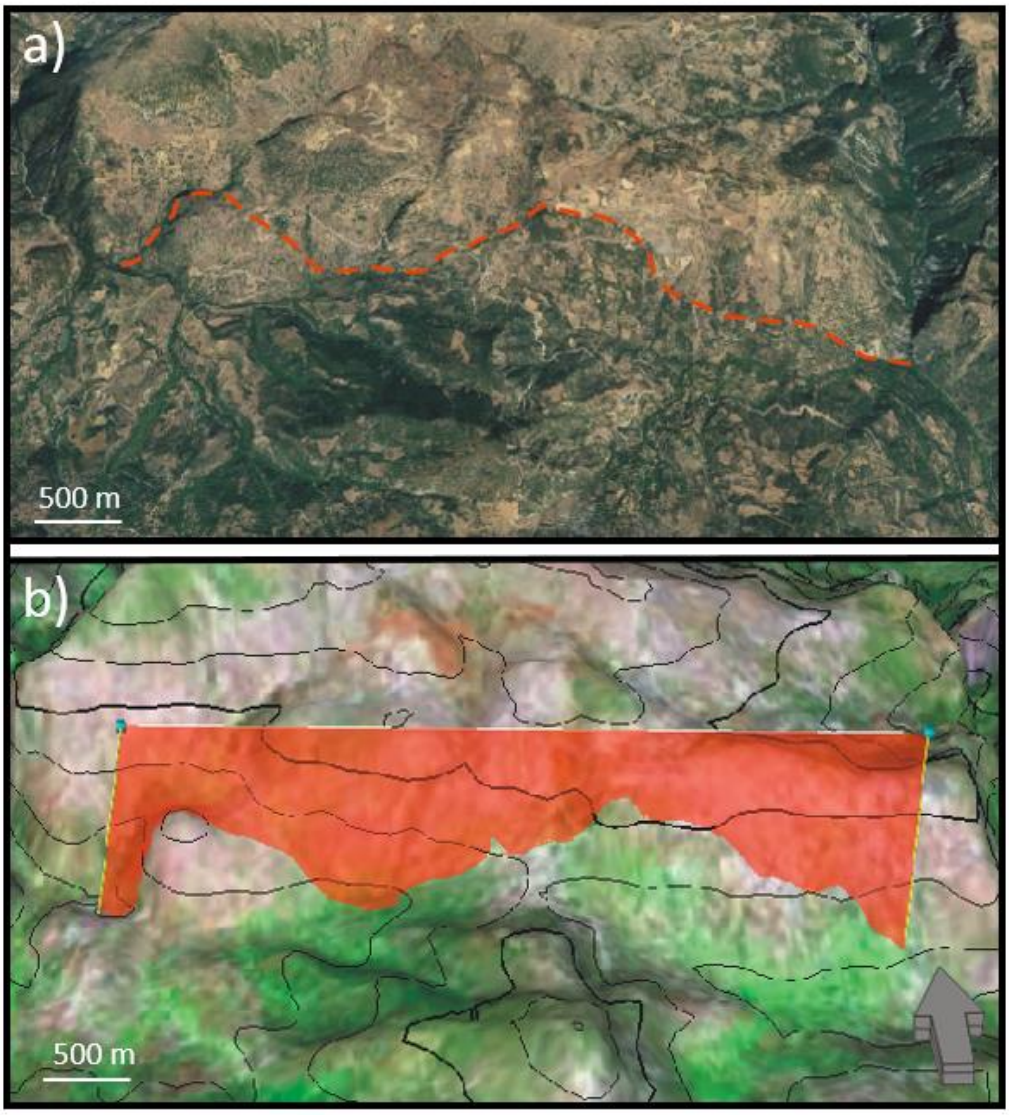

Figure 4.15: Comparison of the observed Doumena Unconformity traced in Google Earth with the modelled unconformity in Petrel. The modelled plane is dipping 25°S.

The sensitivity of the unconformity pattern traced in Google Earth was tested by modifying the unconformity dip by ±5° in Petrel (Figure 4.16). The result show differences, where the contact does not match the topography with the same pattern as traced in Google Earth.

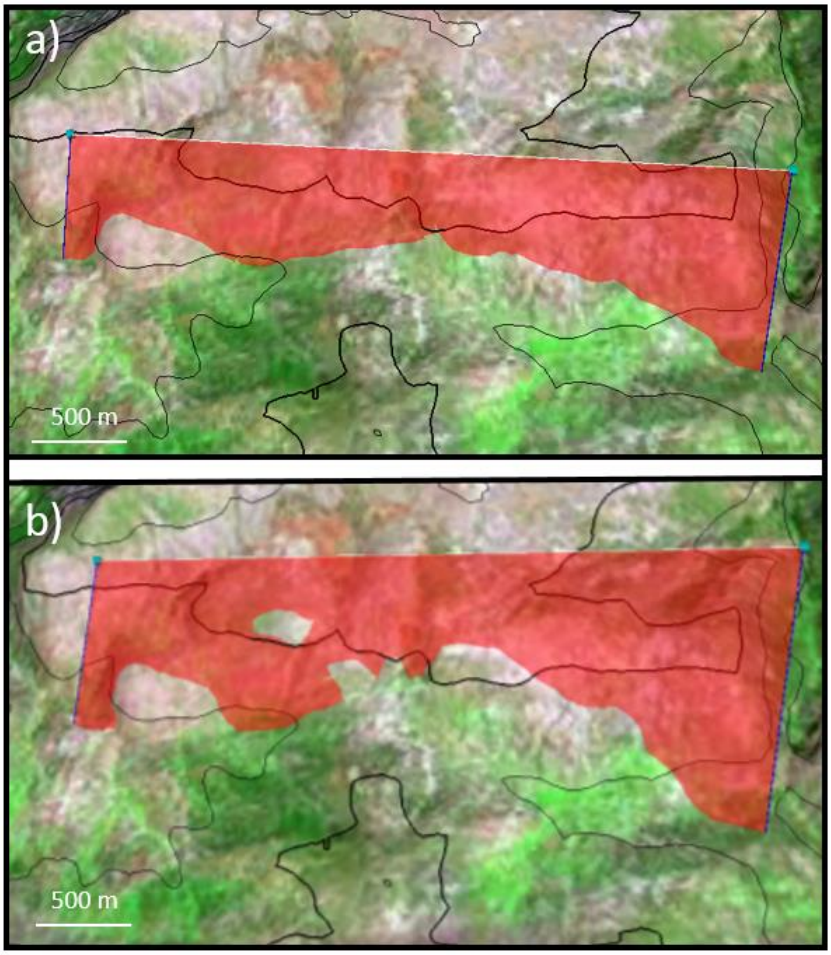

Figure 4.16: Images from Petrel showing how the unconformity pattern is affected by changing the dip of a) +5° and b) -5°.

After finding the better optimum match with the topography compared to that traced in the field, the unconformity was first truncated by the faults; down-dip on the hanging wall side of the southern fault, and up-dip on the footwall side of the northern fault (Figure 4.17). In several cases the truncation by the northern fault was subaerial, meaning it has been eroded. In this case the unconformity was also truncated by the DEM which represents the current-day topography. This operation is done under "Eliminate where" in the settings window (Figure 4.18).

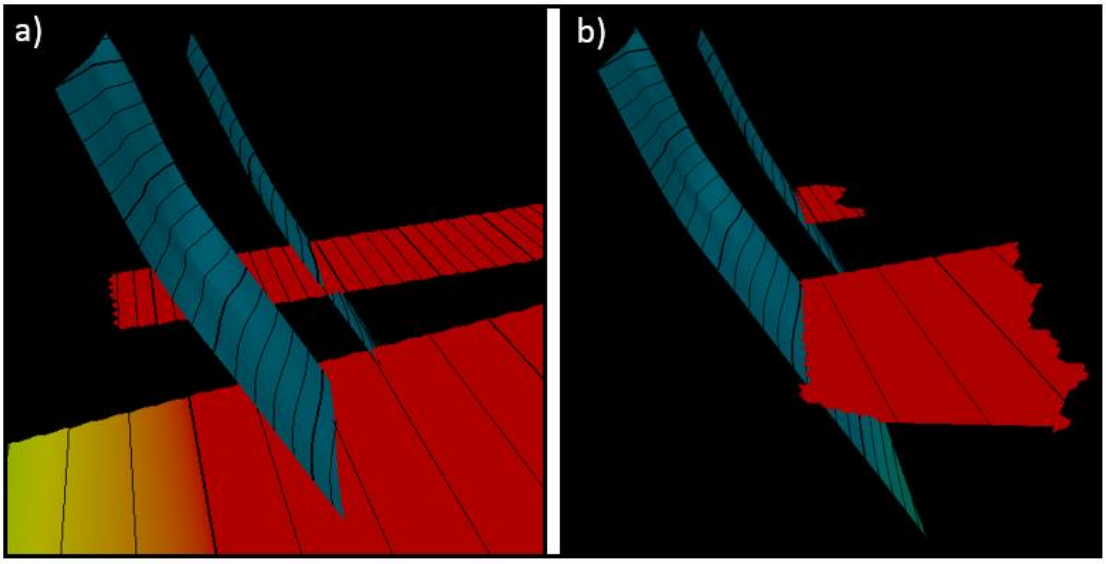

Figure 4.17: Modelled fault plane and unconformity surfaces showing a) Before unconformity cut and b) After unconformity cut with the fault surface and the DEM.

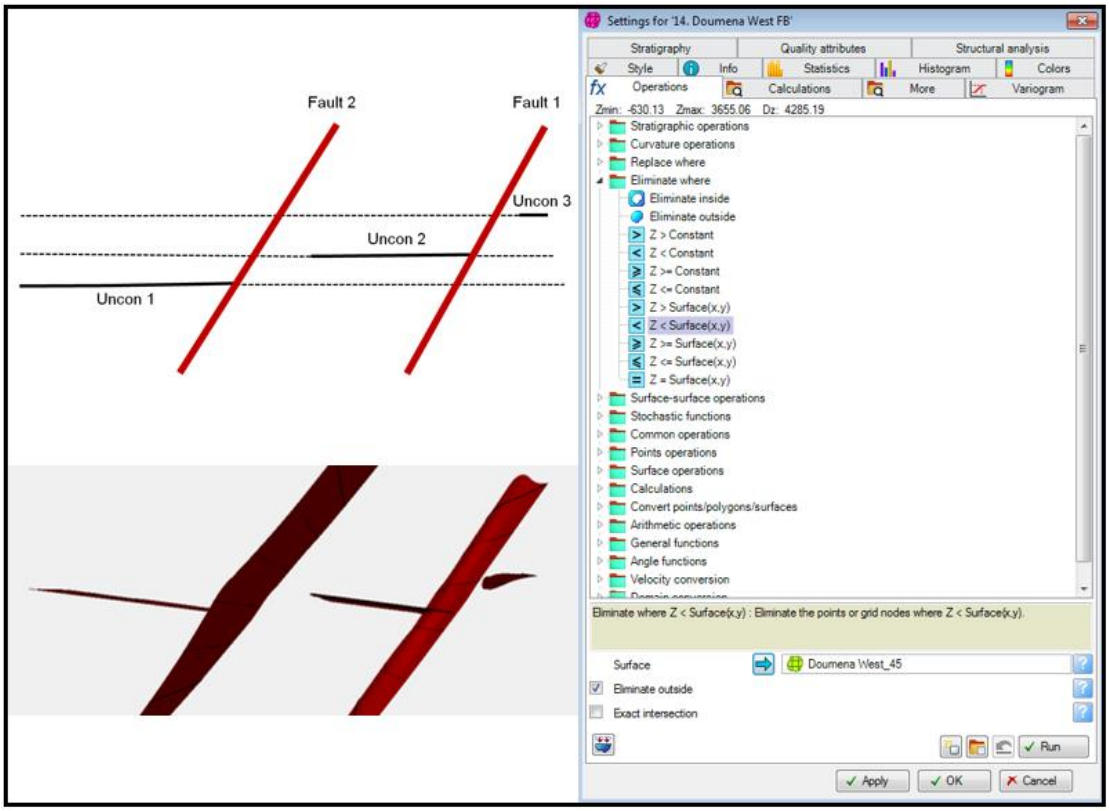

Figure 4.18: The left side is showing a conceptual figure of two faults and unconformities, and how this should be modelled and truncated in Petrel (lower left side). The box to the right shows the "Eliminate where" operation used to truncate the unconformity surfaces.

4.3.2 Structural 3D Modelling

After completing the fault and unconformity modelling, the fault surfaces need to be converted to an active model as fault pillars (Figure 4.19). In this step it is important to select a sufficient number of pillars. If too many pillars are added, it may become unnecessarily complicated and time-consuming when adjusting and making changes to the faults. Alternatively, too few pillars used, the subtle changes along strike may be neglected, and important features may not be included.

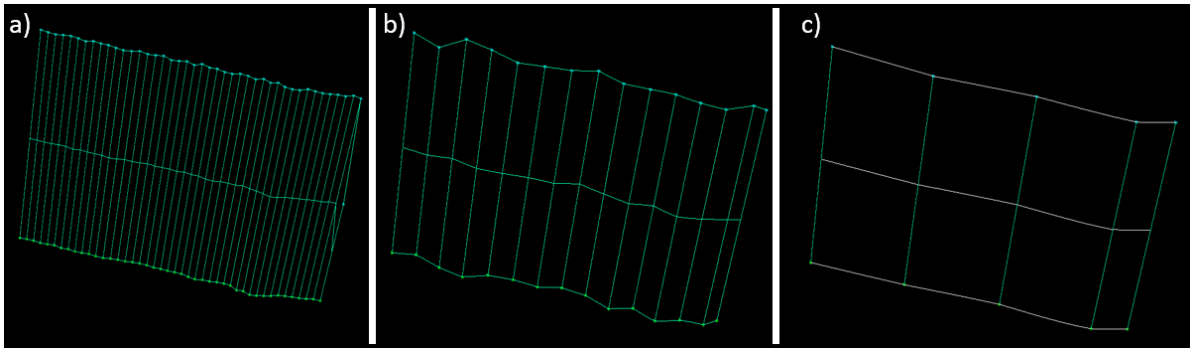

Figure 4.19: A fault surface converted to fault pillars showing different numbers of fault sticks: a) a very dense selection, b) a moderately dense selection and c) a limited selection.

The next step is to quality check (QC) all the faults and identify if there needs to be any corrections made. Changes may be connecting faults that intersect, deleting or adding pillars, checking the fault dip, stretching or cutting the fault lengths (Figure 4.20). It is important to try and honour the input data when doing these adjustments.

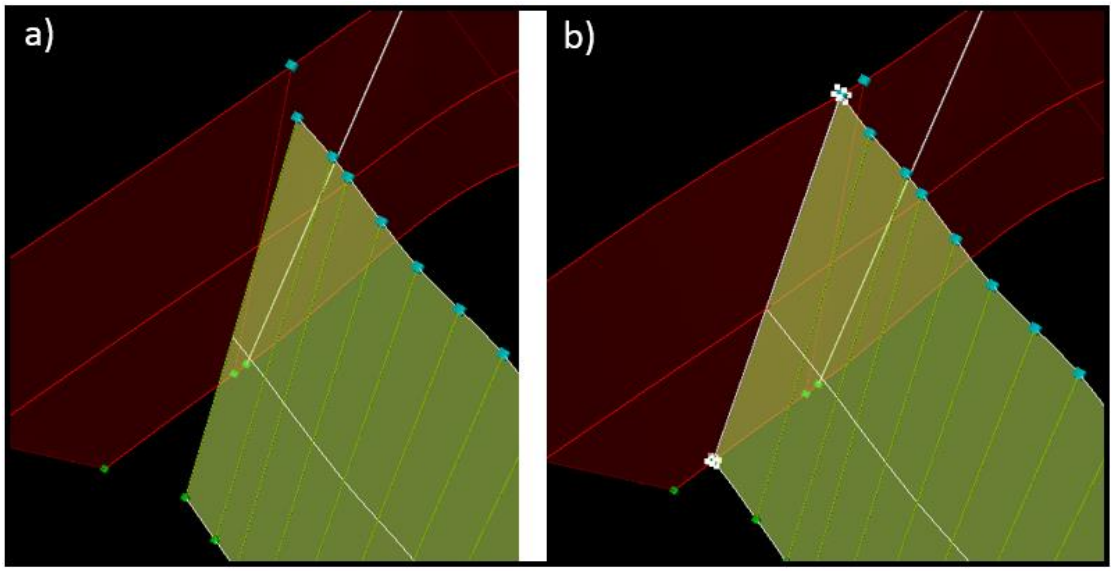

Figure 4.20: Petrel image showing a) before and b) after connection of two faults.

After completing the fault pillar editing, the faults should be displayed in 2D view to check if faults overlap or truncate or need further adjustments (Figure 4.21). In this process, it is possible to define the directions of faults that strike in the same by marking part of a fault as an I- or J-direction. This may help to create a less distorted grid. Most of the N-S striking faults have been assigned the same direction (4.22). Pillar gridding is the next step, where a grid is created.

Figure 4.21: Skeleton image of the modelled faults in 2D view in Petrel.

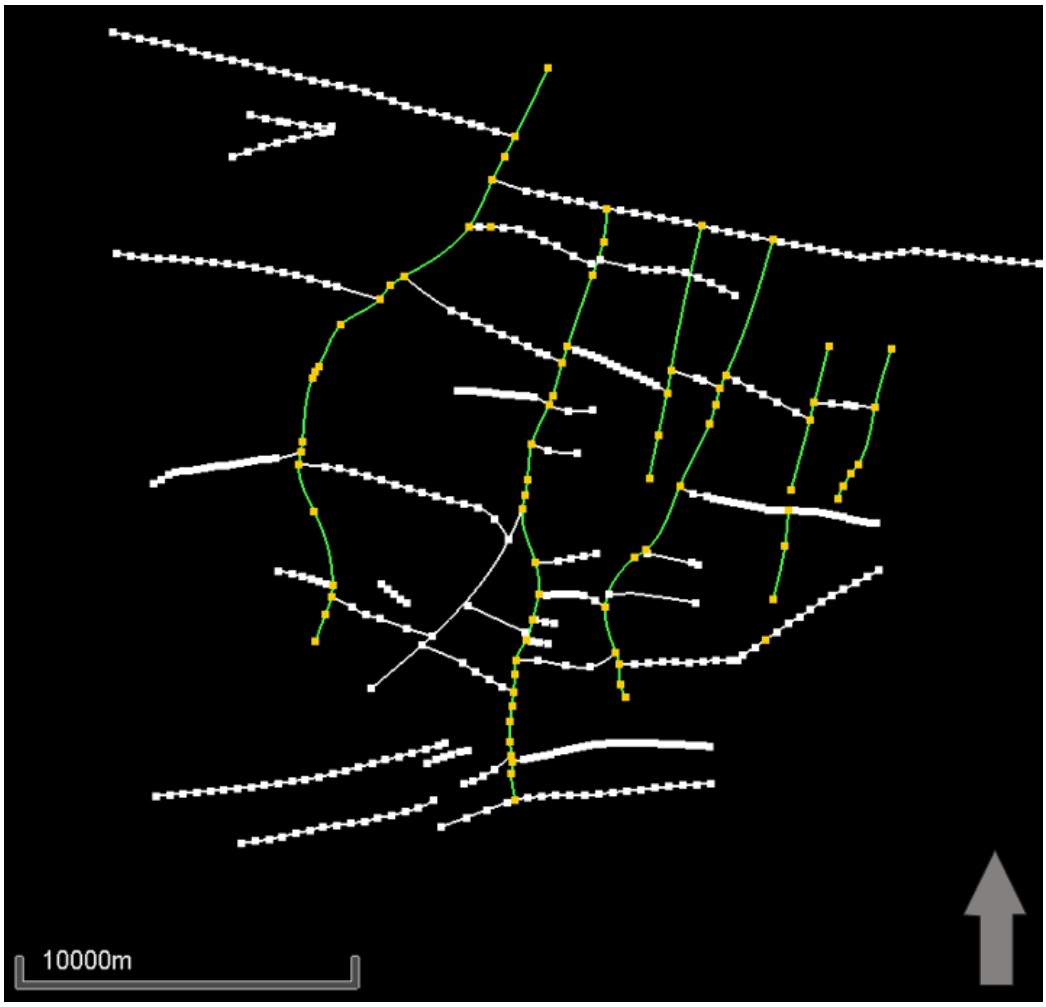

Figure 4.22: Skeleton image of the faults in 2D where the N-S trending faults have been assigned the same I-direction.

The 3D grid form a container to store the geology in, so when building a grid it is important to optimise the number of cells. This means that by minimising the number of cells, the calculation time in property modelling and volumetric estimations reduces, and by maximising the number of cells, reservoir heterogeneities is more likely to be accounted for. Different grid types can be generated depending on input data. In this study the zig-zag grid has been used. Zig-zag help to obtain regular shaped grid cells along faults and this option creates a best-fit split of the rectangular shaped grid cells along the faults defined as arbitrary (Figure 4.23).

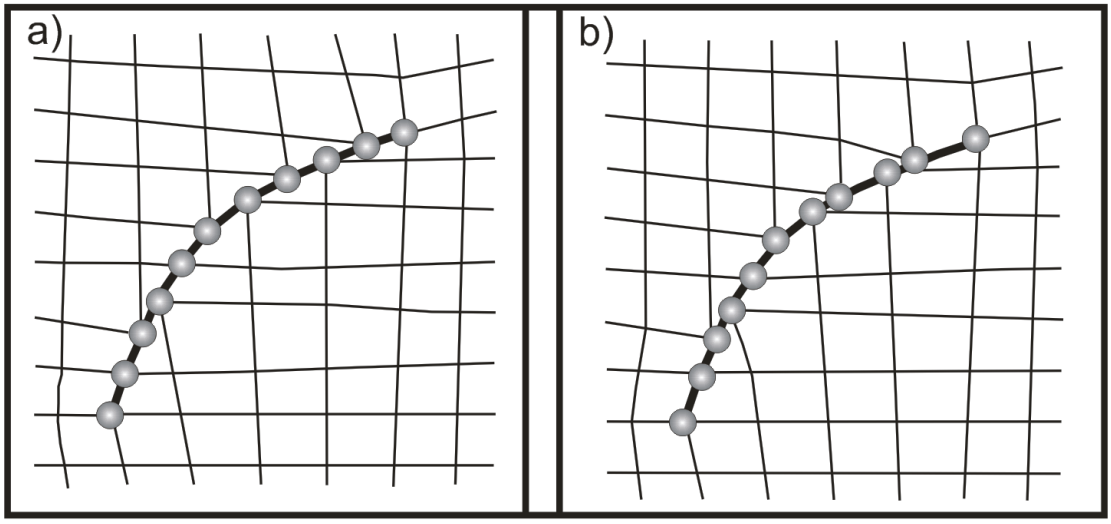

Figure 4.23: a) Grid cells equally spaced along an arbitrary fault and b) Grid cells moved perpendicular to the arbitrary fault where the spacing of grid cells along the fault vary.

After generating a grid, horizons can be added to the model, hereby dividing it into zones. The input surfaces include the DEM, which act as the erosional upper surface, with the unconformity surfaces in the middle and an arbitrary basement base at the bottom. Each unconformity surface is assigned to the segment it belongs to. The geometrical model attribute can be used to display the zones and segments. Figure 4.24 shows a 3D structural model divided into a syn-rift and a basement zone. The final step is to quality check the model in 3D. It is important to keep in mind that the finalized model contains geological simplifications compared to the actual study area. The model is an excellent tool in order to visualize, analyse and to better understand the area despite the simplifications.

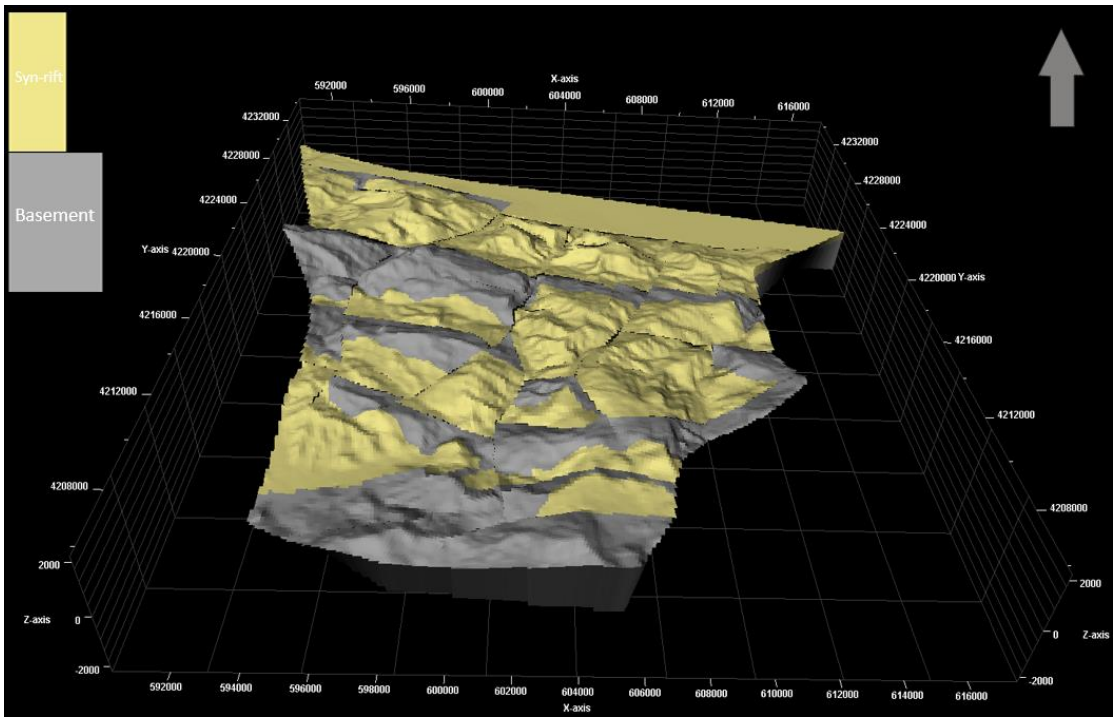

Figure 4.24: 3D Model of the study area showing the syn-rift (yellow) and basement (grey) in Petrel.

4.4 STRUCTURAL CROSS SECTIONS

This sub-chapter will consider and examine the present structural configuration of the study area along N-S cross-sections, to investigate the total displacement along the profiles and possible differences between them.

4.4.1 N-S Cross Sections

Four approximately N-S oriented cross-sections are constructed from the 3D model in Petrel in order to highlight the main features of the structural changes across the study area (Figure 4.25). The location criteria for these cross-sections was based on investigating each fault block separated by river valleys, and are therefore placed sub-parallel to the valleys. The cross-sections were generated in Petrel by drawing polygon lines on the area of interest and intersection of those lines were created in the 3D grid. The depth of the basement in the sub-surface has been approximated in several places where few exposures are present, especially in the central to eastern part (Oppedal, 2017). These are highlighted by "?" in the cross-sections. Wherever the basement deposits are exposed, the dip of its unconformity surface is projected linearly. Also, the depth of the ancient Gilbert-type deltas are assumed to be at approximately -500 m below the sea level (Chapter 5.1 – Case 4) for all of the following analyses.

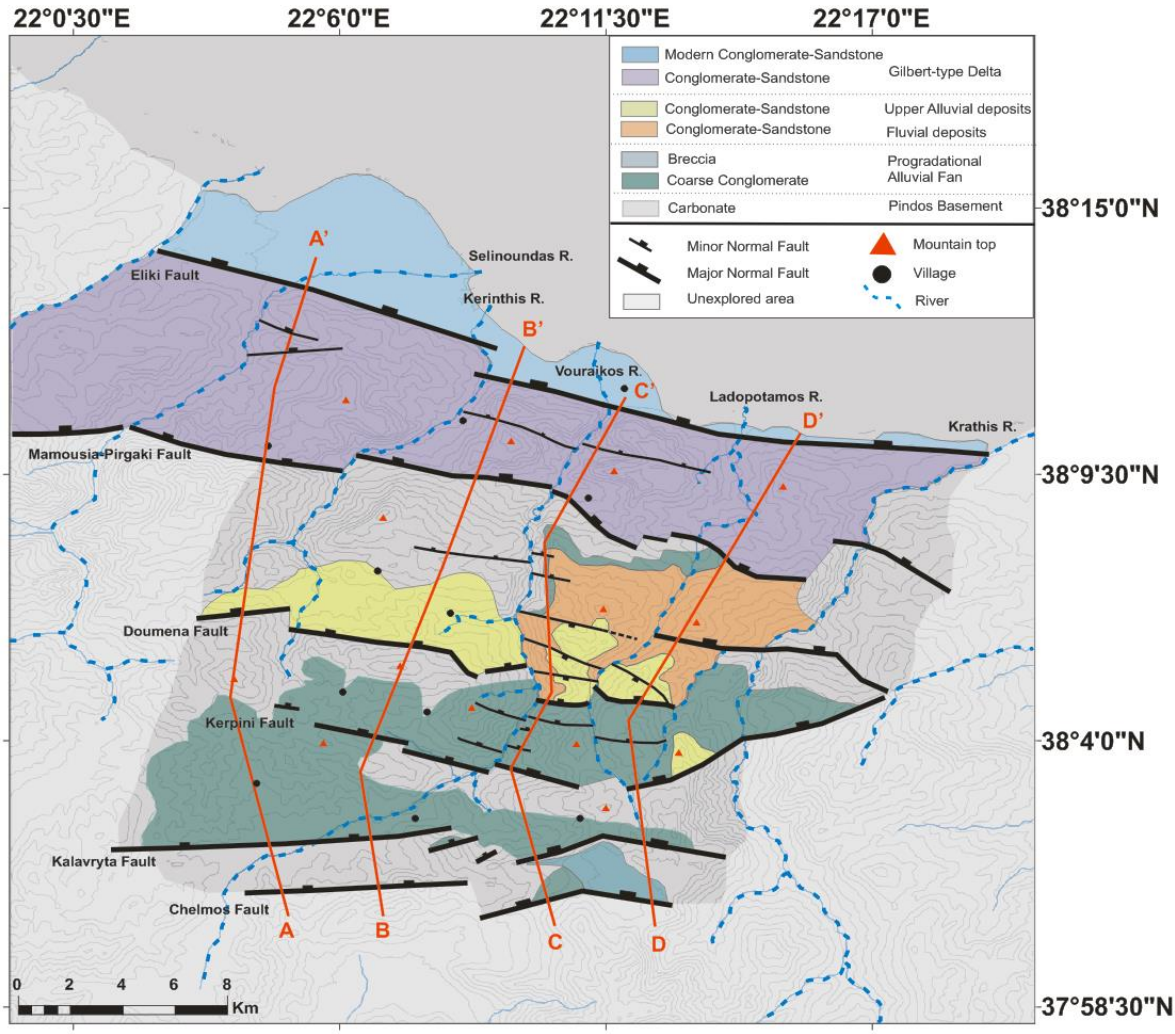

Figure 4.25: Location map showing location of the four N-S cross-sections.

Cross-section A-A' exhibits the longest horizontal distance (24900 m), and contain all of the major north-dipping faults, except for the Kerpini Fault (Figure 4.26). The Mamousia-Pirgaki Fault Block accommodate two minor faults in the Kerinthis Delta, the Kerinthis Fault North and Kerinthis Fault South. The spacing between the major faults are about 4-6 km, apart from the 8 km long distance between the Kalavryta and Doumena Faults and the 2 km distance between the Chelmos and Kalavryta Faults. The syn-rift deposits are coarse conglomerates in the Kalavryta Fault Block in the south, with a modest section of alluvial deposits in the hanging wall of the Doumena Fault. Section A-A' is dominated by a large N-S oriented basement ridge on the

Kalavryta and Doumena Fault Blocks, while the Mamousia-Pirgaki Fault Block host a large ancient delta in the north.

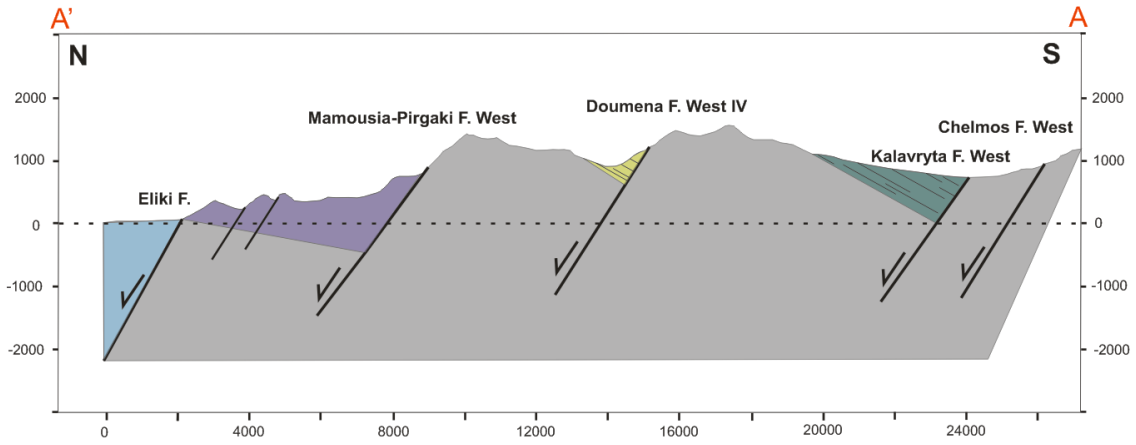

Figure 4.26: Cross-section A-A'.

Cross-section B-B' contain all the major faults, in addition to the Little Doumena Fault and the Dhervini Fault (Figure 4.27). The spacing between the major faults are quite similar, ranging between 4-6 km, with a shorter distance between the Chelmos and Kalavryta Faults of 2 km, as observed from the section A-A'. The Doumena Faults is still characterized by a large basement ridge, but the alluvial deposits gets more pronounced in this section.

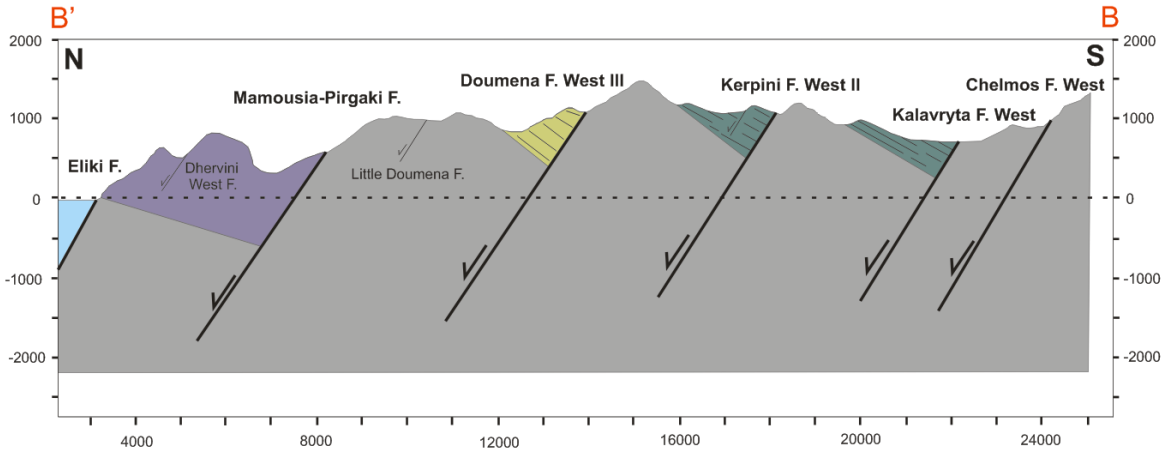

Figure 4.27: Cross-section B-B'.

Cross-section C-C' accommodates all the major faults and feature a graben structure in the central part, enclosed by the Doumena F. East I and an antithetic fault, the North Graben Fault (Figure 4.28). This graben host almost horizontal dipping alluvial deposits underlain by a thick package of fluvial deposits. South of the graben structure, a multitude of smaller scale rotated fault blocks are present, containing south-dipping coarse conglomerates. In this section, compared to the other two sections, the basement ridges are much less pronounced, there are more syn-rift deposits present and several more minor faults. Only minor basement ridges are found in the Chelmos, Kalavryta and Doumena hanging walls.

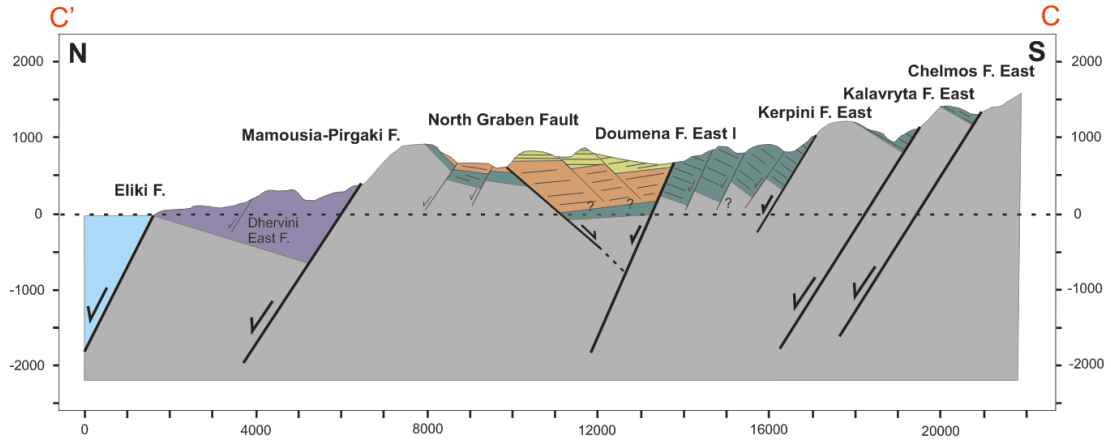

Figure 4.28: Cross-section C-C'.

Cross-section D-D' shows different fault blocks that contain thick packages of syn-rift deposits in the central to northern part of the section, with a general trend of thinning southwards (Figure 4.29). The antithetic fault that created the graben structure observed from the previous section is much less pronounced here. The spacing between the faults are similar in this section, but there are significantly less minor faults in the Kerpini and Doumena Fault Blocks than in section C-C'. A fairly large fault, the Valimi Fault, is located between the Doumena Fault East II and the Mamousia-Pirgaki Fault East.

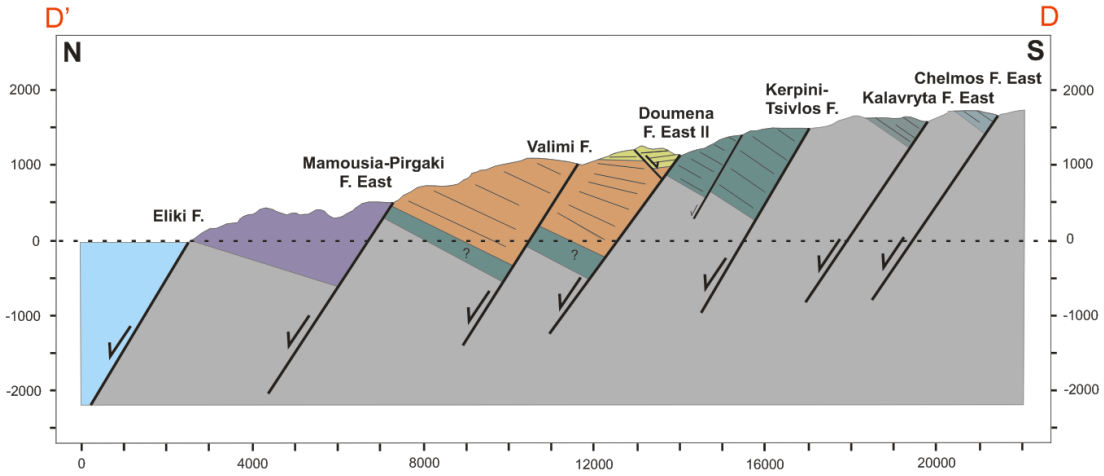

Figure 4.29: Cross-section D-D'.

By positioning the sections from west to east in a 3D view, it is clear that there are heterogeneities between the different cross-sections (Figure 4.30). This 3D figure displays a better view of how syn-rift sediments change from section to section and also the variation in the number of faults.

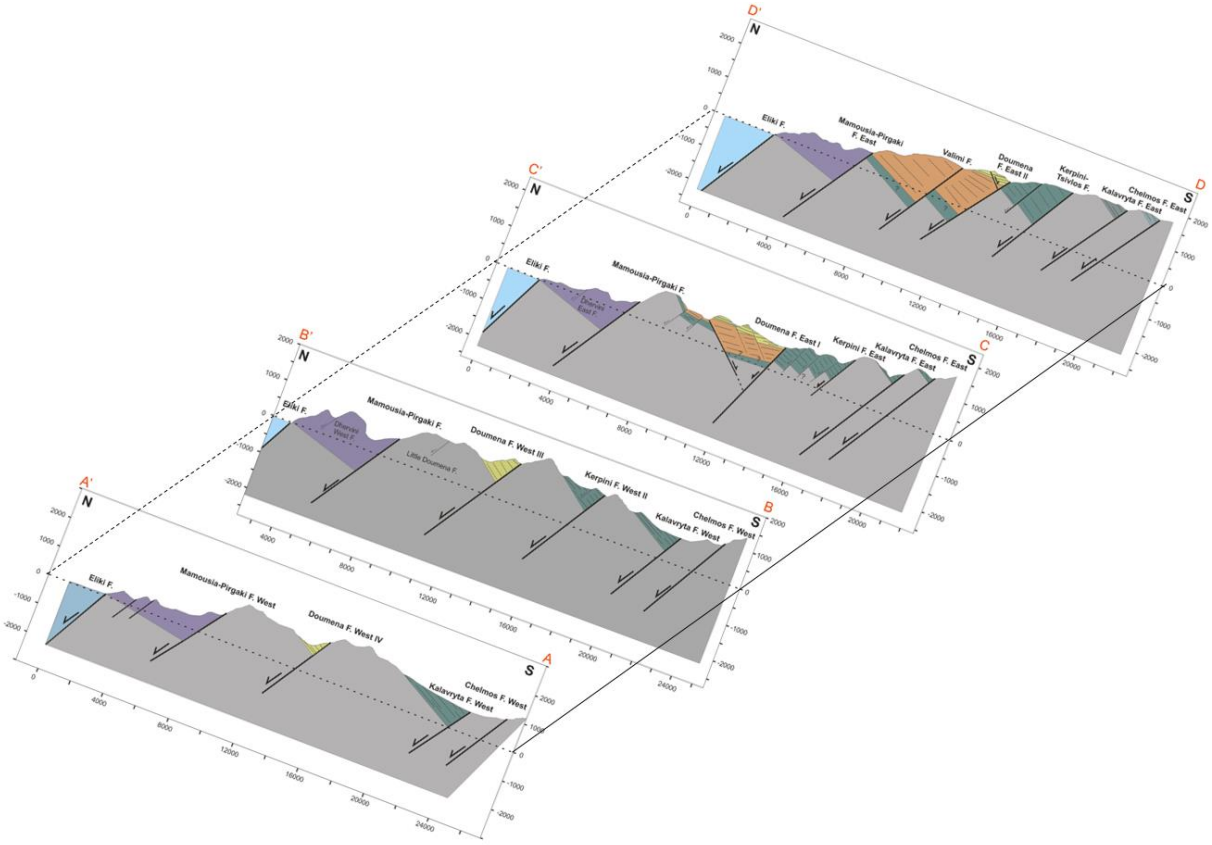

Figure 4.30: 3D view of the four N-S sections, from west (section A-A') to east (section D-D'). The figure show the heterogeneities between the different cross-sections.

Chapter 5 – Displacement Analysis

5.1 INTRODUCTION

A displacement analysis was performed conducting case studies on different parts of the study area in order to quantify the displacements on the major faults and identify any variations along them (Figure 5.1). Displacements have been analysed by constructing basement-syn-rift unconformity surfaces. These surfaces has been constructed both in the subsurface and re-constructed where they have been eroded. In most cases the displacement relies on this construction process. A significant assumption in this process is that the unconformity surface is approximately planar and suffered minimum erosion prior to the extensional faulting. The unconformity surfaces also rely on dip-strike measurements and estimates. The variation associated with these measurements are also assessed to determine their impact on the uncertainty in displacement estimates (Chapter 5.4).

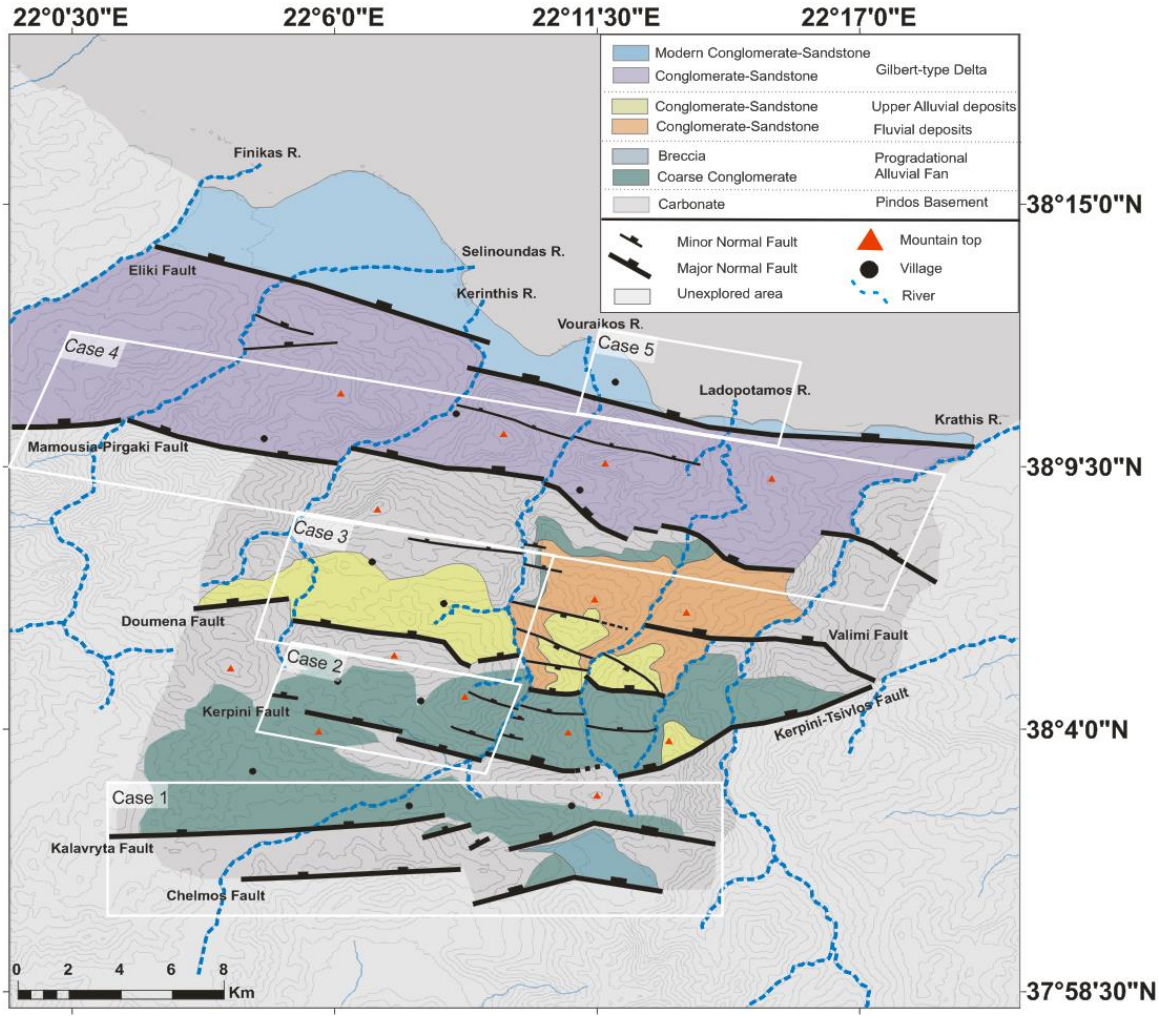

Figure 5.1: Structural map showing the location of the case studies highlighted by white squares.

Case 1. The Kalavryta Fault

The Kalavryta Fault is located in the southern part of the study area and consist of Pindos carbonate basement deposits and progradational alluvial fan conglomerates (Figure 5.2). The Kalavryta Fault is divided into the four fault segments that is the Kalavryta F. East, Kalavryta F. Step 1, Kalavryta F. Step 2 and Kalavryta F. West. The Kalavryta F. East and West have an average strike of N85°E, while the Kalavryta F. Step 1 and Step 2 strike in the N70°E direction. All fault segments are assumed to have

an average dip of 45° north. The strike and dip angles are based on the measurements done by Finnesand (2013). The syn-rift conglomerates, which act as an unconformity marker, start in the valley north of the Kalavryta Fault, passing through the village of Vrachni, moving eastwards towards Kalavryta F. Step 1. The unconformity surface is poorly exposed west of the village of Vrachni, making it challenging to follow and trace. When facing these issues, the solution is to extrapolate the contact between two known points. Taking these challenges into consideration the displacement estimation was determined by projecting the unconformity planes on both sides of the fault to establish the total slip of the fault. The Chelmos Fault Block is located south of the Kalavryta Fault. The syn-rift deposits identified on the Chelmos Fault Block are mainly breccia and coarse conglomerates.

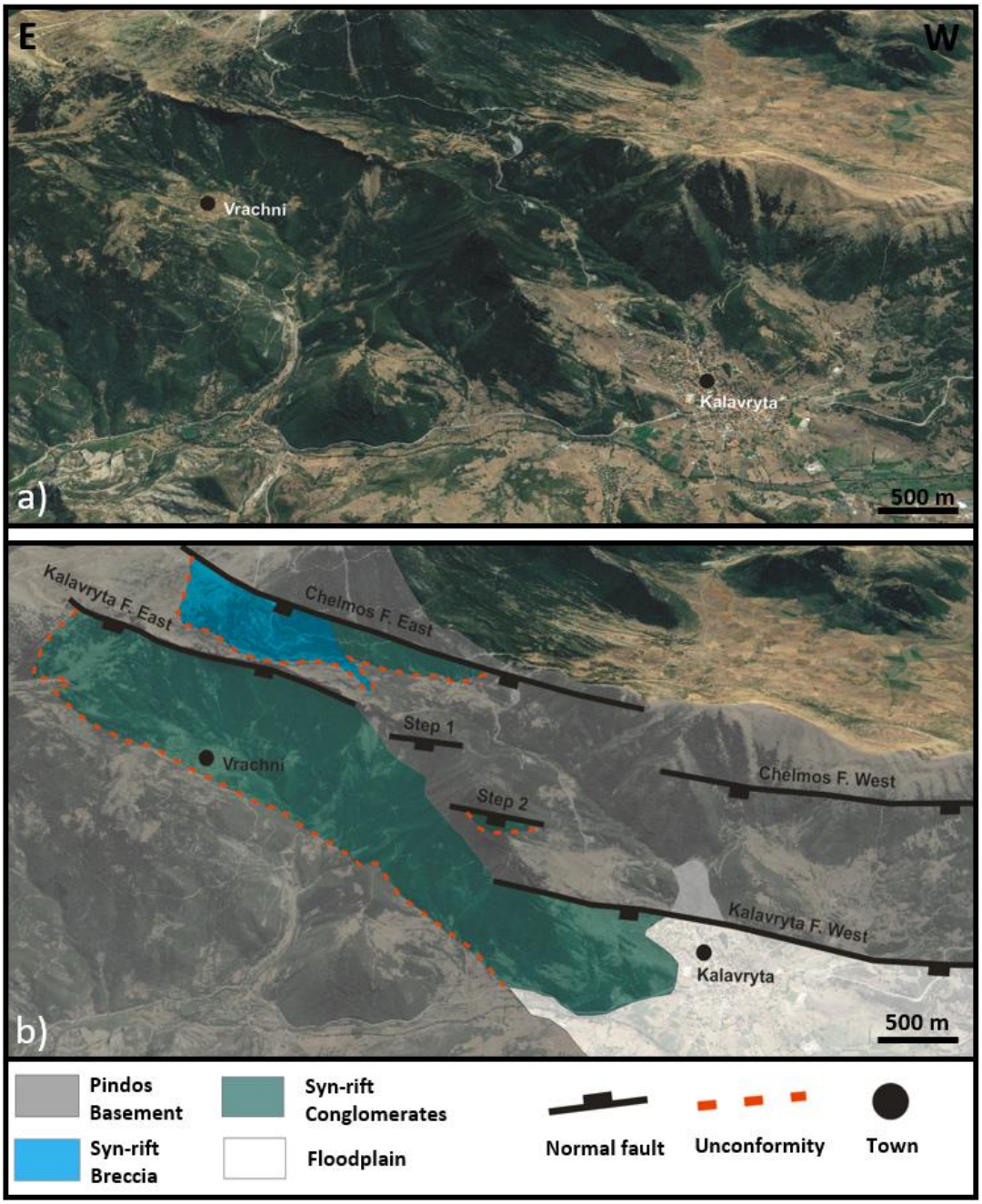

Figure 5.2: a) Original satellite image from Google Earth of the Kalavryta and Chelmos Faults, and b) Structural interpretation with lithological units and contacts.

The displacement analysis of the Kalavryta Fault resulted in a range from 460-825 m, representing the minimum and maximum displacements (Figure 5.3). All the fault segments show increased displacement towards the central part of the fault system. The Kalavryta F. East increases displacement from 620 m in the east to a maximum of

820 m. The eastern limit of this fault is not clear, and it may continue eastwards out of the study area. Both Kalavryta F. Step 1 and Step 2 show similar geometries with increased displacement eastwards. Kalavryta Fault West exhibits a slight displacement gradient, gently decreasing westward, to the western termination of the system shown in the plot. Abrupt changes in displacement is a characteristic feature and illustrate the fault discontinuities or steps. In this analysis, there is no evidence that the fault displacement gradually decrease to zero displacement, allowing the possibility that the fault steps onto another segment outside the study area.

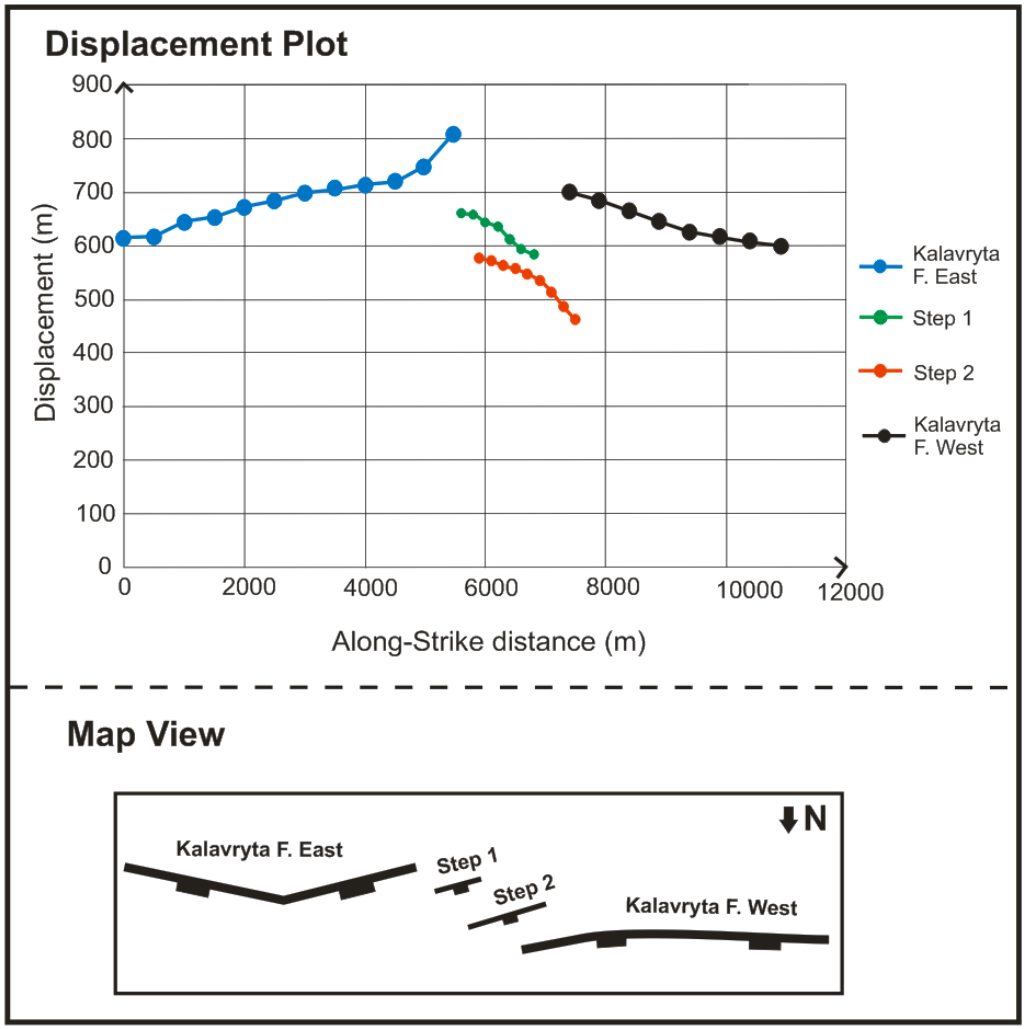

Figure 5.3: Displacement plot of the Kalavryta Fault segments and their relative positions in map view.

Case 2. The Kerpini Fault West

The Kerpini Fault West is located in the south-western part of the study area, north of the Kalavryta Fault Block. The Eastern Kerpini Fault is located east of the Vouraikos Valley. The fault is separated by a 750 m left step in the Vouraikos Valley. The Western Kerpini Fault can be divided into three fault segments, the Kerpini Fault West I, II and III, east to west. The three segments have slightly different strikes: segment I strikes N107°E, segment II strikes N100°E and segment III strikes N110°E. The faults dip approximately 45° north and stretch about 6 km east-west (Figure 5.4). The syn-rift deposits consist of coarse conglomerates that dip 25° south, and traced north of the village of Kerpini and to the south of the village of Roghi (Hadland, 2016). Two additional faults are identified in Roghi Mountain, west of the village of Roghi, named Intra Roghi F. 1 and Intra Roghi F. 2. To the west of the Mountain of Roghi, close to the village of Roghi, a N-S fault has been identified, called the Roghi Fault (Hadland, 2016). The analysis of the Kerpini Fault West investigates the fault displacement on the three fault segments to document possible variations along the strike of the individual faults.

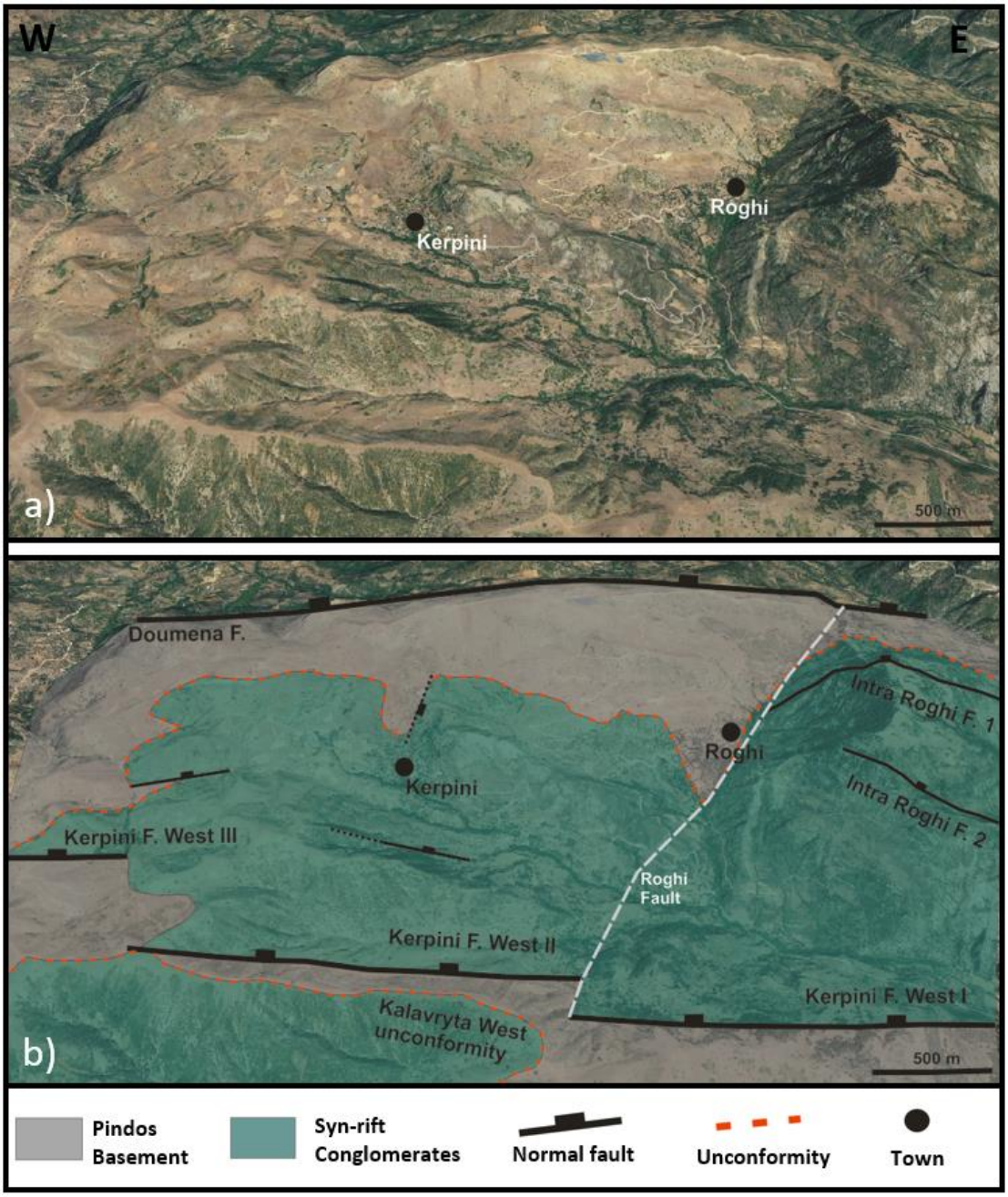

Figure 5.4: a) Satellite image from Google Earth of the Kerpini West Fault and b) Structural interpretation with lithological units and contacts.

The results of the displacement analysis shows a general decrease in displacement from east to west (Figure 5.5). The Kerpini F. West I has a displacement maximum of ~1775 m. The Kerpini F. West II and III have maximum displacement of 1277 m and 570 m respectively, with both segments displaying a slight westward

decreasing displacement gradient. The western end of the Kerpini F. III represents the end of the fault, with a very sharp drop in displacement by 480 m. The abrupt changes in displacement between the fault segments, observed in the Kalavryta Fault Block, is also observed in this area, here with a sharp decrease of 320 m between the Kerpini F. I and II, which step aligns with the Roghi Fault, and 540 m between Kerpini F. West II and III.

The Intra Roghi Fault 2, located in the Roghi Mountain, has an estimated displacement of 750 m, decreasing eastwards to 450 m (Sigmundstad, 2016). Also, Intra Roghi Fault 1 have an estimated displacement of ca 50 m. If Intra Roghi Fault 2 was to be included in the displacement analysis, the total displacement of the Kerpini F. West I would be significantly larger. Additionally, there have not been identified corresponding faults west of the Roghi Fault in the other Kerpini Fault segments.

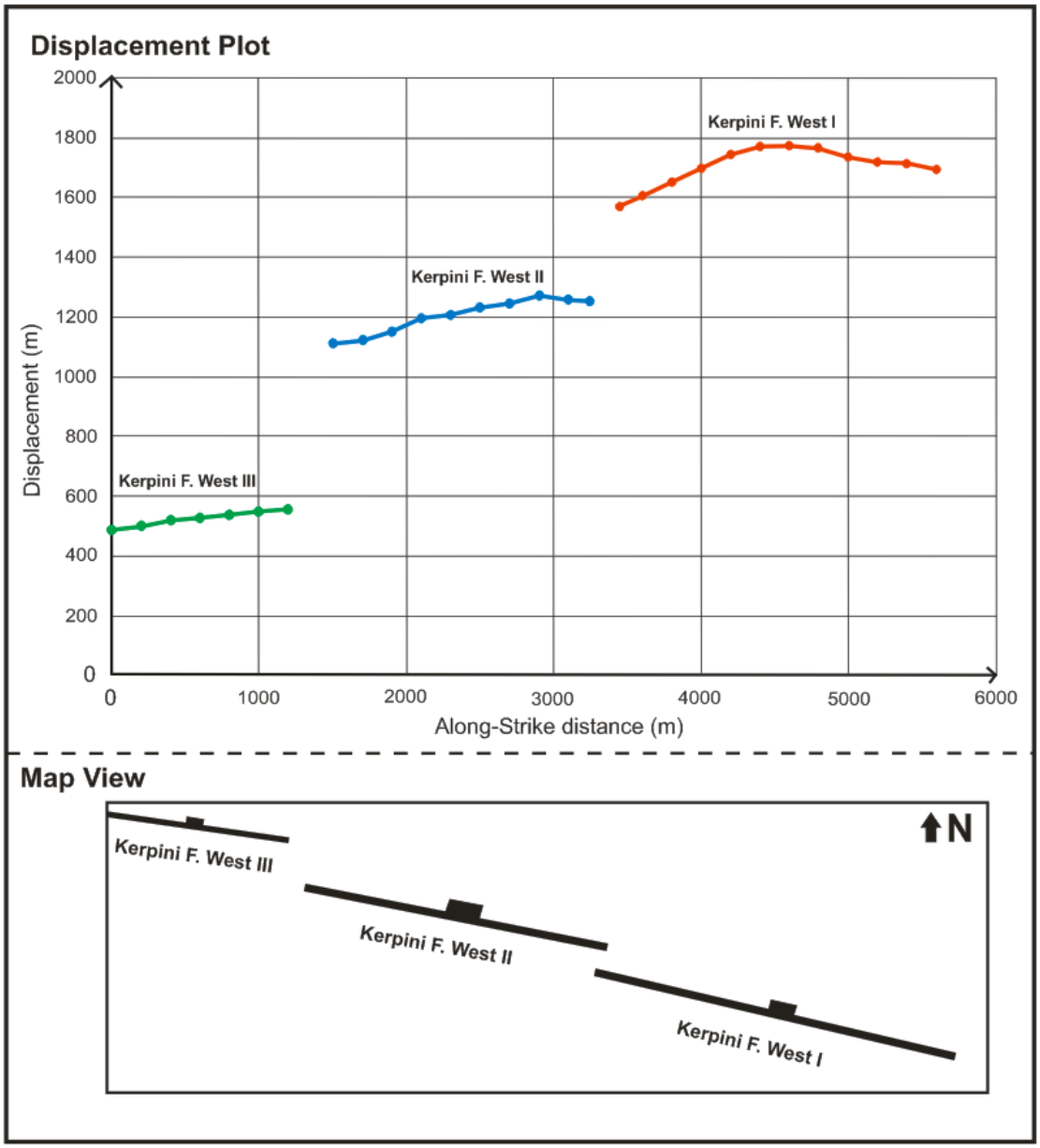

Figure 5.5: Displacement plot of the Kerpini West Fault segments and their relative positions in map view.

A comparison between the displacement of the western and eastern Kerpini Fault was performed to investigate the presence of a major N-S fault in the Vouraikos Valley (Figure 5.6). In the Vouraikos Valley, previous work proposed a major N-S transfer fault that can explain this step. The analysis showed that the Kerpini F. East has a displacement maximum of 1275 m which rapidly decrease eastwards. There is a

sharp decrease in displacement by 430 m between the two segments. The eastern termination of the Kerpini F. East is most likely connected to the Kerpini-Tsivlos Fault in the East, which may also be another step in this large Kerpini Fault. Considering the whole Kerpini Fault, it seems that there is a global displacement maximum in Kerpini F. West I and that the displacement decreases both eastwards and westwards, but with significant changes occurring were the fault steps, most likely explained by the N-S trending transfer faults identified by Hadland (2016).

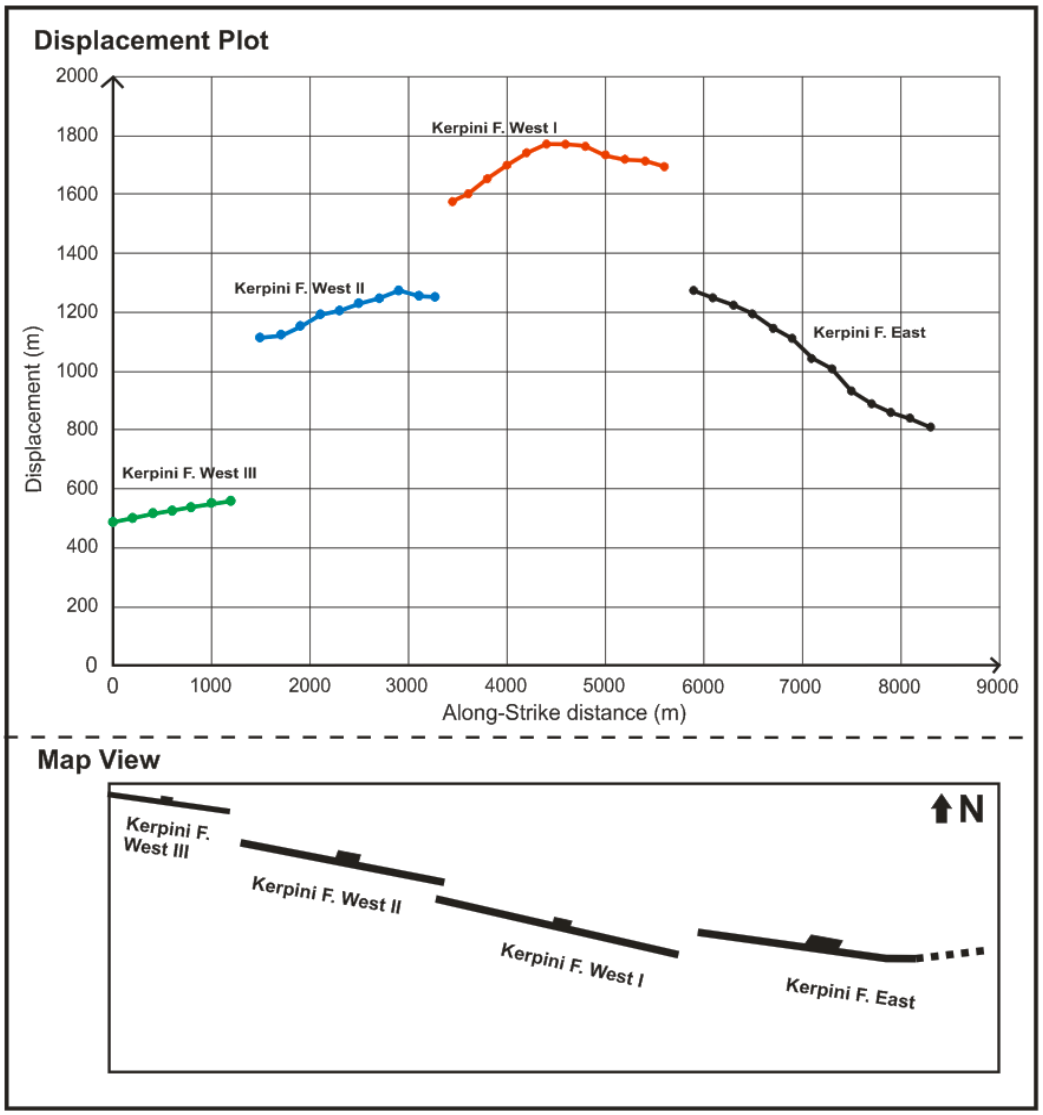

Figure 5.6: Displacement plot of the three Kerpini West Fault segments compared to Kerpini F. West. The faults relative positions are presented in map view.

Case 3. The Doumena Fault West

The Western Doumena Fault is located approximately two km north of the Kerpini Fault and consist of three fault segments (Figure 5.7). The segments is divided into the Doumena Fault West (DWF) I, II and III, respectively, and they stretch a total of five km east-west. Segment I strikes N92°E, segment II strikes N105°E, segment III strikes N100°E, and all the segments dip 45°N after Veiteberg (2017). The syn-rift sediments are primarily fluvial conglomerates with an average dip angle of 25° south. The unconformity surface was traced along the contact between syn-rift sediments and basement, close to the villages of Vilivina and Doumena (Veiteberg, 2017). North-east of the unconformity marker, a relatively minor fault, Little Doumena Fault, is identified by a small topographic high, but sits within the basement with no syn-rift infill present. This fault is described in more detail in chapter 5.2.2.

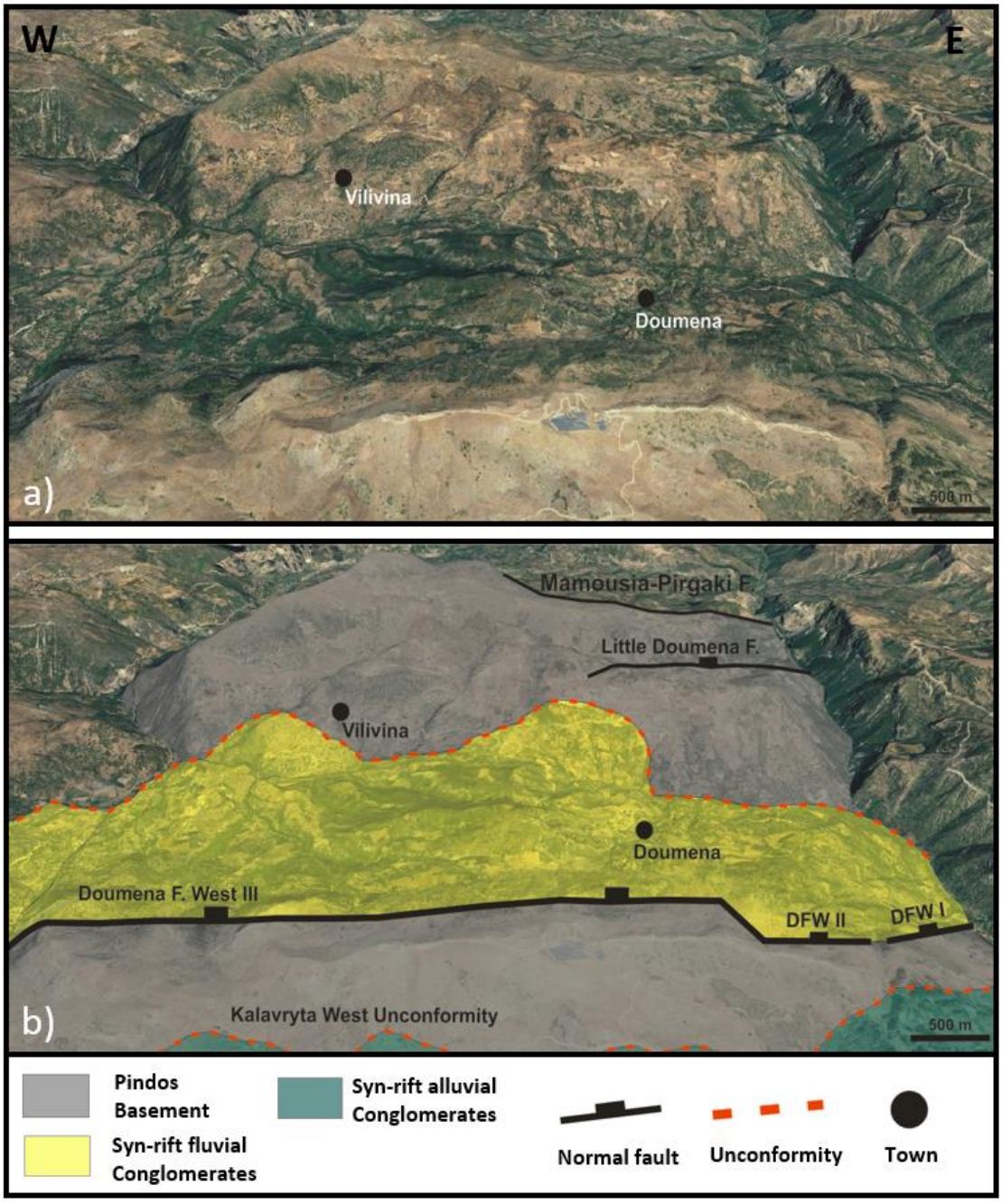

Figure 5.7: a) Satellite image from Google Earth of the Doumena Fault Block and b) Structural interpretation with lithological units and contacts.

The estimated displacement on the different fault segments shows a general increase from east to west (Figure 5.8). The DFW III exhibits a displacement maximum of 1625 m, but all of the fault segments each have a local displacement maximum, DFW II with 1460 m and DFW I with 1250 m. Furthermore, the Doumena Fault West

represent the third example of abrupt fault displacement changes, evident from the sharp transition between the DFW II and DFW I, dropping 150 m in displacement. Also, there are sudden abrupt fault terminations at the western and eastern ends, where the DFW I step in the Vouraikos Valley and DFW III step in the continuation of the Kerinthis Valley to the eastern segment of the Doumena Fault to DFW IV. Figure 5.9 shows the step west of Doumena F. West III, where the fault continues into another segment; the Doumena Fault West IV. Here the fault steps 850 m north (Veiteberg, 2017).

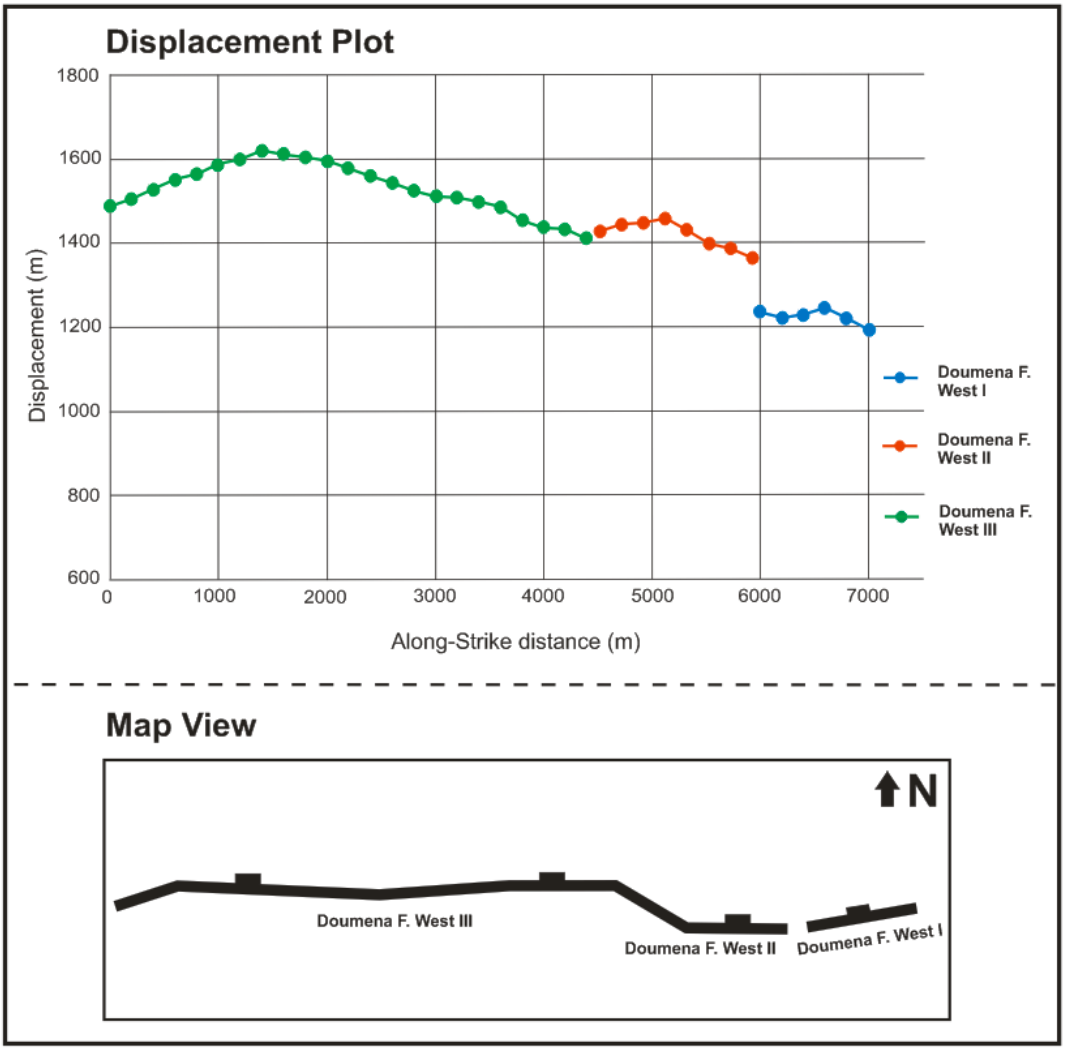

Figure 5.8: Displacement plot of the Doumena West Fault segments and their relative positon in map view.

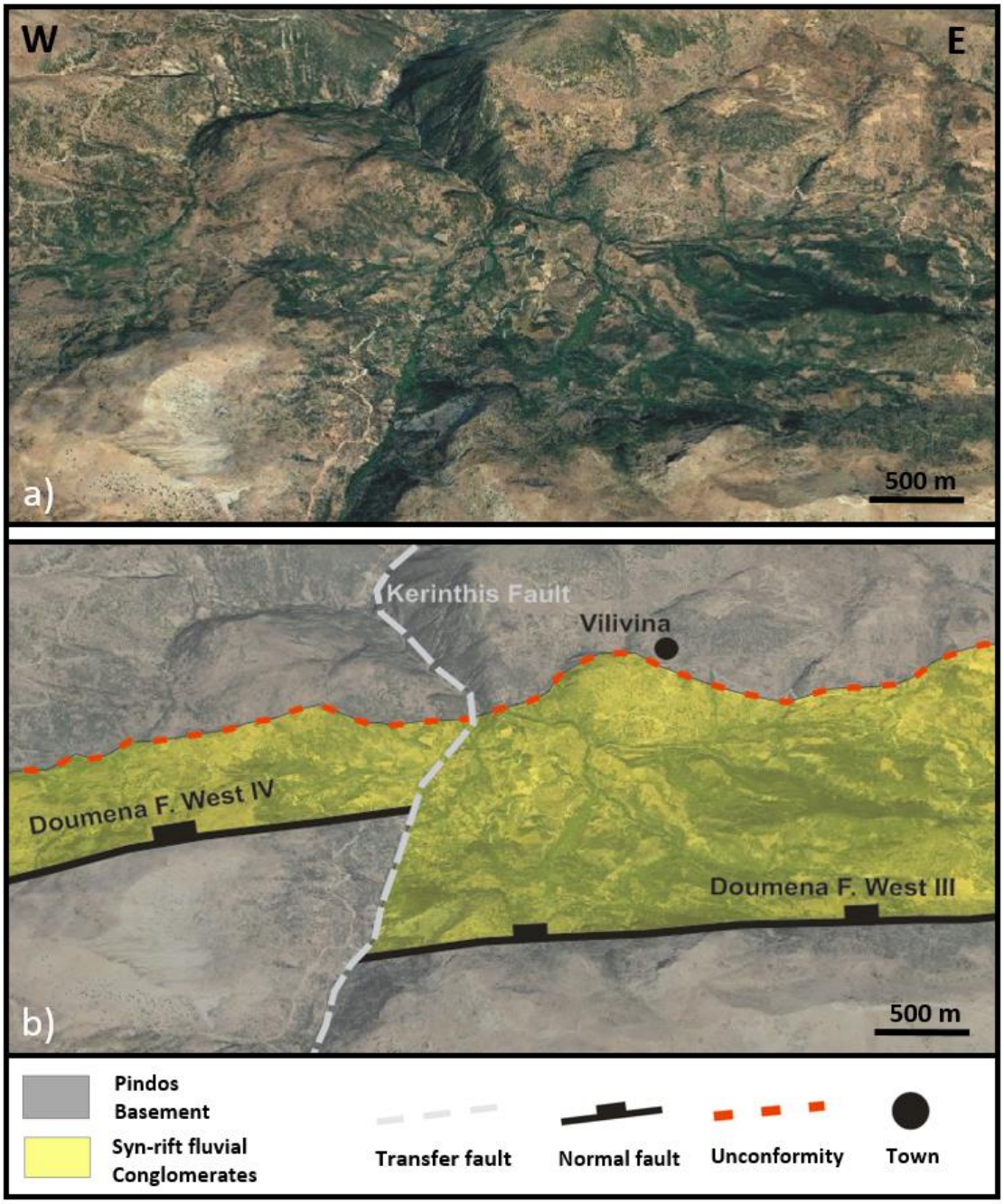

Figure 5.9: a) Satellite image from Google Earth of the western Doumena Fault Block and b) structural interpretation of the fault step between Doumena F. West III and Doumena F. West IV and a proposed N-S Kerinthis Faults.

Case 4. The Mamousia-Pirgaki Fault - Ancient Delta

The Mamousia-Pirgaki Fault (M-P Fault) is located approximately 5.5 km north of the Doumena Fault, stretching all the way through the study area in the east-west direction. The Mamousia-Pirgaki Fault Block has previously hosted accommodation for Gilbert-type deltas to form. Later these have been uplifted due to the Eliki Fault and today feature as ancient deltas, consisting of conglomerate-sandstone facies, characteristic by their sub-horizontal top-sets. The top-sets are important markers representing the paleo sea-level. The depth of the basement beneath these ancient Gilbert-type deltas is generally unclear and not well documented in previous work. An approach has been adopted here to estimate the depth of these deltas using the geometries of the topography in the nearby area; the Vouraikos Delta used as an example (Figure 5.10). The height of the ancient delta is 820 m and the height of the intersection between the Mamousia-Pirgaki Fault and the footwall unconformity is at 2120 m. The results in 1300 m of footwall uplift. Assuming the hanging wall downthrown is equal to the uplift and subtracting 1300 m downwards from the top of the delta, the unconformity should have an approximate depth of 480 m below sea level (bsl). The fifty-fifty assumption can be tested to get a range of likely displacements. For example using a minimum of 0 m, a medium of -250 m bsl and a maximum of -500 m bsl.

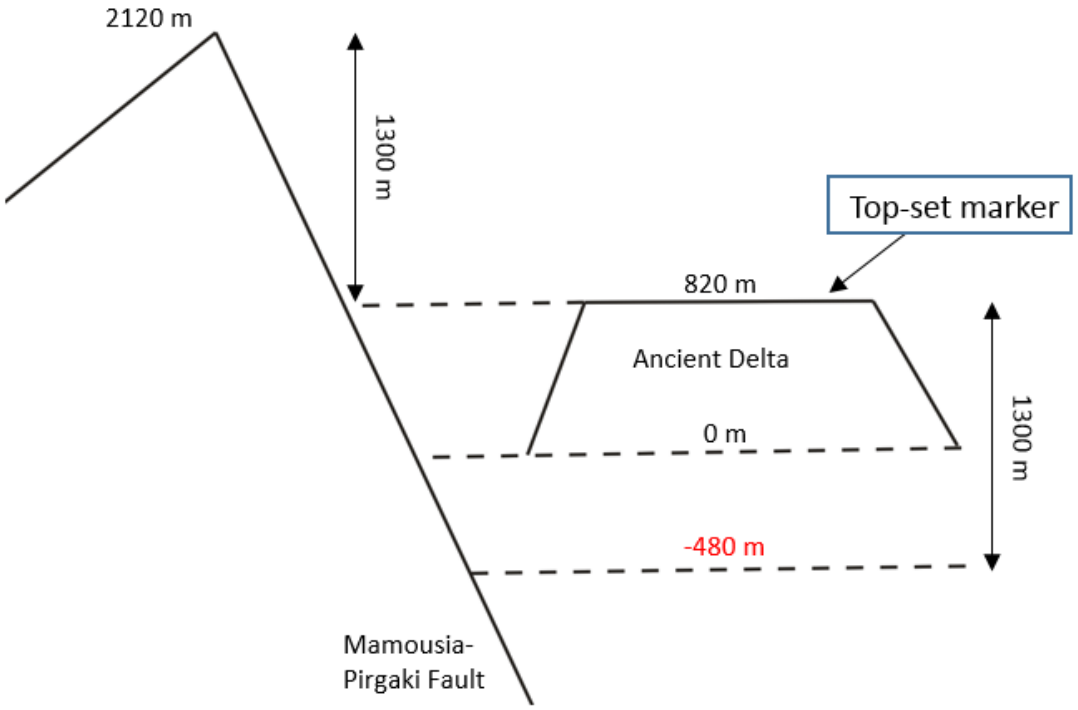

Figure 5.10: Conceptual sketch showing the approach of estimating the depth of the Mamousia-Pirgaki unconformity. Here using the top-sets of the ancient delta as a paleo-marker. Depth estimated to 480 m below sea level highlighted by the red-coloured text.

The Mamousia-Pirgaki Fault features discontinuance and is seen to abruptly step in several areas, generally in the river valleys (Figure 5.11). The Mamousia-Pirgaki Fault has therefore been divided into seven fault segments from east to west; M-P F. I, II, III, IV, V, VI and VII, were the average fault dip is 45°N (Ford et al., 2013). The segments I and II strike N120°E, segment III strikes N110°E, segment IV strike N125°E, segments V and VI strikes N100°E and segment VII strikes N92E. Figure 5.10 shows a correlation between the identified fault trace of the segments in Google Earth and the modelled fault planes in the Petrel model.

Figure 5.11: a) Satelite image from Google Earth 2017 showing the trace of the seven Mamousia-Pirgaki Fault segments, and b) Modelled fault planes of the Mamousia-Pirgaki Fault segments in Petrel.

The observations from the fault displacement analysis of the Mamousia-Pirgaki Fault are summarised in the following points (Figure 5.12):

- The fault segments show a general increase in displacement from the eastern and western flanks, towards the central to western part of the area.
- There is a displacement maxima at the Mamousia-Pirgaki Fault VI of 3600 m, close to the village of Pirgaki.
- There is displacement gradient on individual segments, mostly decreasing from west to east, except for the Mamousia-Pirgaki Fault VII that decrease westwards.
- The Mamousia-Pirgaki Fault V shows less grading, but some minor variations.
- The displacement of the Mamousia-Pirgaki Fault VII decrease dramatically westwards into an area of low topography. This may

suggest that the Mamousia-Pirgaki Fault may head to zero displacement west of this fault segment, but field observations suggest a rapid termination.

- The easternmost fault segment of the Mamousia-Pirgaki Fault probably represents the end of this major fault, which is a very sharp termination in terms of displacement.
- There are clear steps between many of the fault segments, generally in the river valleys, as seen in the other cases. This may be due to N-S trending faults as seen before.

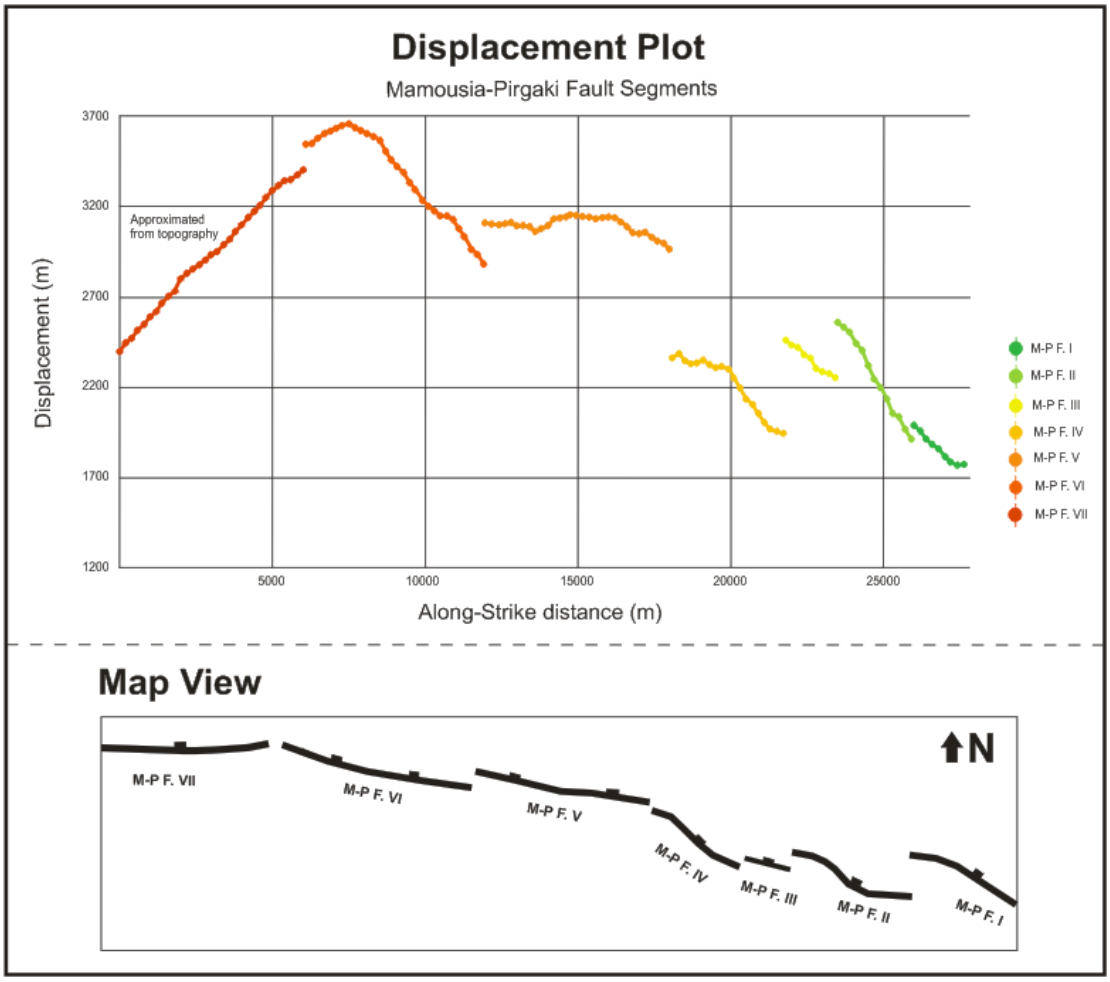

Figure 5.12: Displacement plot of the seven Mamousia-Pirgaki Fault segments and their relative positions in map view.

Case 5. The Eliki Fault - Modern Delta

The Eliki Fault is located in the northernmost part of the study area, stretching 30 km along the shoreline. The fault is divided into the East and West Eliki Faults, separated at the Kerinthis Valley where there is a right hand step of 2000 m. The fault dips 50° north. It separates the onshore mountains to the south, from the modern deltas that are controlled by the fault, and are currently building out into the Gulf of Corinth. The fault is currently active with many recent earthquakes and controls the sedimentary deposition (Leeder et al., 2008; Bell et al., 2009).

The depth of the modern deltas was approximated using a bathymetric map (McNeill and Collier, 2004) covering southern parts the Gulf of Corinth (Figure 5.13). Because the bathymetry map is of large-scale character, the depths of the modern deltas are approximated, along with the distance out to the offshore fault marked on the map. In this case the distance to the offshore fault is approximated to be 2000 m northwards. This fault is recognized by Bell et al., 2008, but not all papers include this interpretation. Taking these challenges into consideration the case study was performed testing different dip angles of the unconformity at the base of the modern deltas, ranging from 0-25° south (Figures 5.14), based on dip estimates from Ford et al. (2007). By applying the minimum, medium and maximum dip angles, the displacement calculations gave a range of probable displacement estimates for the Eliki Fault.

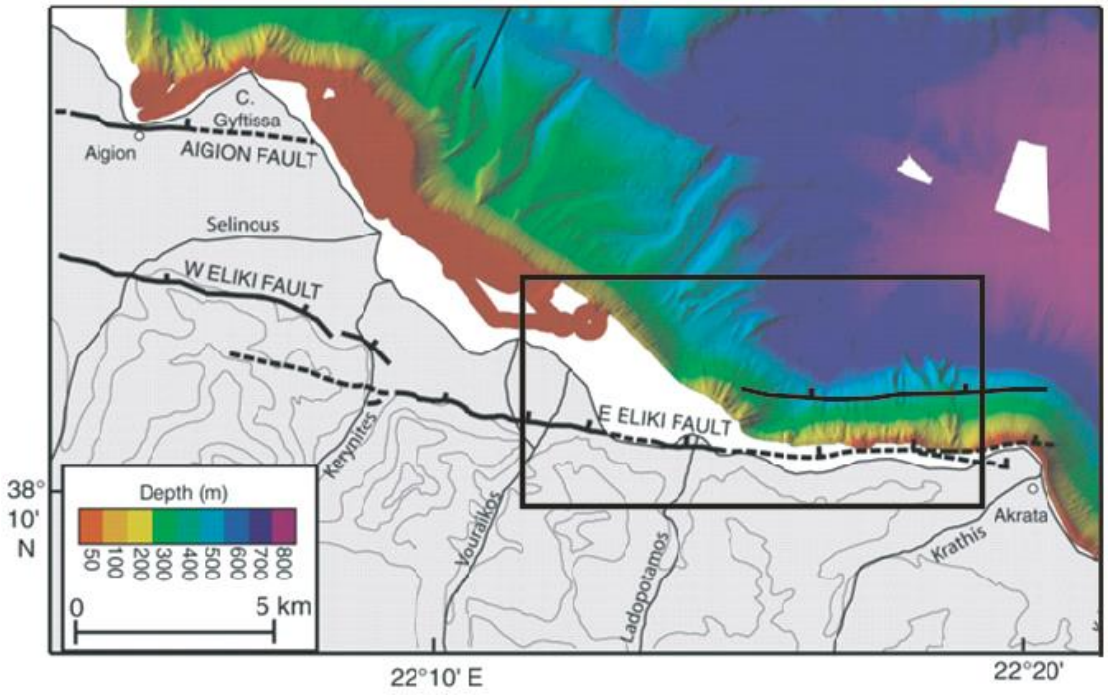

Figure 5.13: Bathymetry map covering the southern parts of the Gulf of Corinth. Case study location, showing parts of the Eliki Fault Block, is highlighted by the black square. Modified from McNeill and Collier, 2004.

The top of the mountain south of the Eliki Fault, the delta top-sets, is 700 m above sea level and clearly indicate the amount of uplift in the footwall. The depth down to the offshore hanging wall block is less certain. The bathymetry map indicates it is about 600 m below sea level. This corresponds well to the footwall uplift, assuming that there is a fifty-fifty slip on the Eliki Fault. The displacement estimates range 500 m, from a minimum of 2022 m using an unconformity dip of 0°, to a maximum of 2529 m, using a dip of 25° (Figure 5.14).

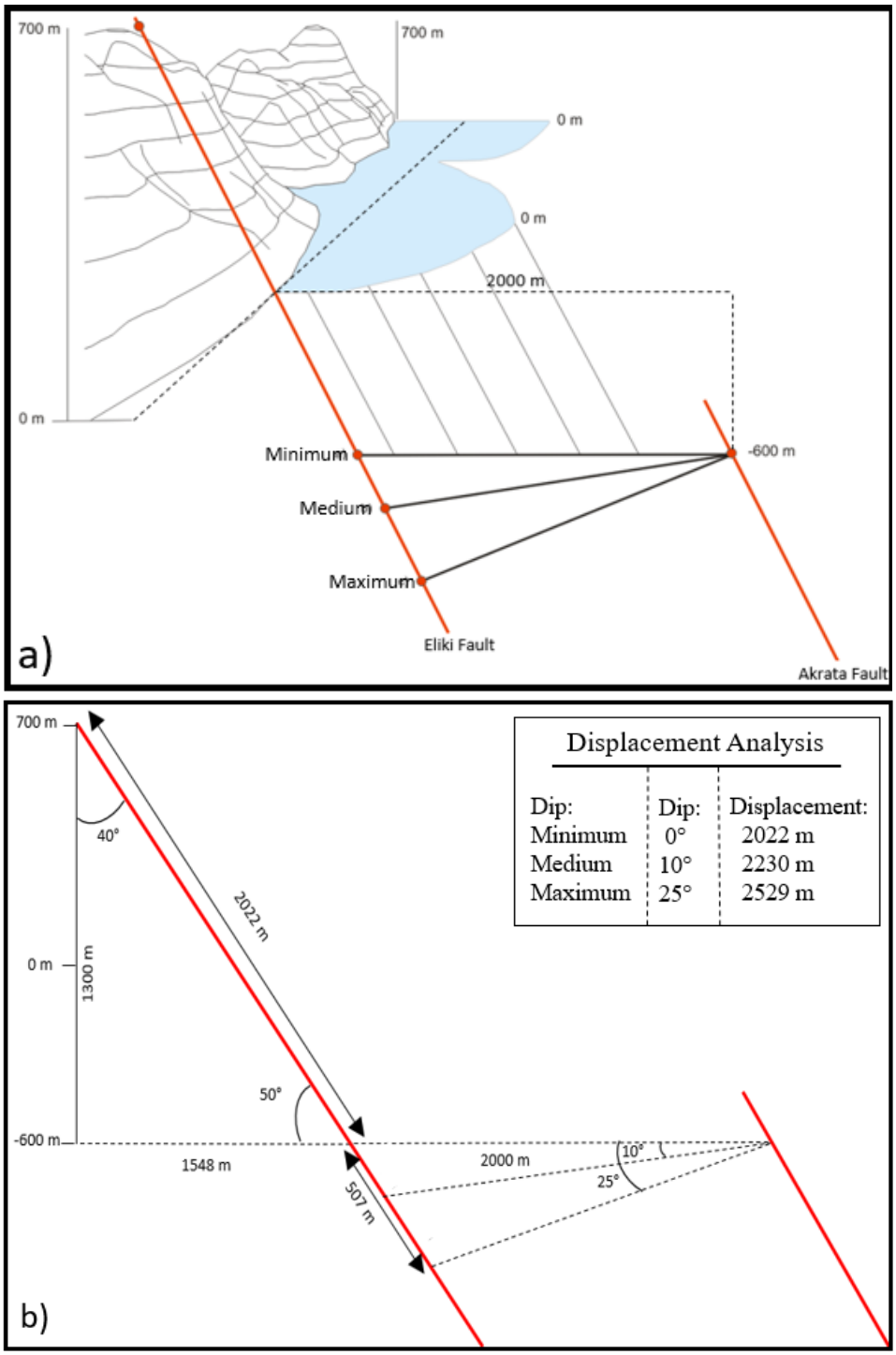

Figure 5.14: a) Conceptual cross section showing the minimum, maximum and medium displacement cases and b) Calculated displacement for the different minimum, medium and maximum dip angles.

5.2 Additional Geometrical Analysis

This sub-chapter show a selection of additional fault plane analyses, or geometrical exercises, which were performed to test different hypotheses on structural features in the study area.

5.2.1 Fault Plane Analysis

A geometrical exercise was conducted on the Mamousia-Pirgaki Fault VI segment to validate the dip angle that has previously been documented to range between 45-50° (Ford et al., 2013). A topographic feature can be observed which appears to mimic the fault plane. It is clearly planar and can be seen on both sides of the Vouraikos Valley. A triangle of points was created in Google Earth 2017 on what is believed to be the fault plane (Figure 5.15). The points were transformed to a plane surface where the dip angle was calculated at 27.3°.

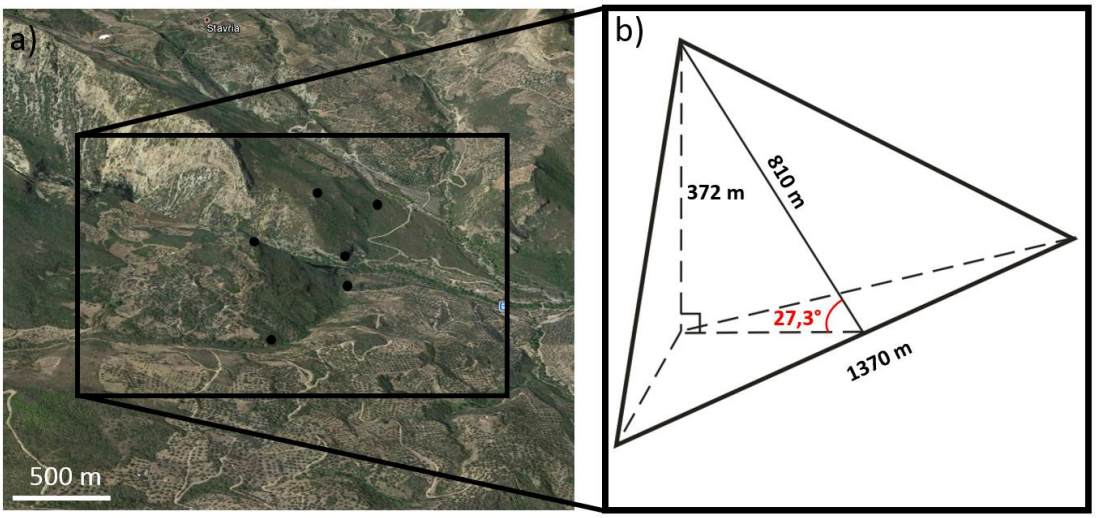

Figure 5.15: a) Google Earth image of a possible fault plane belonging to the Mamousia-Pirgaki Fault and b) Calculated fault dip on the exposed plane, marked in red-coloured text.

A similar study was implemented to the Kerpini West Fault II, investigating an exposed plane that may resemble the fault plane. A square of points was created in

Google Earth on the surface (Figure 5.16), and transformed to a plane surface where the dip angle was estimated to 24.5°.

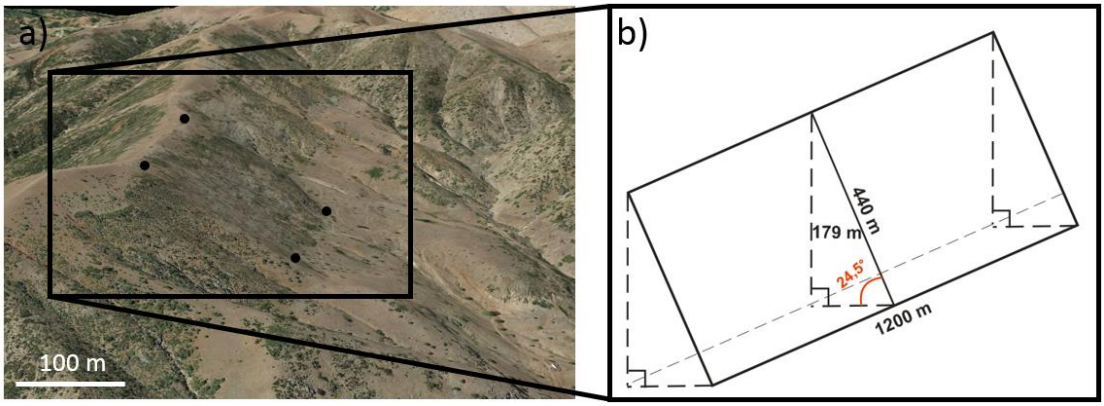

Figure 5.16: a) Google Earth image of a possible fault plane belonging to the Kerpini Fault West I and b) Calculated fault dip on the exposed plane marked in red.

These geometrical exercises did not give the expected result of a fault dip close to 45-50°. This suggests that there has been some erosion related to these surfaces (Figure 5.17). These features in the field might not be actual fault planes even though they may resemble one. Nevertheless, this has shown to be a valuable method to investigate amounts of erosion the faults may be exposed to.

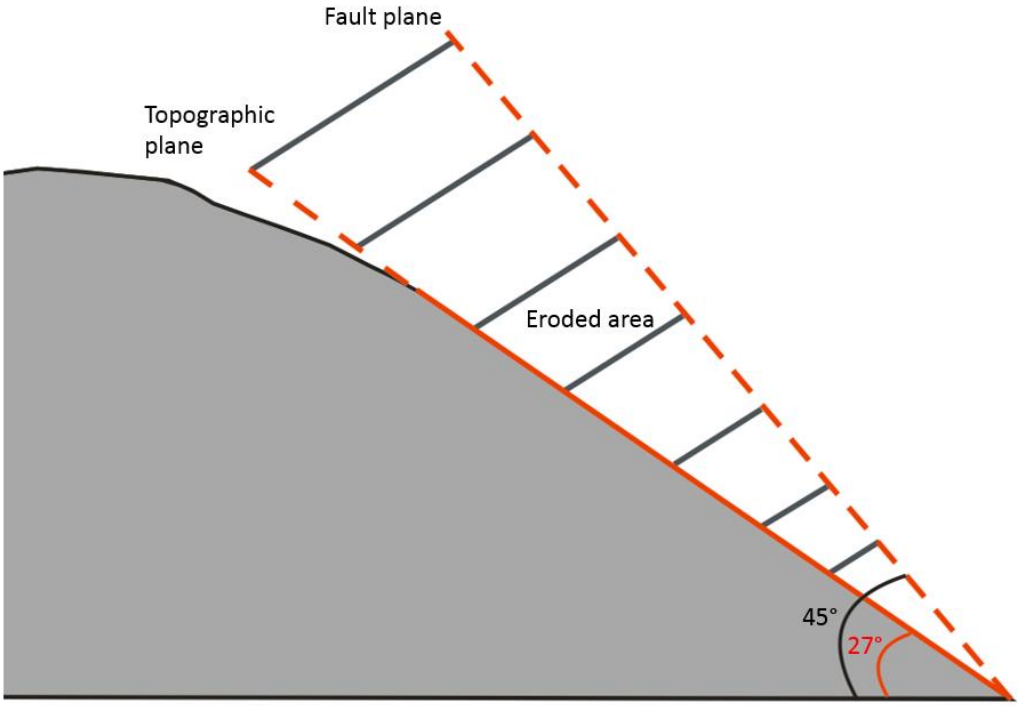

Figure 5.17: Conceptual model showing the possible amount of erosion between the topographic plane and the fault plane.

5.2.2 Little Doumena Fault

A geometrical exercise was used to further investigate the total displacement of the Mamousia-Pirgaki Fault V segment and the Little Doumena Fault. The Little Doumena Fault is located in the Doumena Fault Block, it lies 2 km south of the Mamousia-Pirgaki Fault, separated by the Mountain of Rouskio, and stretches 3 km in the east-west direction (Figure 5.18). The fault has a mean strike of N110°W and a dip angle of 55° north (Veiteberg, 2017). The displacement of the Little Doumena Fault is based on the approximation of topography, because no syn-rift sediments are present, only basement. The maximum displacement is estimated to 400 m (Veiteberg, 2017), close to the Vouraikos Valley and decreases gradually westwards.

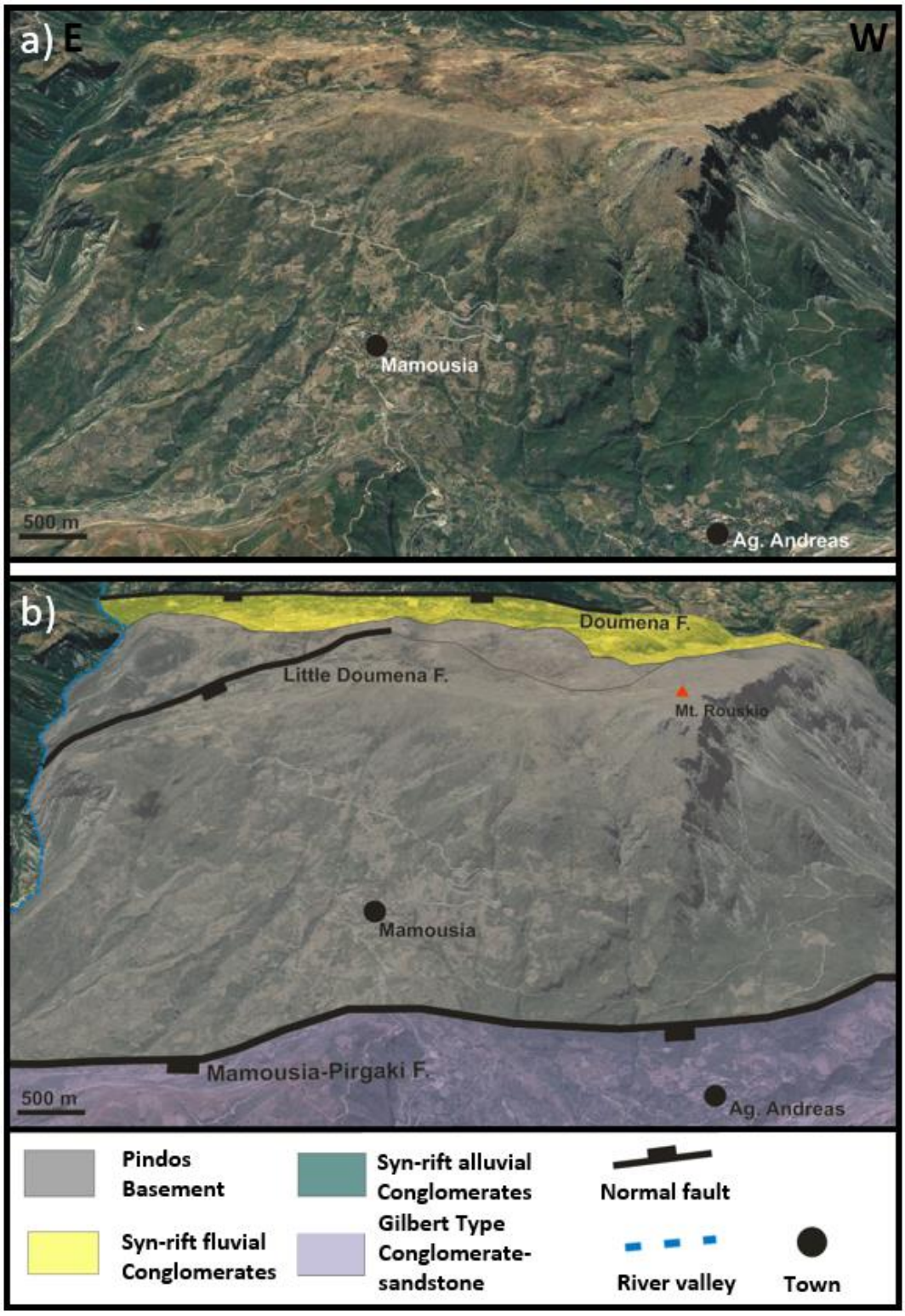

Figure 5.18: a) Satellite image from Google Earth of the Mamousia-Pirgaki Fault and the Doumena Fault Block and b) Structural interpretation with lithological units and contacts.

The displacement of the Mamousia-Pirgaki Fault V ranges from 2950 to 3200 m. It is increasing westward to a maximum of 3200 m, then decreasing down to 3050 m (Figure 5.19). The displacement of the Little Doumena Fault has a maximum of 400 m from the Vouraikos Valley, decreasing westwards. A displacement curve, created to form the sum of the two fault displacements, has been generated and shows a curve with a very low displacement gradient. The plot indicates that the Mamousia-Pirgaki Fault V might be passing displacement on to the Little Doumena Fault at the horizontal distance of 3500 m, which might explain why the total displacement curve show a sub-horizontal nature.

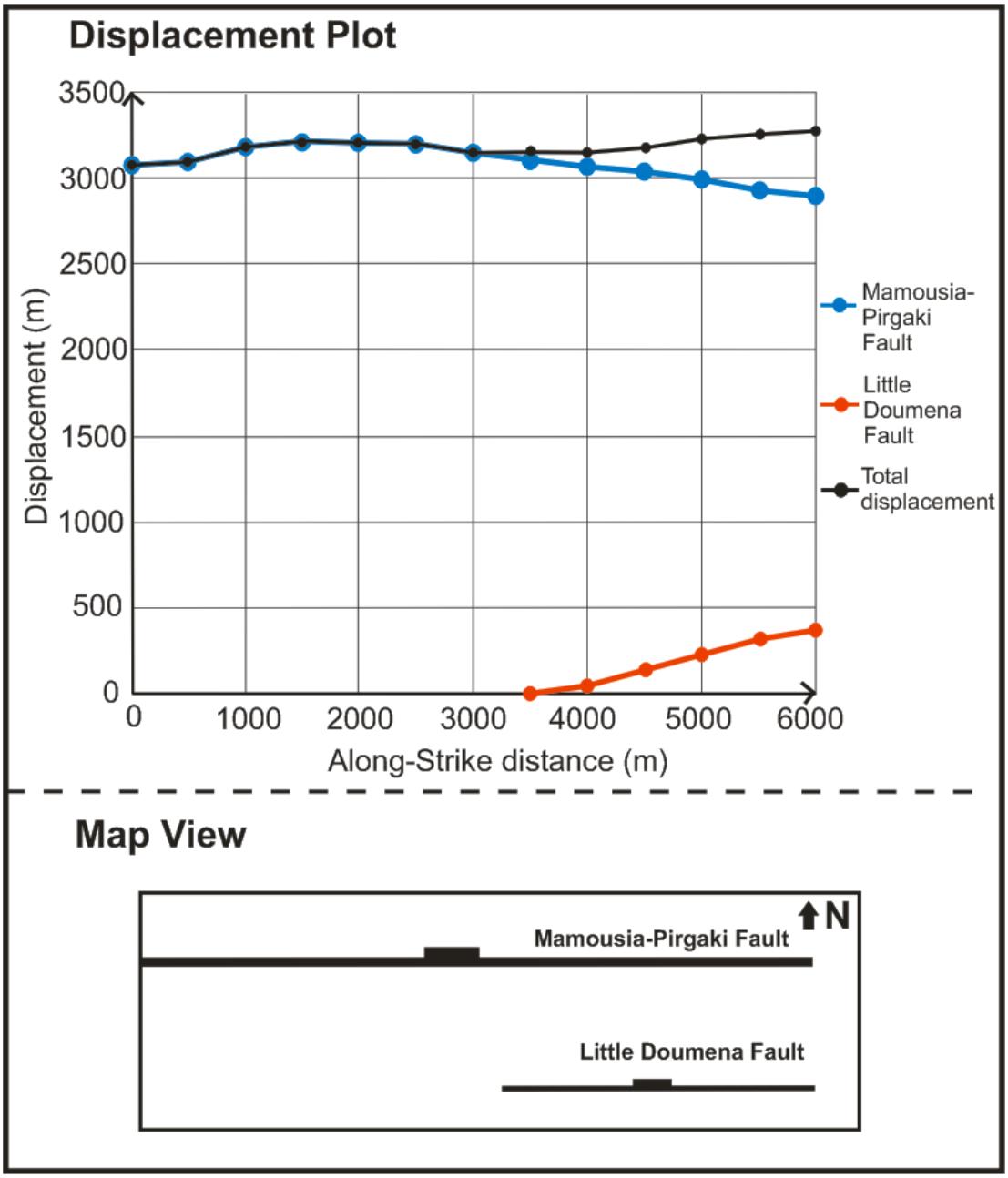

Figure 5.19: Displacement plot of the Doumena Fault West and the Little Doumena Fault, and their relative positions in map view. The black curve represents the total displacement of the two faults.

5.3 CUMULATIVE DISPLACEMENT

This sub-chapter will investigate and compare the cumulative displacements of the structural N-S cross-sections introduced in Chapter 4.4. Also, look into the uncertainty error-range related to the estimated displacements.

The cumulative displacement, which is the total displacement for the faults, were estimated for the four N-S cross-sections (Figure 5.20). The heterogeneity between the cross-sections may lead to questions about the variability in the total extension across the Gulf of Corinth. For example, could there be a consistent change in extension from east to west, or will it be difficult to assume similar extension due to the heterogeneities between the sections? The cumulative displacements range between 9300 and 10700 m (Figure 5.20), which is approximately 13 %. Despite the major structural heterogeneity between the cross sections, and that the number of faults varies, the total displacements are quite similar between the sections, even in an area with a horizontal distance up to 25 km.

The profiles show that the number of faults vary between the sections. When comparing profile A-A' which exhibits the fewest number of faults, to profile C-C' which contains the highest, the displacement difference lie around 5%, which is well within an acceptable range. In profile A-A', the Mamousia-Pirgaki and the Kalavryta Faults have the largest displacement so that the profile is not that far off from the other.

An important observation, seen in all of the profiles, is that there is a general increasing displacement moving from the Chelmos Fault in the south (~900 m) to the Mamousia-Pirgaki Fault in the north (~3500 m) throughout the profiles. This might suggest that the rifting was more extensive in the later stages when the Mamousia-

Pirgaki and Eliki Faults were forming, in comparison to the activity of rifting when the first faults were forming.

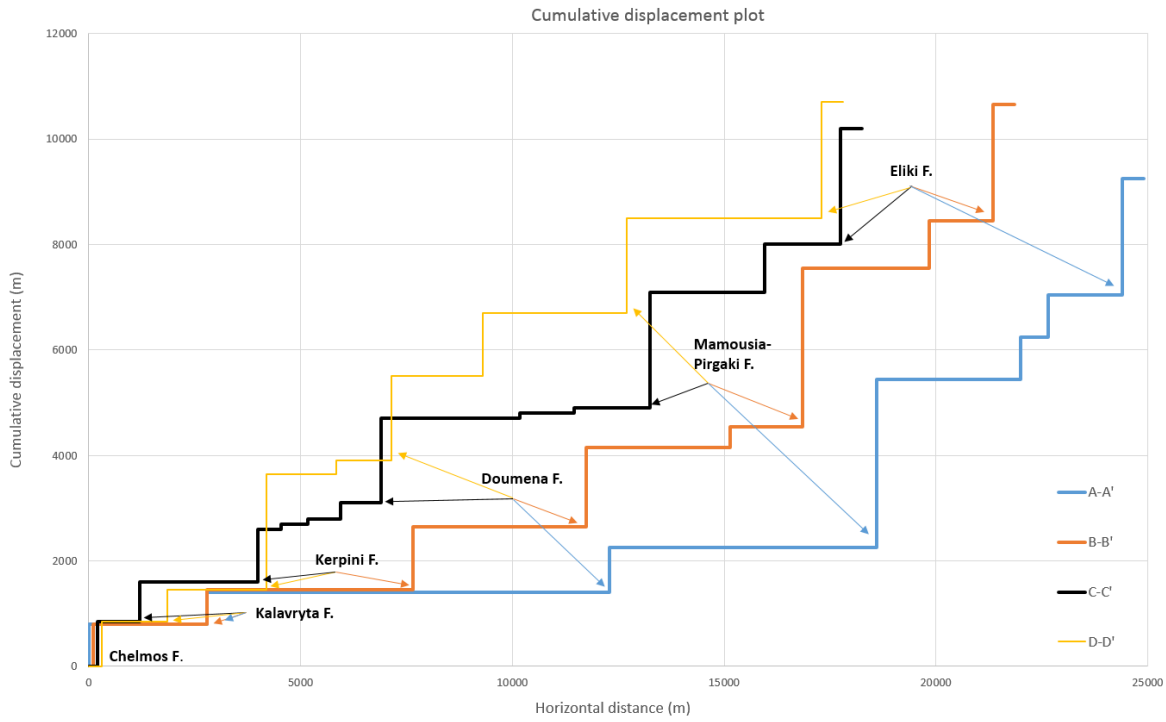

Figure 5.20: Cumulative displacement plot of cross-sections A-A', B-B', C'C' and D-D', showing the cumulative displacement of the major and minor north dipping faults. The Chelmos Fault is located by the zero-point for all four sections. The cumulative displacement is calculated by summing the estimated displacements of all the basement-involved faults.

To include the uncertainty of the displacement analysis of the N-S cross-sections, maximum and minimum displacements have been estimated to show a possible range (Figure 5.21, 5.22, 5.23 and 5.24). The error estimations are based on the uncertainties related to fault dip and unconformity strike and dip. Important to notice is that the minimum and maximum displacements are not uniform for each fault. The uncertainty error related to the Mamousia-Pirgaki Fault, as an example, shows difference in the maximum from the minimum error, were the maximum error is higher than the minimum. In this example, the lower minimum error is due to the topography,

that one can be more certain of the minimum displacement, while the possible maximum displacement is more uncertain.

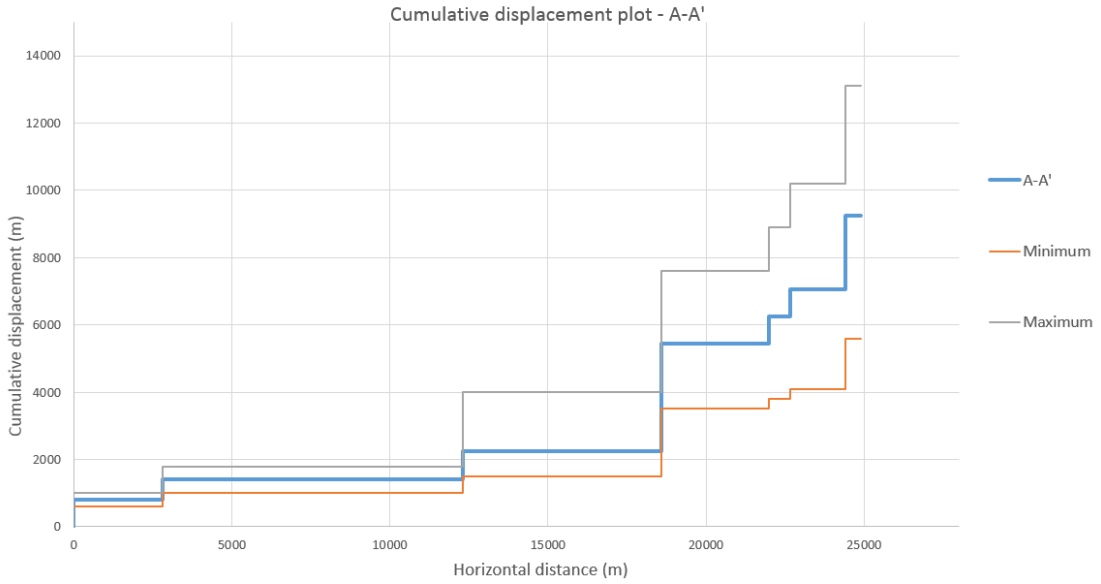

Figure 5.21: Cumulative displacement plot of cross-section, A-A'. The black and the orange lines represent the minimum and maximum displacements.

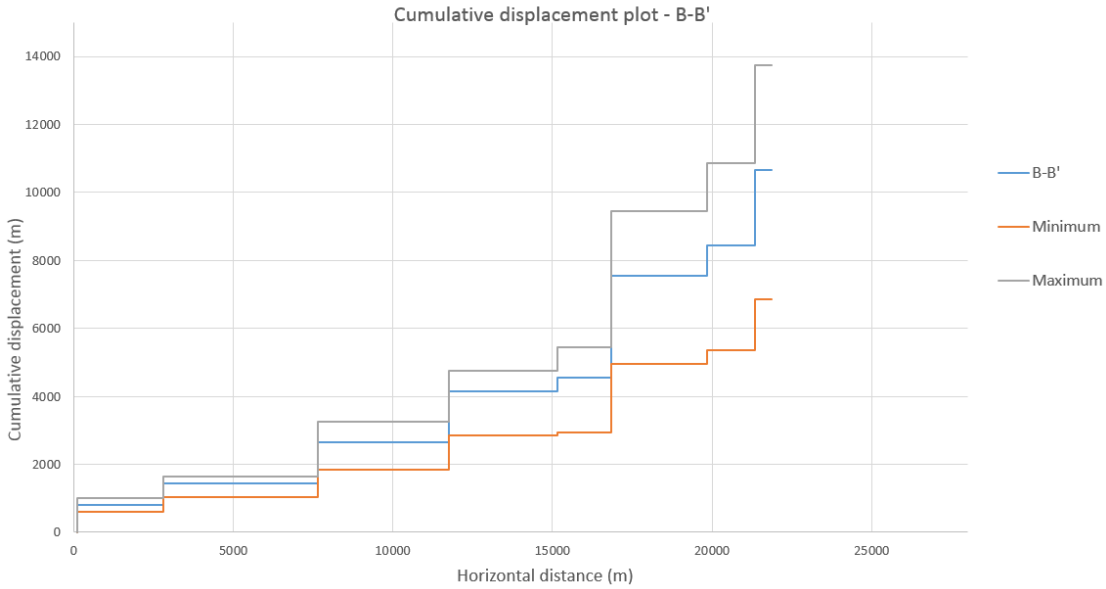

Figure 5.22: Cumulative displacement plot cross-section, B-B'. The black and the orange lines represent the minimum and maximum displacements.

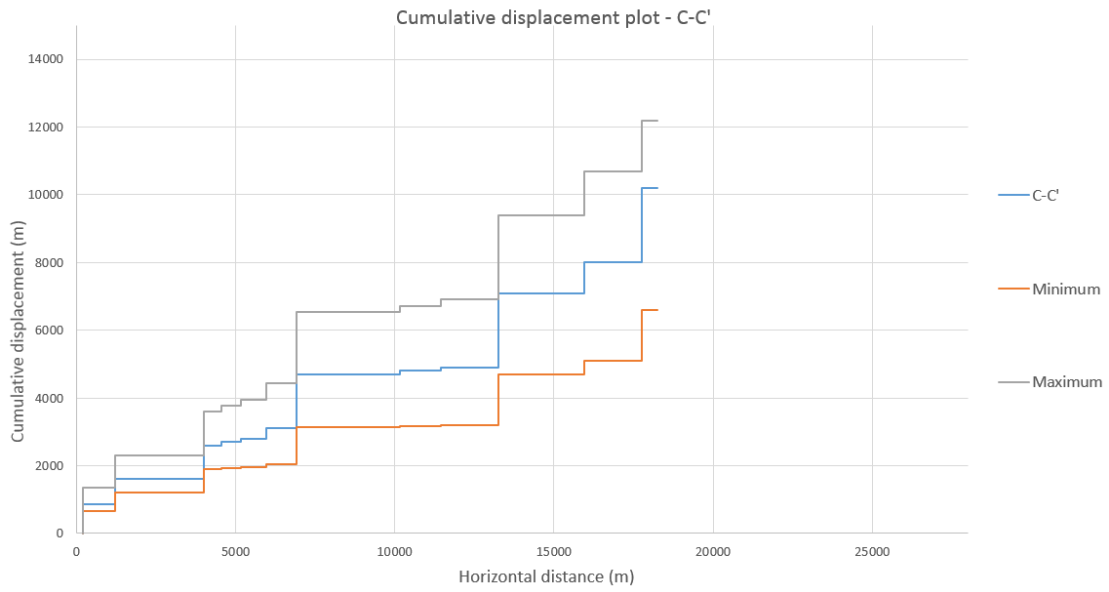

Figure 5.23: Cumulative displacement plot of cross-section, C-C'. The black and the orange lines represent the minimum and maximum displacements.

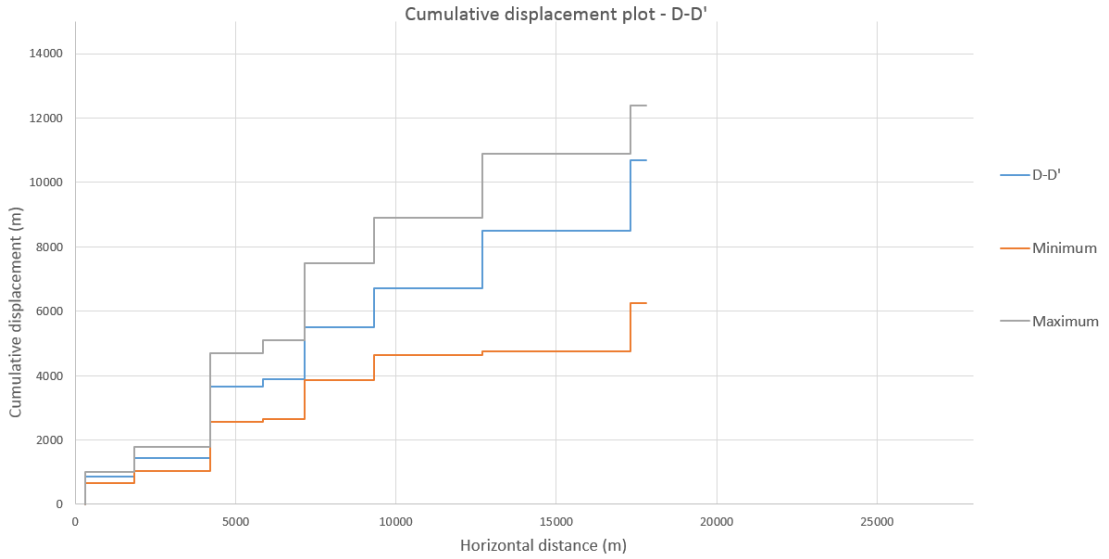

Figure 5.24: Cumulative displacement plot of cross-section, D-D'. The black and the orange lines represent the minimum and maximum displacements.

The error-range of the cumulative displacement analysis of the N-S cross-sections, maximum and minimum displacements have been displayed as error bars to be able to compare uncertainties between the different cross-sections (Figure 5.25).

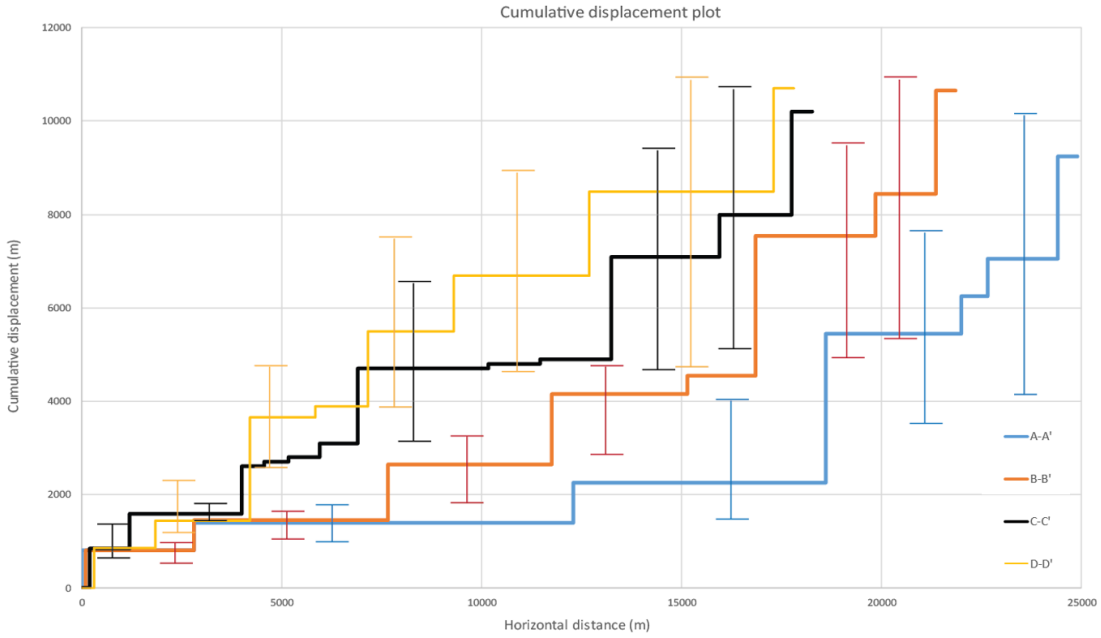

Figure 5.25: Cumulative displacement plot of cross-sections A-A', B-B', C'C' and D-D', with cumulative error bars showing the minimum and maximum cumulative displacement.

A result, which lies within 15 % difference in cumulative displacement, suggest a similar total displacements among the sections that may lead to the assumption of a uniform extension in this area. The results indicate an extension similar across the Kalavryta-Eliki area, probably having some gradual changes within the system. Perhaps there are minor steps that create the displacement range between the sections. The offshore faults, which are not taken into the consideration, could also affect the total displacement. When uncertainty is included, the difference in cumulative displacement is well-within the error-range. So the variation in cumulative displacement could be real, but it could also be due to the uncertainty in the displacement estimates.

5.4 UNCERTAINTY ANALYSIS

Geological three-dimensional (3D) models are constructed to reliably represent a given geological target. The reliability of a model is heavily dependent on the input data and that these parameters honour the geology. In this thesis, the displacement has been determined by using constructed unconformity and fault surfaces. The input for their construction is highly dependent on the dip and strike angles, which in some areas are poorly constrained. The parameters retrieved in the field, such as strike and dip measurements of faults and unconformity surfaces, may vary depending on whom is performing the observation. Furthermore the quality check of the surfaces in Google Earth, although optimised, allows some freedom for a possible range of values. So, how sensitive is the fault displacement in regards to the strike and dip measurements?

The Doumena Fault West III and the Kerpini Fault West have been analysed to investigate how displacement is affected by the dip and strike. The fault dip and unconformity dip was changed by ±5° increments (Figure 5.26). The "x" marked in Figure 5.26, indicates the incremental distance, which is the distance the displacement changes by 5° dip change. The strike direction were changed by ±1° increments (Figure 5.27), where the change in displacement is prominently greater at the flanks of the unconformity surface and decreasing to zero displacement at the mid-point.

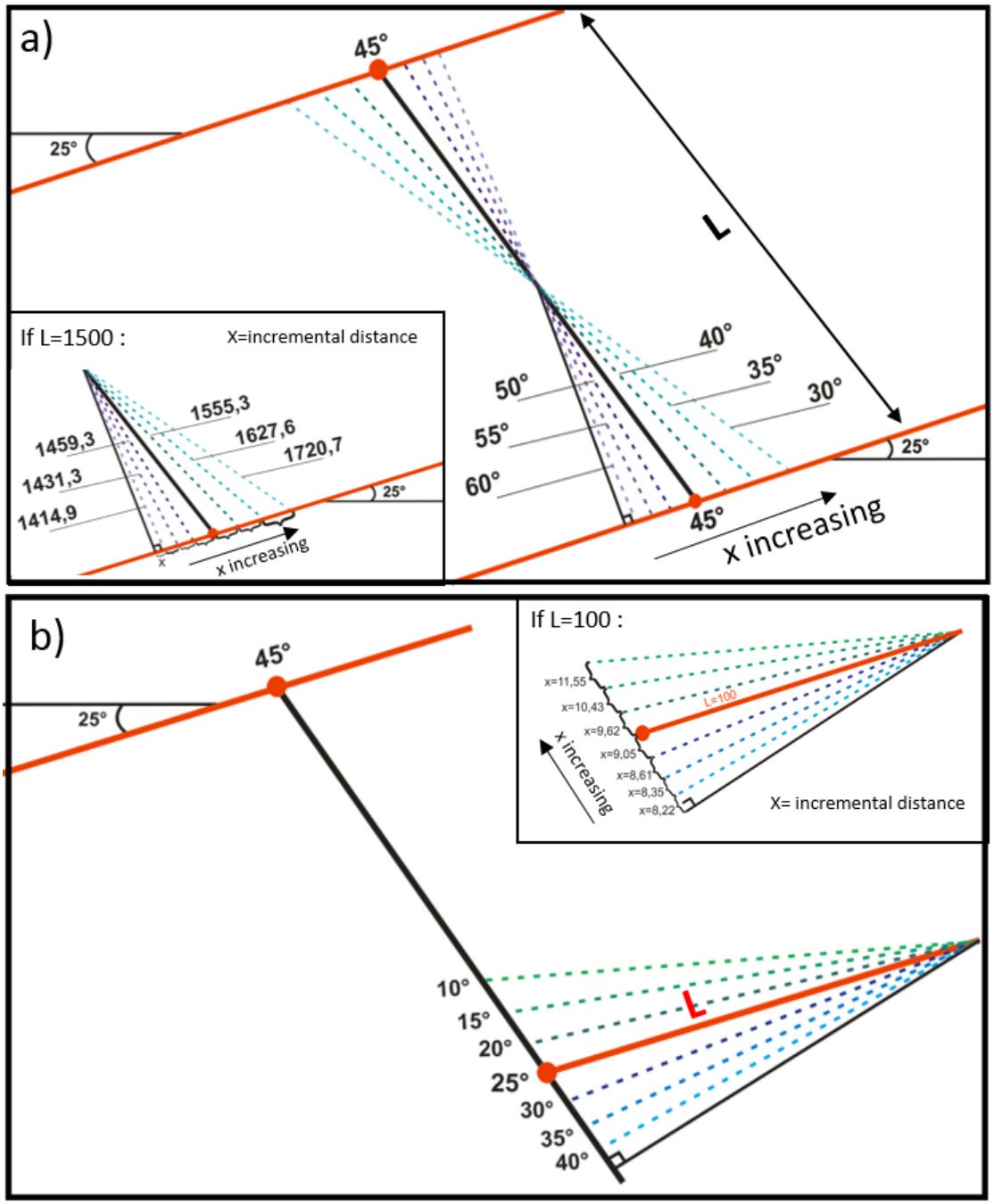

Figure 5.26: Conceptual sketches of a) Change in fault dip by 5° increments. The minimum displacement will be when the fault dip is 90° on the unconformity plane. The black box in the lower left corner shows an example of displacement estimations if the 45° line is at 1500. b) Change in unconformity dip by 5° increments. The black box in upper right corner show an example of how the incremental distance is changing every 5° if L=100. Both figures are showing increased x moving away from the black 90° line.

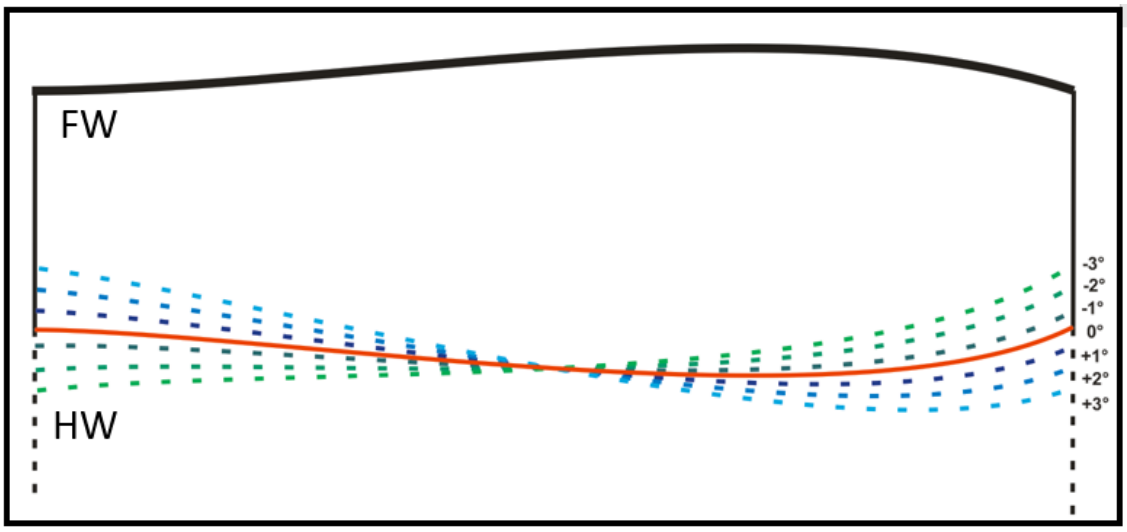

Figure 5.27: Conceptual sketch showing the unconformity surface on a fault plane, with a change in strike direction by ±1° increments. The change in displacement is prominently greater at the flanks of the unconformity surface and decreasing to zero displacement at the mid-point.

5.4.1 The Doumena Fault West

The Doumena Fault West III has an average displacement of around 1500-1600 m using the parameters of fault dip of 45° north and unconformity dip of 25° south. In order to investigate the sensitivity of the displacement, the fault dip was adjusted ±5, 10 and 15° (Figure 5.28). The results showed that the displacement changes are not constant. By decreasing the fault dip from the original 45°, the change in displacement increases with the decrease in dip increment. In contrary, when increasing the fault dip, the displacement will decrease less and less. The displacement distance between the 30° and 35° is 15.2 m, while the displacement distance between 55° and 60° is 87.7 m. The "X" marked on the plot shows how the incremental distance increase with decrease in fault dip.

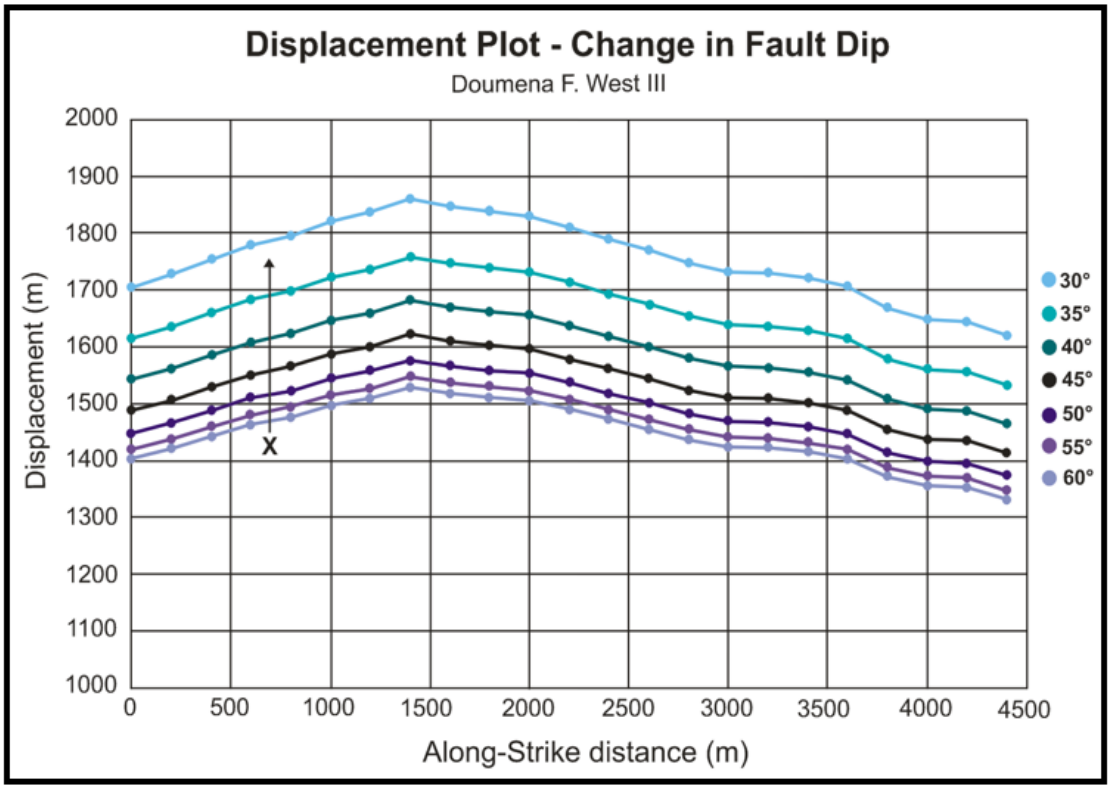

Figure 5.28: Displacement plot showing the different displacements using different fault dip angle by 5° increments. The incremental distance (x), is increasing more and more with decrease in fault dip.

A similar analysis was conducted by adjusting the dip of the unconformity surface by ±5, 10 and 15° (Figure 5.29). The results showed a similar trend to the fault analysis, but not as prominent changes in the incremental distance. Here, the "X" marked on the plot shows how the incremental distance increase with decrease in unconformity dip. The displacement distance between the 40° and 35° is 91.9 m, while the displacement distance between 15° and 10° is 127.5 m.

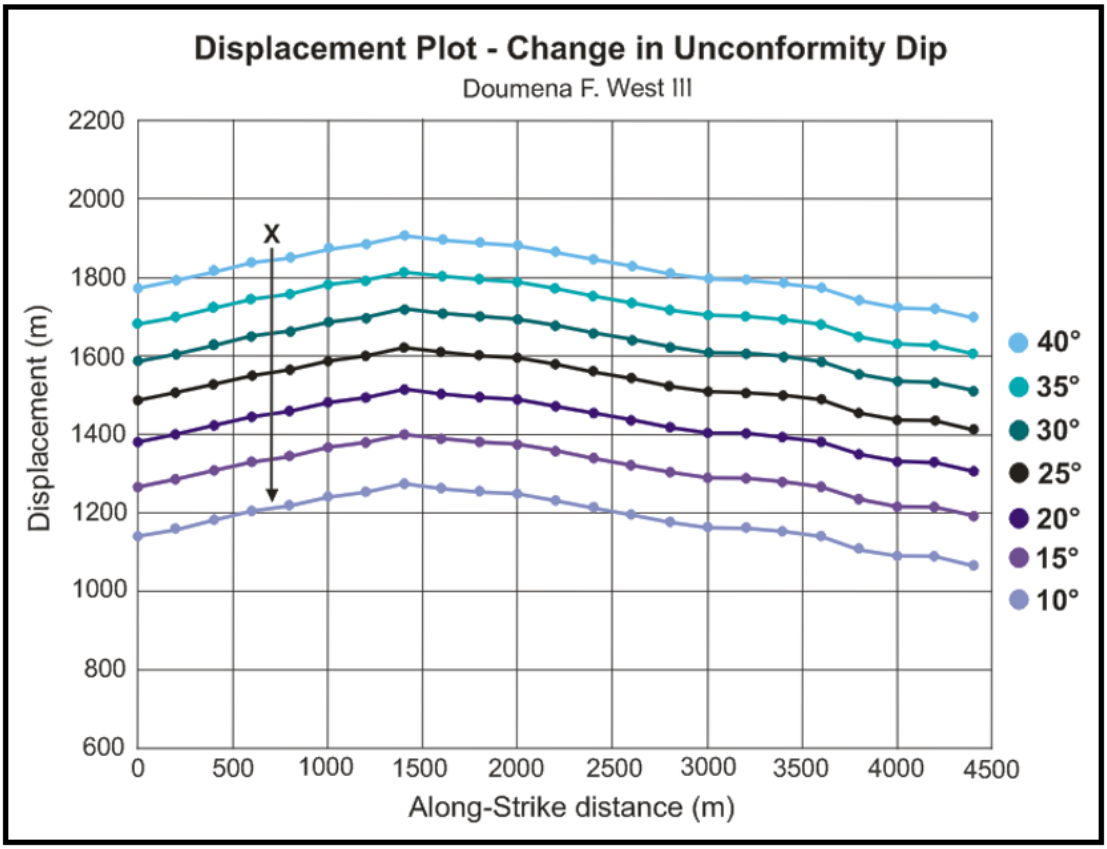

Figure 5.29: Displacement plot of the Doumena F. West with change in displacement with change in unconformity dip by 5° increments.

A comparison between the uncertainty analysis between the fault dip and the unconformity dip, show that the change in the unconformity dip has a larger impact on the displacement than changing the fault dip. But that the fault dip is more sensitive at lower dips and less so with higher dips. Figure 5.30 shows a comparison between the minimum displacement (steep fault and shallow unconformity) versus the maximum displacement (shallow fault and steep unconformity) from the analysis above. Here it is evident that the unconformity dip has a larger impact on the displacement.

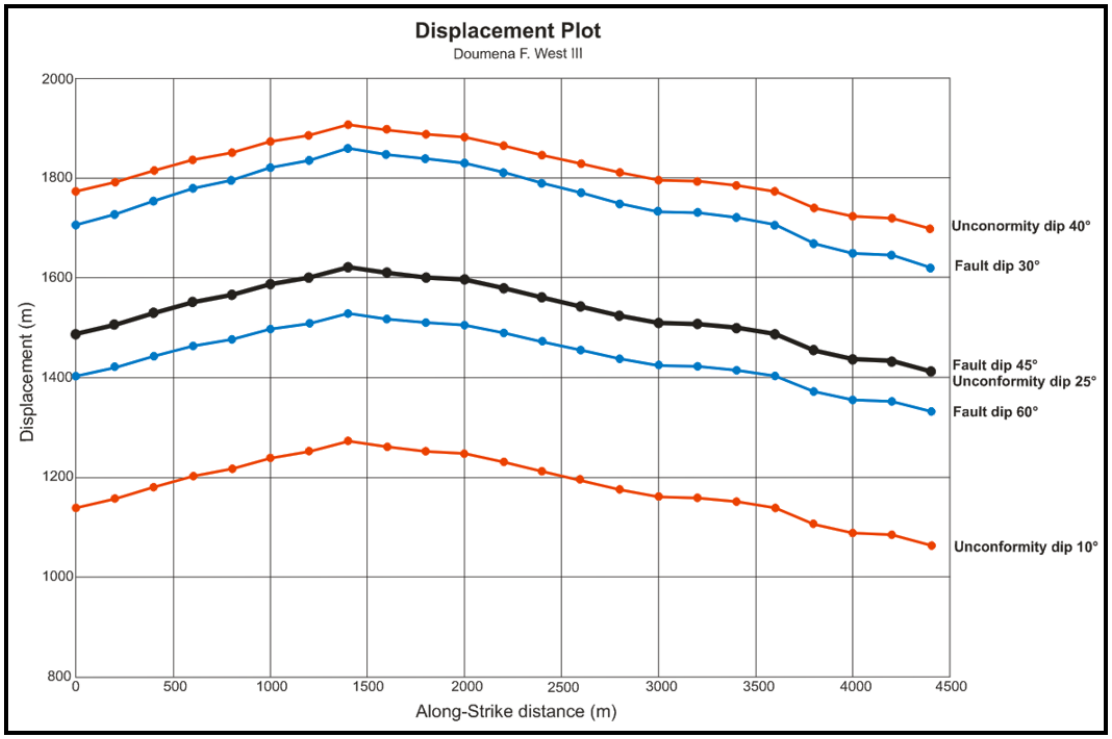

Figure 5.30: The results from the previous analysis of the steepest unconformity and fault versus the shallowest unconformity and fault dip. The black line represent the displacement of the Doumena Fault West III with fault dip of 45° and unconformity dip of 25°.

A final analysis tested how sensitive the displacement is to the strike direction of the fault. The strike was changed by ±1, 2 and 3°. By changing the strike of the fault by 1°, there was a displacement change up to 30 meters at the flanks of the fault, which corresponds to a change by an average percentage of 1.3-1.6 % in the flanks per 1° (Figure 5.31). This result shows that by incorrectly estimating the strike by 5°, a displacement error of 150 m can occur. This error is also dependant on the fault length, whereby longer faults will have an increased error.

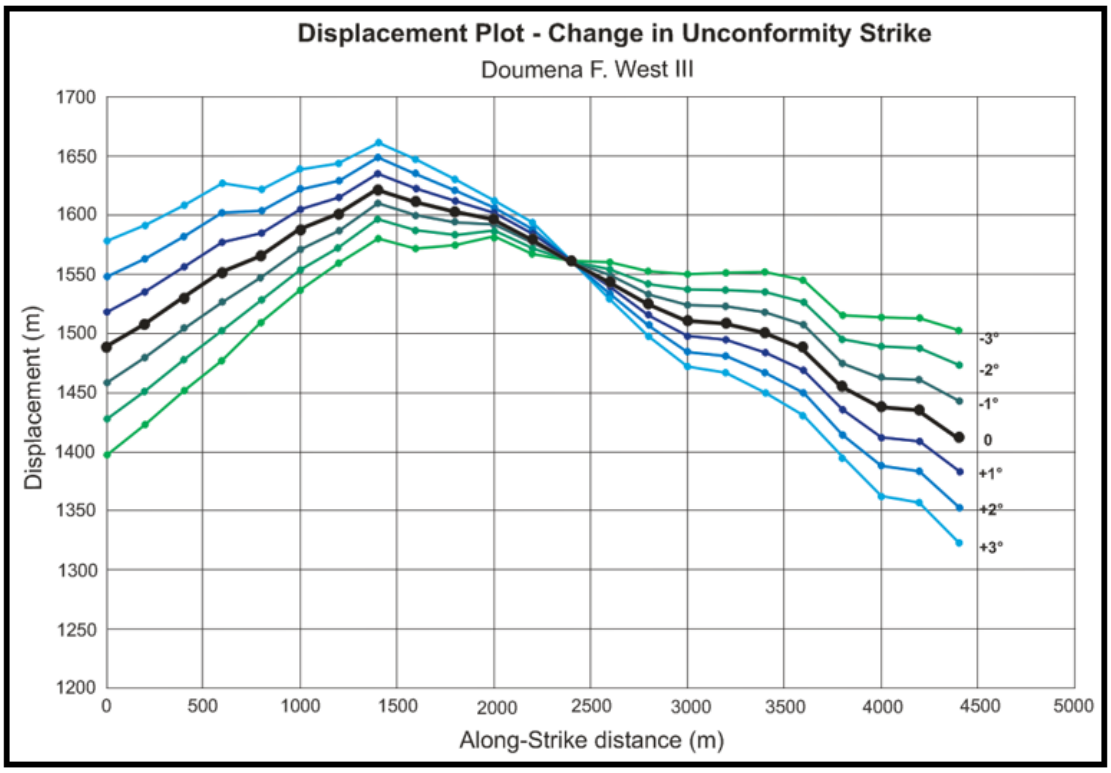

Figure 5.31: Displacement plot showing different displacements adjusting the strike direction by 1° increments.

5.4.2 The Kerpini Fault West

A second analysis was conducted on the Kerpini Fault West, in this case investigating three fault segments. First, the fault analysis showed increased displacement with decrease in fault dip. And a decrease in fault displacement with increased fault dip, but the decrease is less and less for every 5th degree, similar to the results from the Doumena West Fault III analysis (Figure 5.32).

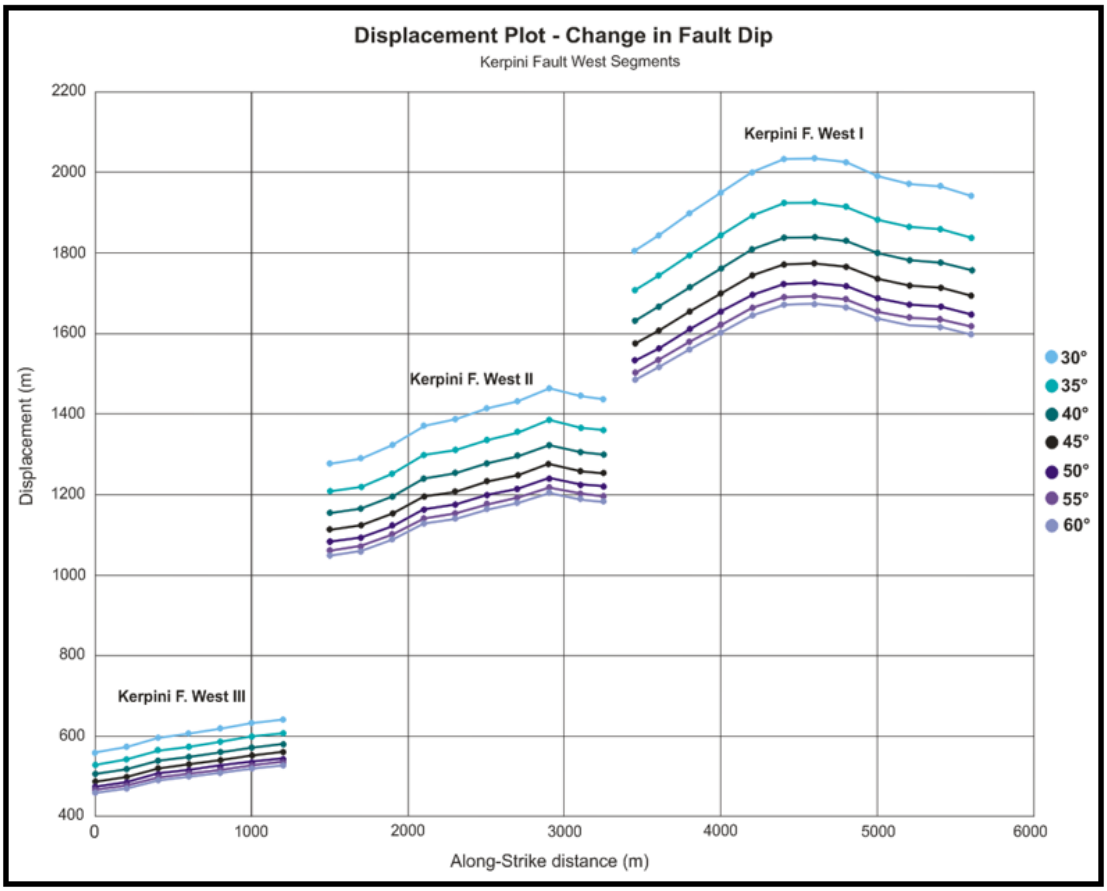

Figure 5.32: Displacement plot of the Kerpini F. West segments showing the different displacements with change in fault dip of 5° increments.

The unconformity analysis on the Kerpini F. West segments resulted in the same pattern as for the unconformity analysis done on the Doumena Fault West III. A larger decrease in displacement by every 5° decrease in dip, and the opposite with every 5° increase in dip (Figure 5.33).

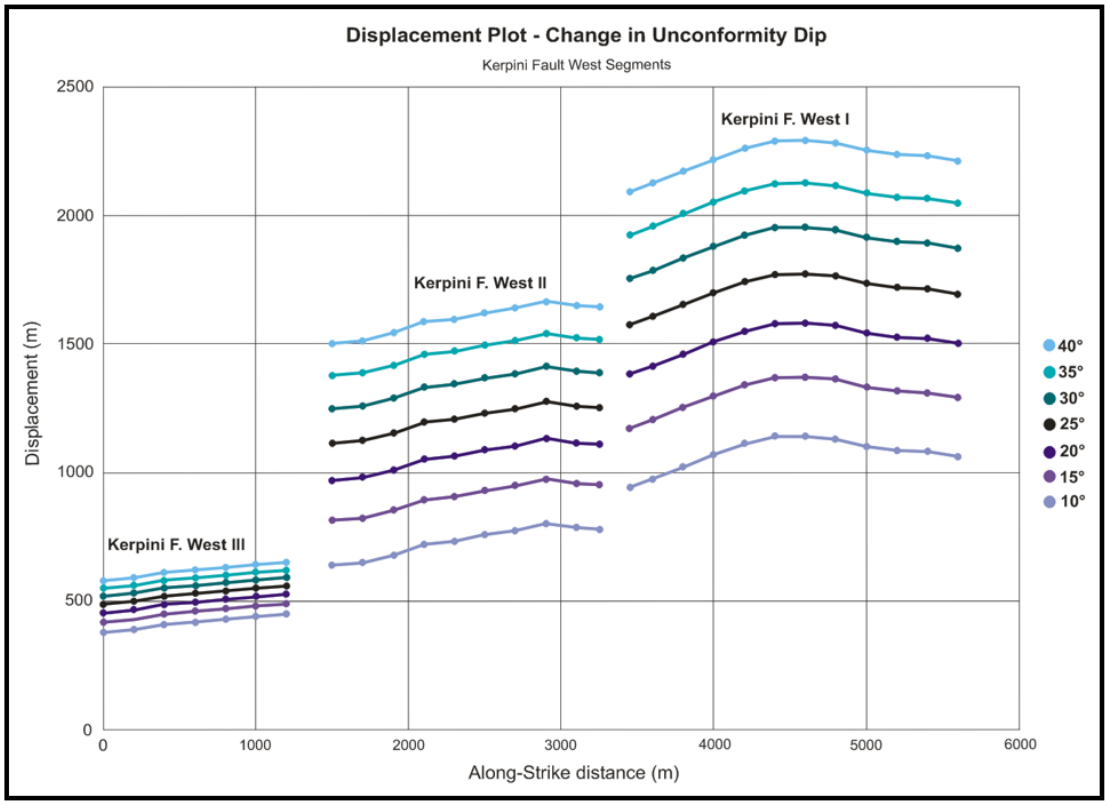

Figure 5.33: Displacement plot of the Kerpini F. West segments with change in unconformity dip by 5° increments.

Finally, a second analysis of displacement related to the strike direction was performed to compare with the results from the Doumena Fault West. The analysis showed that the displacement of the Kerpini F. West segments change by an average percentage of 1.3-1.6 % in the flanks per 1°. In meters, this correspond to the Kerpini F. West Segement I increasing displacement by 20 m on the flanks, Segment II by 14 m and Segment III by 8 m (Figure 5.34). These displacement errors outline the impact of fault length.

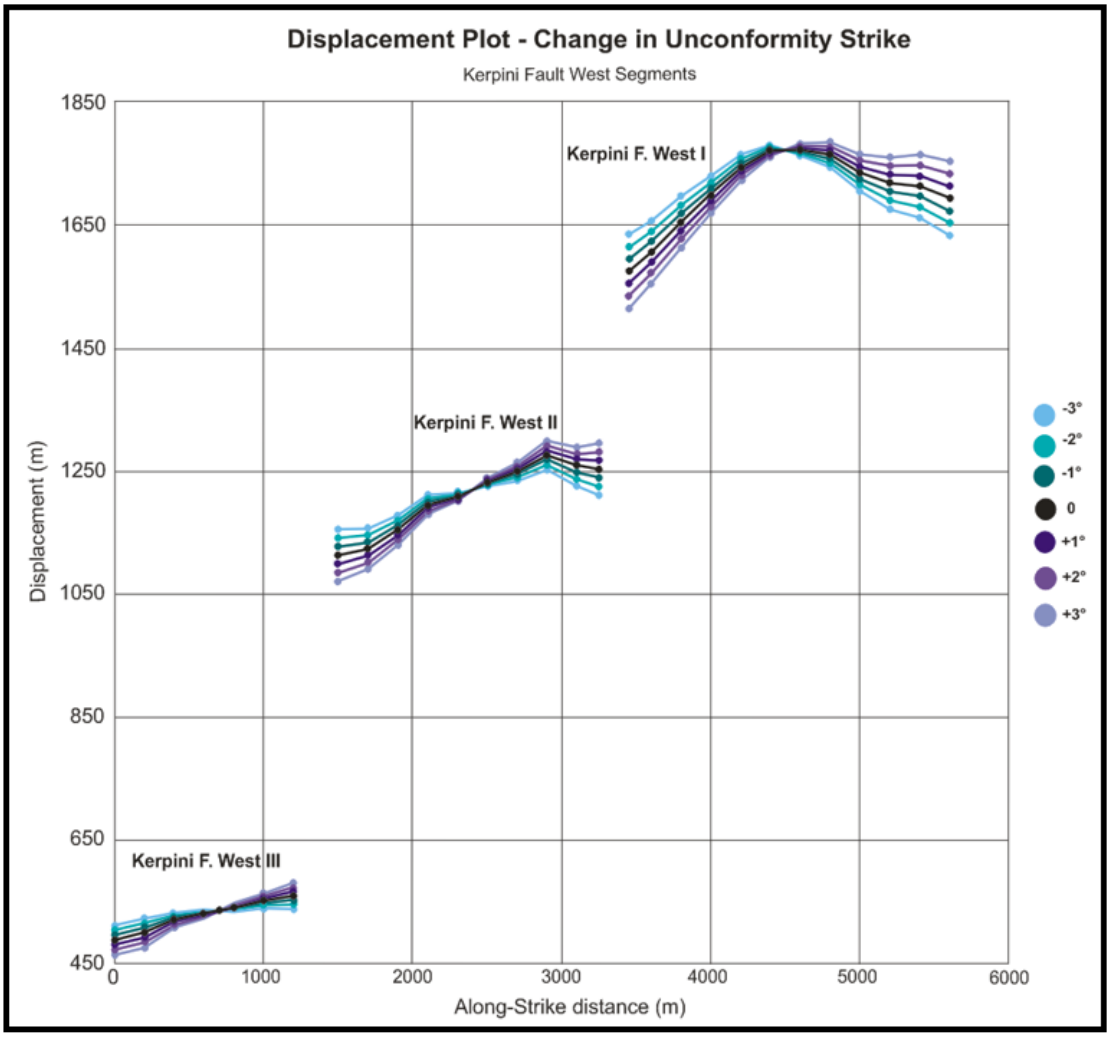

Figure 5.34: Displacement plot of the Kerpini F. West segments with change in strike direction by 1° increments.

Chapter 6 – Discussion

This chapter will discuss the key observations and results from the previous chapters, and attempt to address some of the geological problems that have been raised. This will be done by discussing methods performed in previous work and comparing the results from the displacement analysis. Also investigate displacement patterns and gradients considering rift segmentation.

6.1 Displacement Analysis

Previous work on fault displacement estimations on the major faults in the Kalavryta-Eliki area are mentioned in papers (Doutsos and Poulimenos, 1992; Ghisetti and Vezzani, 2005; Ford et al., 2013; Wood, 2013), but it is generally un-clear on how these were calculated. It is also unclear if the estimated values are local or maximum values. In several cases it is also not stated the locations along strike of the faults where the displacement is estimated. Some cases give a range of displacements, but it is not clear if this represents the variability on individual faults or uncertainty around a single local estimate.

Ghisetti and Vezzani (2005) and Doutsos and Poulimenos (1992) estimated a range of displacements calculated from offset of geological markers and along-strike variations of throw are bracketed by the extreme values. In this case, the estimated displacement represents the variability on individual faults, ranging from maximum to minimum displacements. When presenting the results, it is not stated where exactly along-strike the displacement estimations have been performed, making it challenging to compare results. It is also difficult for the reader to get an understanding of how the displacement gradients act, and where along-strike their displacement maximums and minimums are located. Variations that occur along faults and what kind of error

associated with these displacement estimations are hardly mentioned and not properly considered.

Ford et al. (2013) calculated the displacement along several cross-sections using the basal unconformity as reference, where the faults are extrapolated as planar structures to a depth of 1 km below sea level (bsl). This is similar to the method used in this project, however, the displacement analysis is presented on the basis of three cross-sections throughout the Kalavryta-Eliki area. This gives a rough overview of the displacement of the major faults in the area, but it difficult to follow the along-strike variations along a fault in any detail and to get an understanding of the variations between the faults. The range of minimum and maximum displacement are also not stated, which is important information for the reader to understand the possible amount of variability along the faults.

In this thesis, a detailed and robust displacement analysis has been performed on major and minor faults in the Kalavryta-Eliki area, based largely on constructing 3D surfaces of fault planes and stratigraphic surfaces, which are the basement-syn-rift unconformities. This allows analysis of displacement gradients and patterns, showing how the faults grow, propagate and interact. It opens for analysis of displacement continuity across fault steps, along with estimations of maximum and minimum displacements. Table 1 shows a comparison of displacement estimates calculated for four faults, and Figure 6.1 is showing the location of the estimates. Table 1 shows that there are especially large deviations between the estimates of the Mamousia-Pirgaki and Eliki Faults. The low displacement estimates calculated by Ford (2013) and Ghisetti and Vezzani (2005), compared to this study, could be because the depth of the deltas are not considered, but rather they calculated the minimum displacement based on the

topography. It is also difficult to compare results as the methodology is not clearly explained.

Table 1: Comparison of displacement estimations of four major faults. Note that Ghissetti and Vezzani, 2005, has estimated displacement ranges, while Ford, 2013 and this study have displacement estimates from exact local points.

	Ford, 2013	**Ghisetti and Vezzani, 2005**	**This study**
1.Doumena Fault West III	945 m	695-1250 m	1525 m
2.Kerpini Fault	a. 1109 m b. 2634 m	-	a. 1233 m b. 2200 m
3.Mamousia-Pirgaki Fault	a. 1622 m b. 1445 m	a. 925-1320 m b. 500-1058 m	a. 3028 m b. 2001 m
4. Eliki Fault	-	375-755 m	2230 m

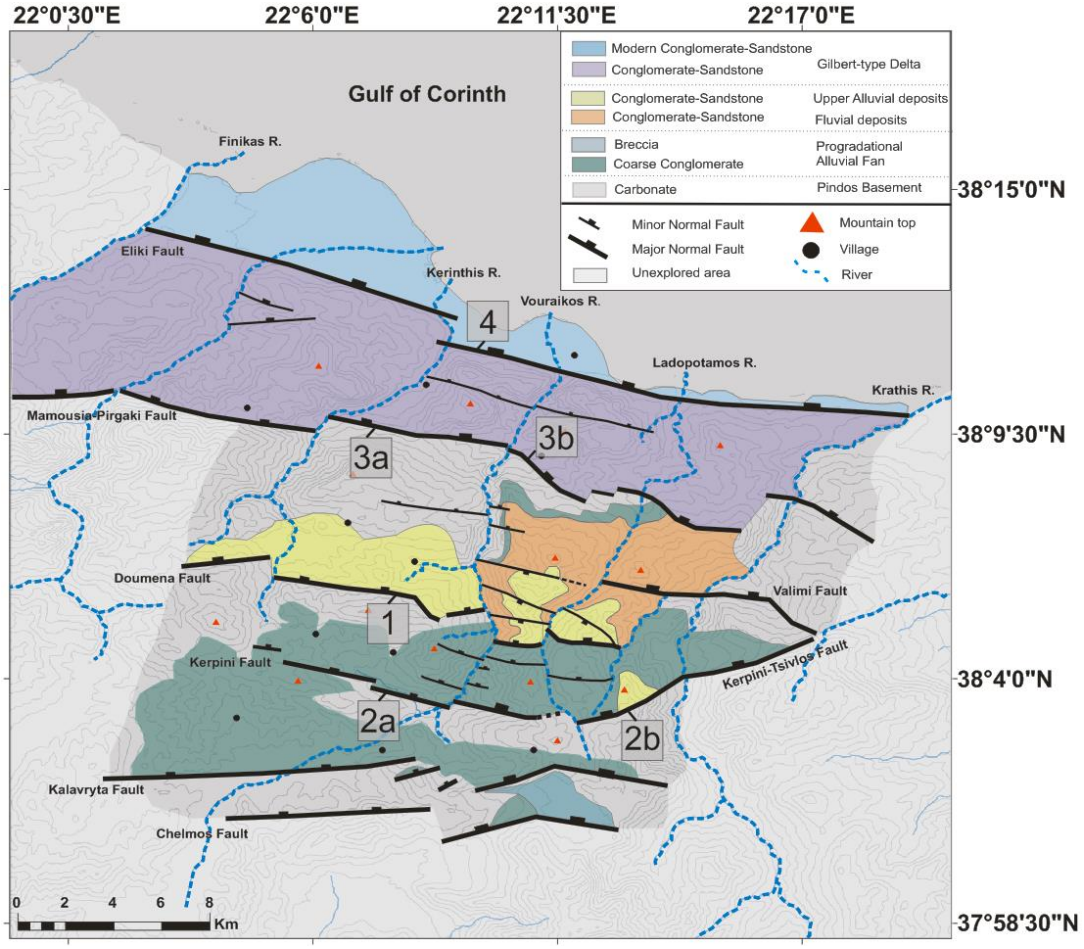

Figure 6.1: Map of the study area showing the location of displacement estimations from Table 1. The estimations from Ghisetti and Vezzani (2005) does not apply to these exact locations since they estimated ranges of displacements, probably considering entire faults.

This methodology of estimating fault displacement is not perfect as it relies on surface construction techniques, knowledge of surface dip and strike, and assumption of a planar pre-faulting unconformity surface (i.e. no erosion). Considering these points, it allows for uncertainty analysis in order to get an understanding of how accurate the estimations are. As seen from the uncertainty analysis, the fault displacement changes differently according to which parameters are changed. It was clear that the change in the unconformity dip has a greater impact on the displacement, than the change in fault dip, and that the displacement change is not uniform for every 5° changed due to the geometries of the planes. In additions, the results from the displacement analysis

showed that there are asymmetry in dip impact that by increasing the dip gives larger error than decreasing dip, both for the unconformity and fault cases.

The displacement analysis shows that the method of 3D model construction is a good approach to highlight how the displacements are and how they vary across single faults and fault segments. And by implementing the uncertainty analysis, it gives a range of possible outcomes, which in many cases will strengthen the reliability of the analysis and represent the errors associated to the method.

6.2 DISPLACEMENT GRADIENTS AND PATTERNS

6.2.1 Displacement Distribution

Displacement variation along faults is common and displacement gradients are typically steeper near fault terminations than on the whole. Classical displacement patterns on normal faults usually tend to show a maximum displacement in the central part of the fault trace, gradually decreasing toward the tips (Figure 6.2). As seen in the displacement analysis the displacement patterns on segmented faults often show significant jumps in the displacement which cannot be explained by the displacement gradient alone. According to Ferrill and Morris (2001), lateral displacement gradients are around 10:1, where a fault's lateral extent is approximately ten times its maximum displacement. The displacement analysis also showed sudden displacement decrease at fault terminations and this do not conform to the gradual decrease to zero displacement in the fault tip model by Fossen (2010). This comparison of displacement patterns suggests that there must be other features that cause these sharp displacement changes.

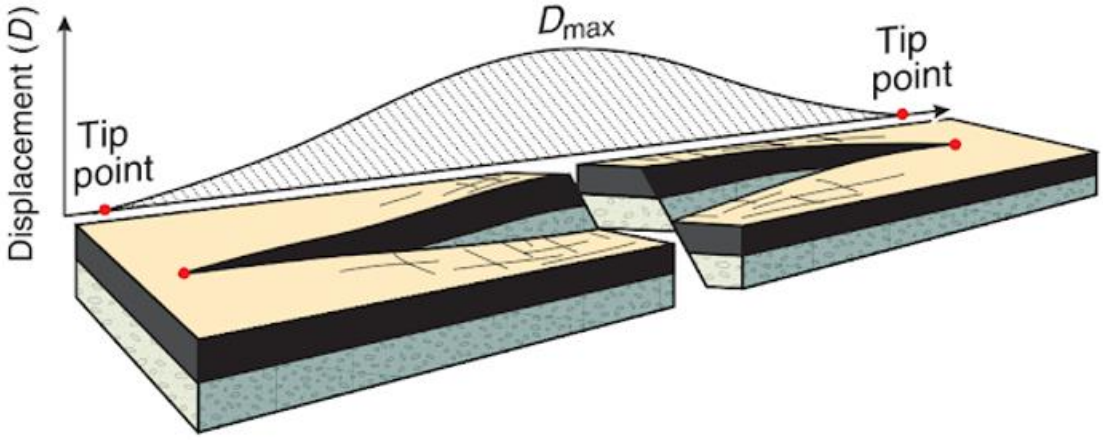

Figure 6.2: Conceptual model of an ideal, isolated fault. The displacement profile indicates maximum displacement near the centre (Dmax), gradually decreasing towards the tip points. Modified from Fossen, 2010.

Relay ramps, proposed by Ford et al. (2013) to be present in the Kalavryta-Eliki area, are the products of opposite displacement gradients on two overlapping, laterally terminating, and subparallel normal faults. They transfer displacement between overlapping normal faults by accommodating horizontal heave gradients and vertical throw gradients on the faults (Ferrill and Morris, 2001). Figure 6.3 shows the displacement pattern for a classical relay ramp, where there is a depression in the curve as the faults overlap. Also, when the approaching faults develop further, the depression tends to be removed. Comparing this ideal displacement profile for relay ramps, with the displacement plots compiled from the displacement analysis on the Kalavryta-Eliki area, there are clearly differences where the sharp changes in fault displacement have been observed. It is difficult to explain these occurrences with the relay model proposed by Ford et al. (2013) as the displacement patterns do not coincide and are not expected to allow for such displacement jumps.

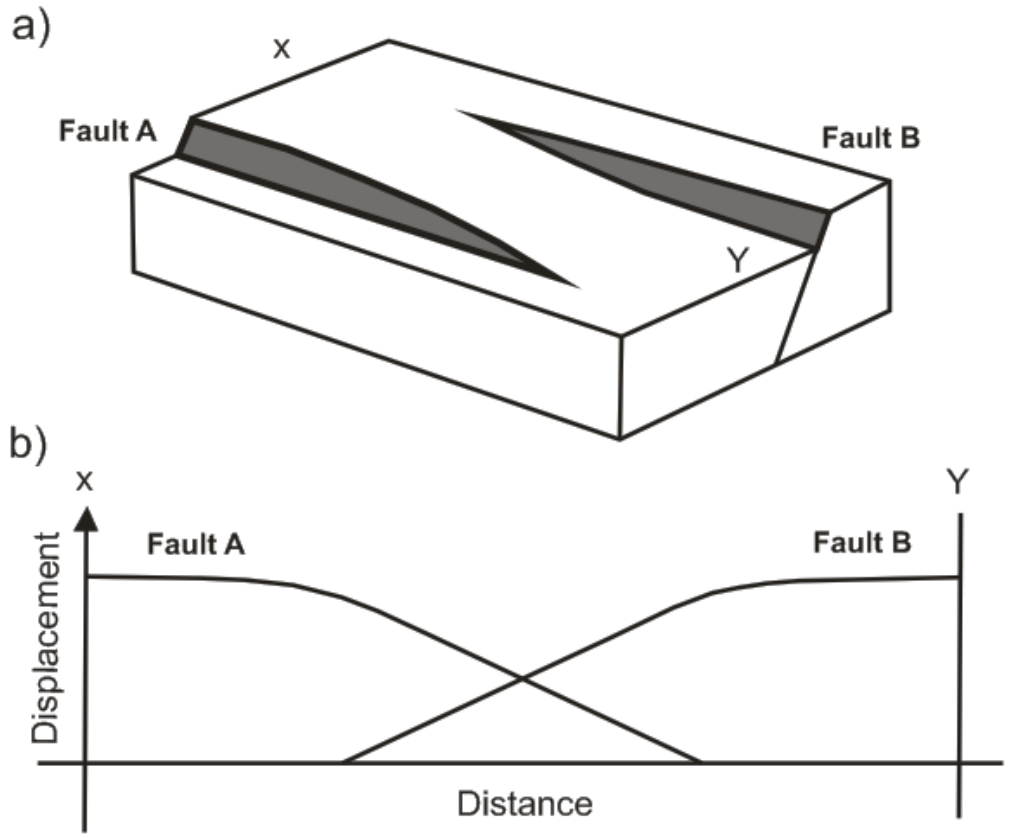

Figure 6.3: a) Conceptual model illustrating a relay ramp and b) Ideal displacement profile diagram for the profile XY of the relay ramp in a). Modified from Ferrill and Morris, 2001.

6.2.2 The Kerpini Fault West

The displacement on segmented faults is well illustrated on the Kerpini Fault West as observed in the displacement analysis (Figure 6.4). There is a large fault step in the Vouraikos Valley between the Kerpini Fault West and the Kerpini Fault East, where the displacement decreases sharply by 430 m (Figure 6.5). This is most likely explained by a N-S trending fault in the Vouraikos Valley. There are also large steps between segments I and II (320 m), where the step is aligned with the Roghi Fault, as previously proposed by Hadland (2016). Both the fault step and the unconformity trace east of the village of Roghi can be explained by this N-S trending fault. The

displacement jump between segments II and III (540 m) and also the western termination of the Kerpini Fault seem to align well with the proposed Kerinthis Fault I and II by Hadland (2016) and later supported by Birkeland (2017). It seems that the Kerinthis Fault is dividing south of the Doumena Fault, forming a fork in the transfer fault, where the Kerinthis Fault II cause the step between the Kerpini Fault West segments II and III. The Kerinthis Fault I continues on the western side, probably terminating the Kerpini Fault. Evidences for proposing the Kerinthis Faults are not only supported by the step in the Kerpini Fault, but also by the step in the height of the unconformity (Hadland, 2016). Figure 6.4 shows the proposed transfer faults along with the step in the unconformity on the western side. The evidences presented, align with previously proposed N-S fault from previous work (Dahman, 2015; Hadland, 2016; Birkeland, 2017; Oppedal, 2017; Veiteberg, 2017), and may suggest that all fault steps could be related to N-S trending faults.

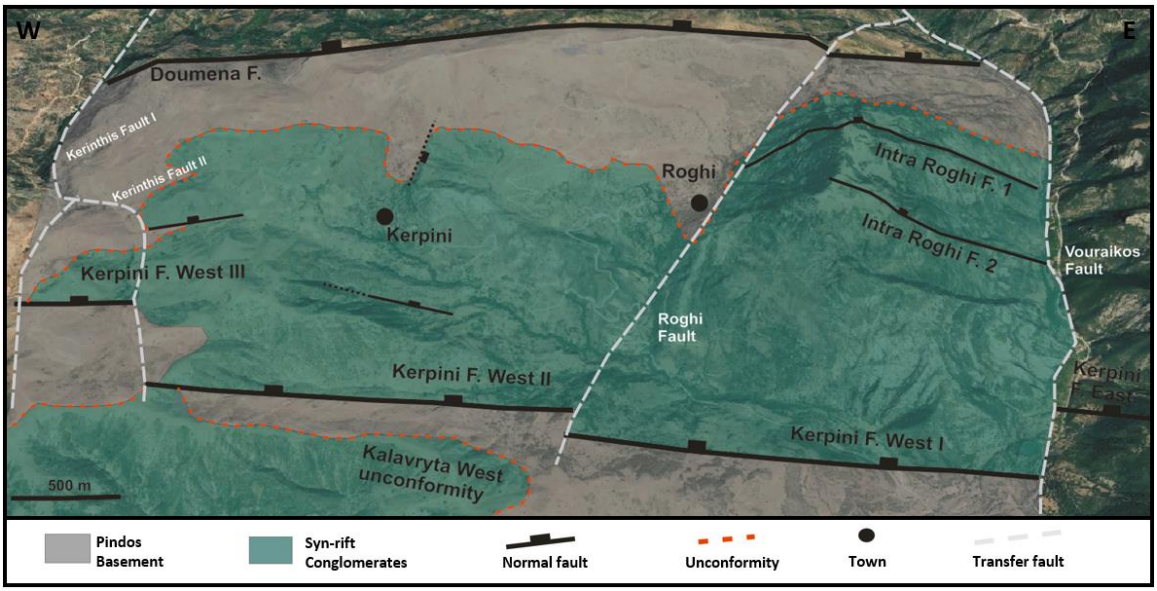

Figure 6.4: Satellite image from Google Earth with proposed transfer faults that aligns with the steps in the Kerpini Fault West, highlighted by white-coloured, stippled lines.

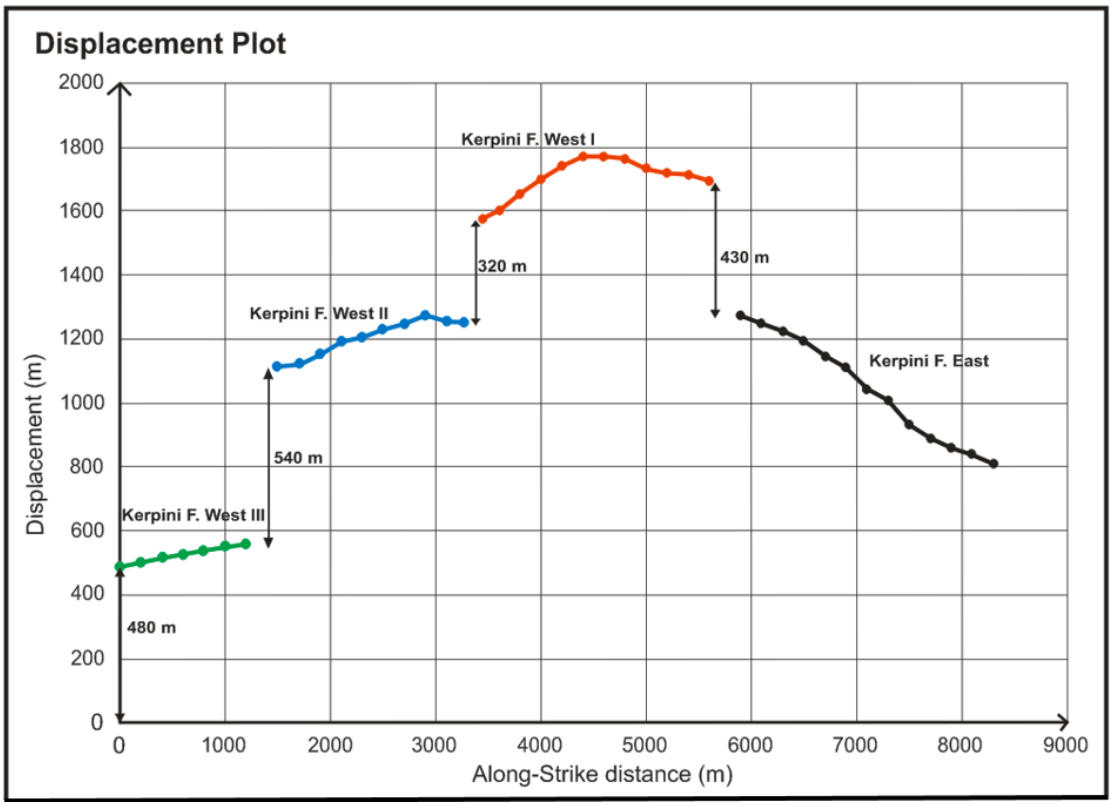

Figure 6.5: Displacement plot of the Kerpini Fault, showing the sharp changes in displacement between the segments highlighted by black arrows.

6.3 SEGMENTATION

6.3.1 Maintenance of Extension

The results from the cumulative displacement analysis showed that the cumulative displacement through the study area is within 13 % displacement difference between the sections. The cumulative displacement plot showed that each fault block has similar extension even though there are heterogeneities between the profiles. Geological mapping of the Kalavryta-Eliki area suggests that the eastern Vouraikos area (profile C-C') is considerably more deformed, hosting several faults, than in the area between the villages of Pirgaki and Skepasto (profile A-A'). In profile A-A' there is only one small fault between the Kalavryta and Mamousia-Pirgaki Faults, whereas further east in profile C-C' there is several faults between the Kerpini and Doumena Faults. This would lead to the suggestion that there is differential extension in the Corinth Graben.

The displacement analysis shows that the cumulative heave, the total horizontal extension for each profile, range between 6540 m and 7560 m, which is 13% difference between the minimum (A-A') and maximum (C-C') cumulative heave in the profiles. (Figure 6.6). The result show a total horizontal extension around 7 km. Bering in mind the geological observations, as the differences between the profiles addressed in chapter 4.4, this is somewhat unexpected. It would be reasonable to predict a more variable extension, with the main deformation area around the Vouraikos Valley, and decreasing deformation eastwards and westwards, evident from the presence of less faults in the profiles. The maintenance of displacement in this case can be explained by the incremental displacement on the Mamousia-Pirgaki Fault, near the village of Pirgaki. However, it is reassuring that there are not significant differences as the change in extension would have to be explained.

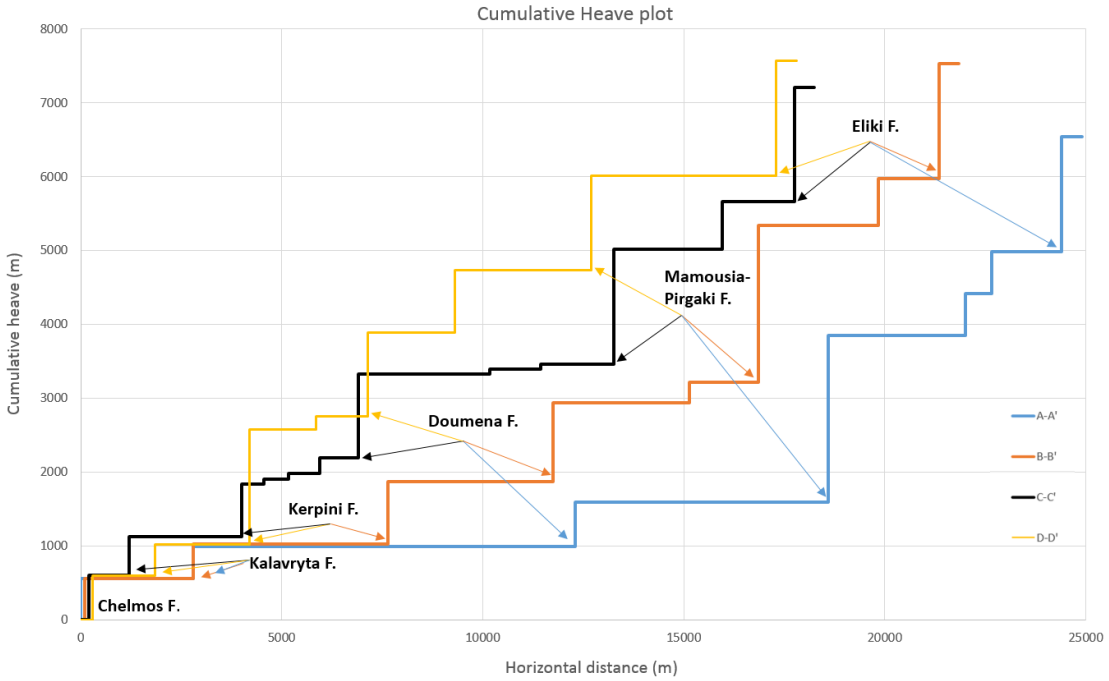

Figure 6.6: Cumulative heave plot of cross-sections A-A', B-B', C'C' and D-D', showing the total horizontal extension of the major and minor north dipping faults. The Chelmos Fault is located by the zero-point for all four sections. The cumulative heave is calculated by summing the estimated heave of all the basement-involved faults.

Even though the extension is relatively similar, there are differences. These differences can be explained as being either i) real and could be compensated for by including the analysis of the faults in the offshore Gulf of Corinth, or ii) they are a result of the uncertainties in the displacement estimates. The uncertainty analysis shown in Figure 6.7, highlighted by error bars, clearly illustrates that the uncertainty is much greater than the range of cumulative displacement, which again supports that the displacement differences between the sections are well-within the range of acceptance.

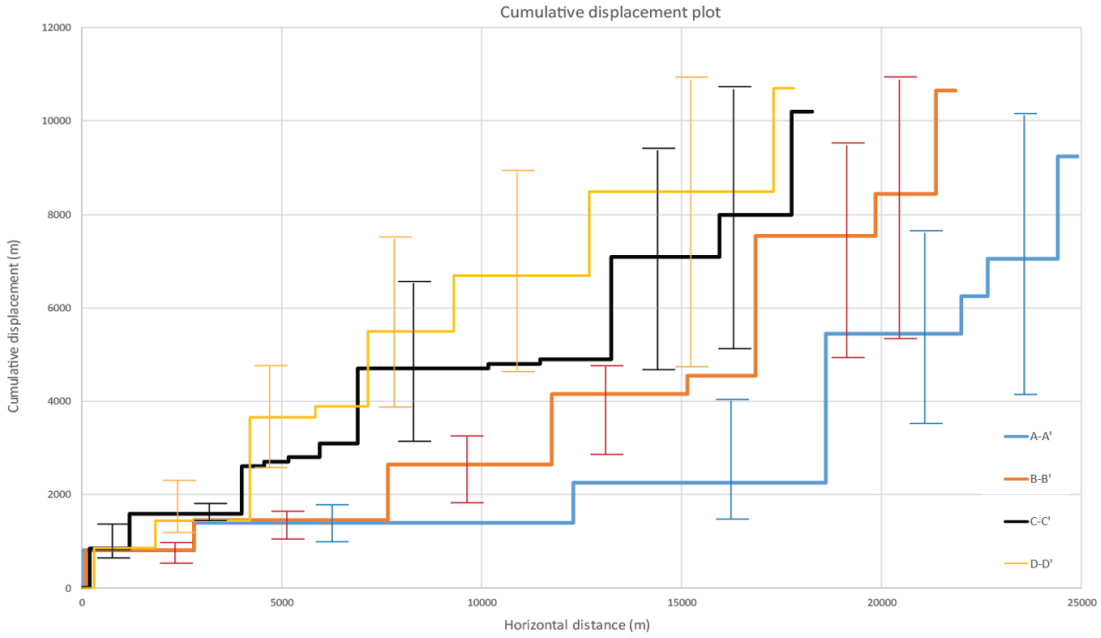

Figure 6.7: Cumulative displacement plot of cross-sections A-A', B-B', C'C' and D-D', with cumulative error bars showing the minimum and maximum cumulative displacement.

6.3.2 Rift Segmentation

Rift segmentation is evident in the Kalavryta-Eliki area. First and foremost by the fact that the displacement patterns from the displacement analysis cannot easily be explained with classical displacement patterns or with relay ramps. The cause of the fault stepping must therefore be from something else. In addition, the Kerinthis, Vouraikos, Ladopotamos and Krathis River Valleys, comprise extensive NNE-SSW intervals across which faults do not correlate. This is concurrent to the observations and conclusions by Dahman (2015) in the Vouraikos Valley, Hadland (2016) on the Kerpini Fault Block and Oppedal (2017) east of the Vouraikos Valley, enclosed by the Kalavryta and Mamousia-Pirgaki Faults.

In studying this area, the river valleys seem to have an underlying fault control. The intervals of miscorrelation are therefore interpreted as quite linear, high-angle

transfer faults enclosing individual segments (Figure 6.8 and Figure 6.9). Also, the displacement analysis of the fault segments are not tipping to zero displacement, evident from the displacement patterns. A more realistic hypothesis would be that they step and continue in another fault segment. The proposal of relay structures provides a simple field explanation but is not favoured due to the severe amount of miscorrelations along relatively straight intervals. The relay ramp displacement pattern does also not agree with the observations from the displacement analysis. Field evidence of overlapping faults are not clear and the 3D models indicate that relays or hard links are very difficult to justify.

By including the interpretations from Dahman (2015), Hadland (2016) and Oppedal (2017), six extensive SSW-NNE trending transfer faults are interpreted to cause the fault discontinuities and ultimately segmenting the area are (Figure 6.8):

1. Kerinthis Transfer Fault
2. Vouraikos Transfer Fault
3. Roghi Transfer Fault
4. Ladopotamos Transfer Fault
5. Potamia Transfer Fault
6. Krathis Transfer Fault

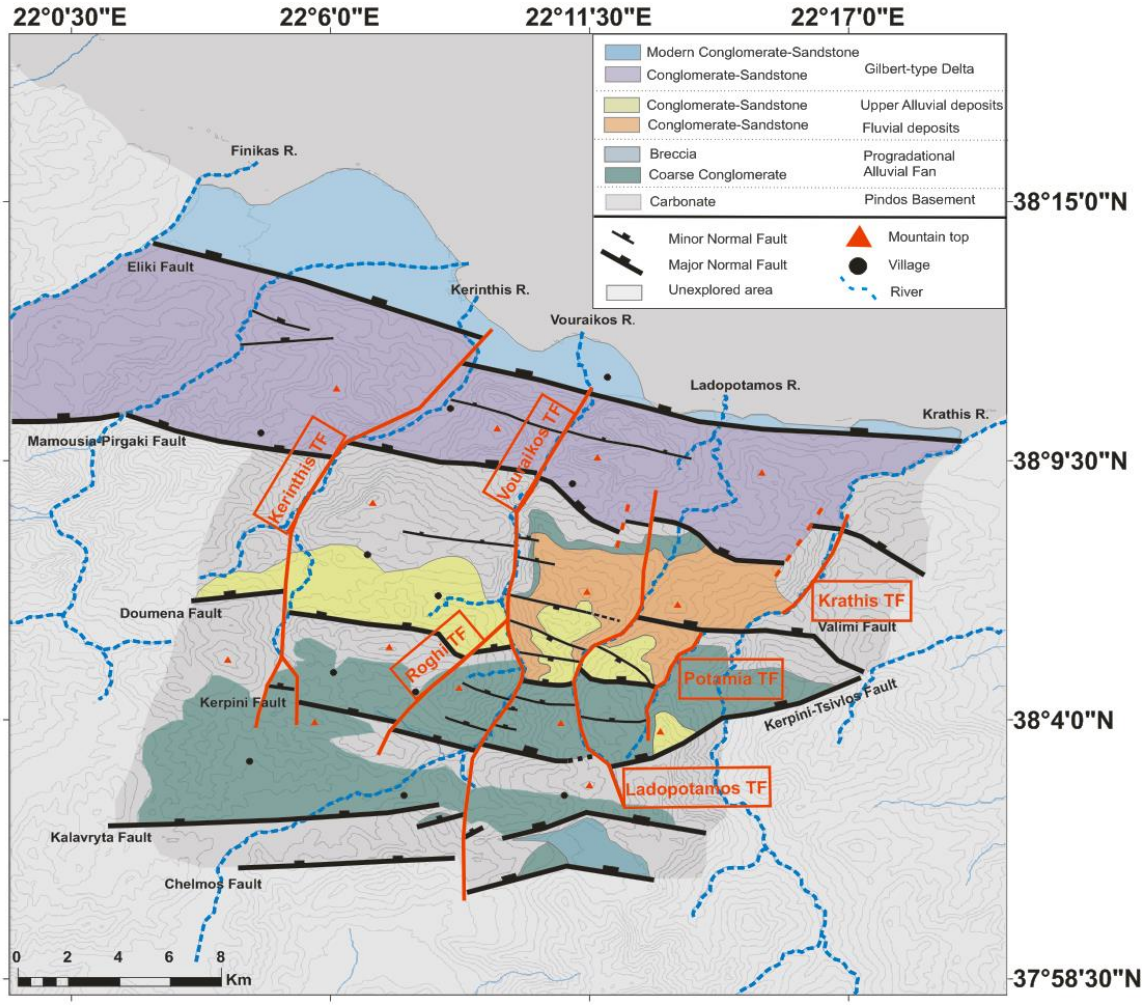

Figure 6.8: Location map showing the proposed transfer faults in the study area.

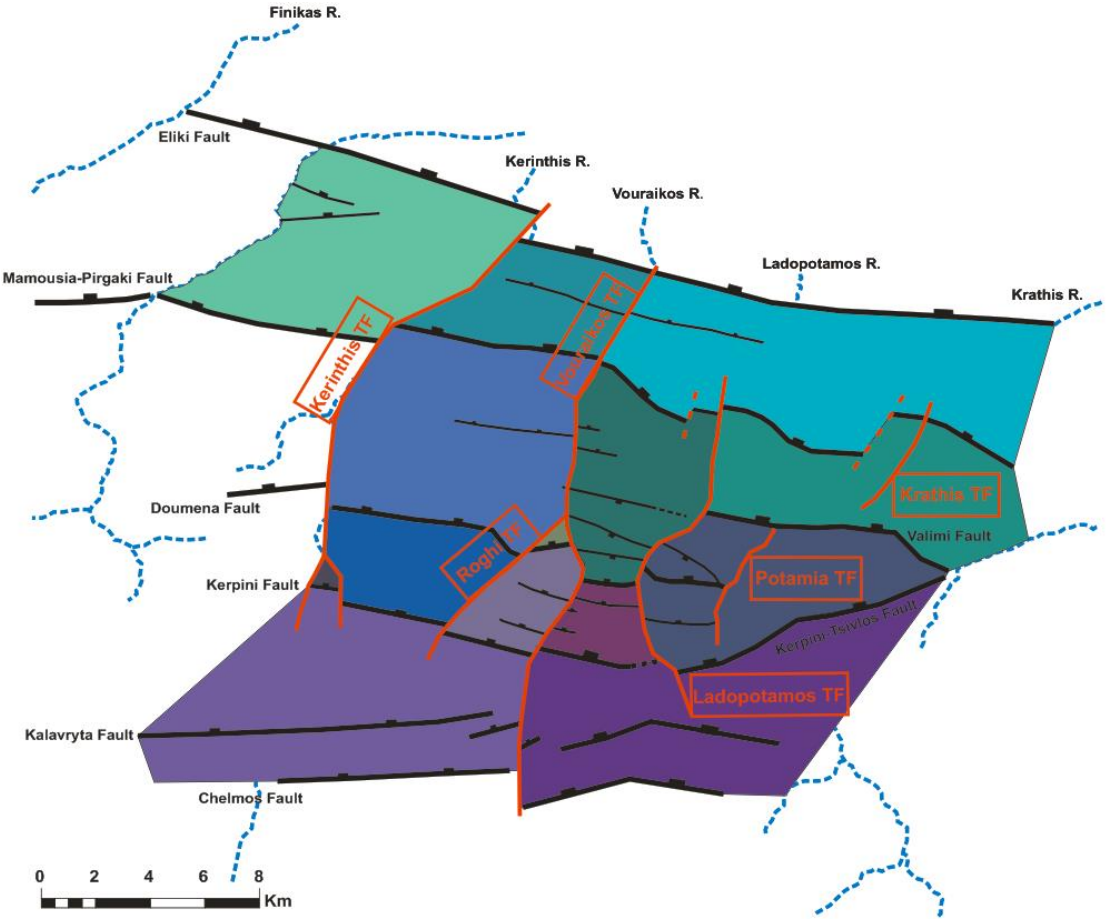

Figure 6.9: Structural map of the study area, highlighting the different segments enclosed by inferred high-angle transfer faults.

Chapter 7 – Conclusion

The study has provided valuable contributions to the understanding of the structural configuration that is the Corinth Rift. The conclusions are summarized in the following points:

- Field observations from the rift system in the Kalavryta-Eliki area are that some faults step, and others terminate abruptly along the N-S river valleys, with these valleys forming an alignment of breaks in fault continuity.
- Relay structures provides a simple field explanation. However, field evidence of overlapping faults are not clear and the 3D models indicate that relays or hard links are very difficult to explain.
- Displacement patterns and gradients show sharp changes in displacement in several areas, and are not conformable with classic displacement patterns or relay displacement patterns.
- The range of displacements estimated for each major fault:
    - Eliki Fault: 2022-2529 m
    - Mamousia-Pirgaki Fault: 1768-3655 m
    - Doumena Fault: 1622-1195 m
    - Kerpini Fault: 1775-488 m
    - Kalavryta Fault: 815-460 m
- In the 3D models, inheritance from underlying linear features controlling transfer zones along the valleys is the most geometrically suitable solution. However, uncertainty on the main contacts, in particular the unconformities needs to be considered.
- There are extensive SSW-NNE trending rift-segmenting structures in the Ladopotamos, Potamia and Krathis valleys, concurrent to the conclusion by Dahman (2015) in Vouraikos Valley, Hadland (2016) in the Kerpini Fault Block and Oppedal (2017) east of the Vouraikos Valley. These are most likely high-angle transfer faults, and they partially control the present-day location of the rivers.

- The cumulative displacement from the N-S profiles in the study area show that there are small differences (~13%) in displacement, suggesting a uniform extension.
- The estimated uncertainties tend to be well-within the error-range of 15 %, which is an acceptable result. It is believed that the method of 3D model construction is a good approach to highlight how the displacements are and how they vary across single faults and fault segments.

Interesting aspects that are recommended for a future project will be to include a displacement analysis of the offshore faults in the Gulf of Corinth. This to build on and investigate further the possibility of segmentation and a uniform extension in the Corinth Rift.

References

ARMIJO, R. M., BERTRAND HUBERT, AURÉLIA BARKA, AYKUT 1999. Westward propagation of the North Anatolian fault into the northern Aegean: Timing and kinematics. *Geology,* 27**,** 267-270.

BALLY, A. 1981. Atlantic-type margins.

BELL, R. E., MCNEILL, L. C., BULL, J. M., HENSTOCK, T. J., COLLIER, R. E. L. & LEEDER, M. R. 2009. Fault architecture, basin structure and evolution of the Gulf of Corinth rift, central Greece. *Basin Research,* 21**,** 824-855.

BIRKELAND, H. 2017. *A Study of Several Proposed Alluvial Fan Deposits in the Kerpini Fault Block, Greece.* M.Sc, University of Stavanger.

CARTWRIGHT, J. A., MANSFIELD, C. & TRUDGILL, B. 1996. The growth of normal faults by segment linkage. *Geological Society, London, Special Publications,* 99**,** 163-177.

CARTWRIGHT, J. A. & MANSFIELD, C. S. 1998. Lateral displacement variation and lateral tip geometry of normal faults in the Canyonlands National Park, Utah. *Journal of Structural Geology,* 20**,** 3-19.

CHÉRY, J. 2001. Core complex mechanics: From the Gulf of Corinth to the Snake Range. *Geology,* 29**,** 439-442.

CHILDS, C., WATTERSON, J. & WALSH, J. J. 1995. Fault overlap zones within developing normal fault systems. *Journal - Geological Society (London),* 152**,** 535-549.

COLLIER, R. & JONES, G. 2004. Rift Sequences of the Southern Margin of the Gulf of Corinth (Greece) as Exploration / Production Analogues*. *Search and Discovery* 50007.

COWIE, P., GUPTA, S. & DAWERS, N. 2000. Implications of fault array evolution for synrift depocentre development: insights from a numerical fault growth model. *Basin Research,* 12**,** 241-261.

COWIE, P. A. & SCHOLZ, C. H. 1992. Displacement-length scaling relationship for faults: data synthesis and discussion. *Journal of Structural Geology,* 14**,** 1149-1156.

COWIE, P. A., UNDERHILL, J. R., BEHN, M. D., LIN, J. & GILL, C. E. 2005. Spatio-temporal evolution of strain accumulation derived from multi-scale observations of Late Jurassic rifting in the northern North Sea: A critical test of models for lithospheric extension. *Earth and Planetary Science Letters,* 234**,** 401-419.

DAHMAN, A. 2015. *The Vouraikos Valley: an example of rift segmentation in the Corinth Graben, Greece.* M.Sc, University of Stavanger.

DAWERS, N. H. & ANDERS, M. H. 1995. Displacement-length scaling and fault linkage. *Journal of Structural Geology,* 17**,** 607-"609,611-614".

DAWERS, N. H., ANDERS, M. H. & SCHOLZ, C. H. 1993. Growth of normal faults: Displacement-length scaling. *Geology,* 21**,** 1107-1110.

DEWEY, J. & ŞENGÖR, A. C. 1979. Aegean and surrounding regions: complex multiplate and continuum tectonics in a convergent zone. *Geological Society of America Bulletin,* 90**,** 84-92.

DOUTSOS, T., KONTOPOULOS, N. & POULIMENOS, G. 1988. The Corinth-Patras rift as the initial stage of continental fragmentation behind an active island arc (Greece). *Basin Research,* 1**,** 177-190.

DOUTSOS, T. & KOUKOUVELAS, I. 1998. Fractal analysis of normal faults in northwestern Aegean area, Greece. *Journal of Geodynamics,* 26**,** 197-216.

DOUTSOS, T. & PIPER, D. J. W. 1990. Listric faulting, sedimentation, and morphological evolution of the Quaternary eastern Corinth rift, Greece: First stages of continental rifting. *GSA Bulletin,* 102**,** 812-829.

DOUTSOS, T. & POULIMENOS, G. 1992. Geometry and kinematics of active faults and their seismotectonic significance in the western Corinth-Patras rift (Greece). *Journal of Structural Geology,* 14**,** 689-699.

FAURE, J. & CHERMETTE, J.-C. 1989. Deformation of tilted blocks, consequences on block geometry and extension measurements. *Bulletin de la Société géologique de France,* 5**,** 3.

FERRILL, D. A. & MORRIS, A. P. 2001. Displacement gradient and deformation in normal fault systems. *Journal of Structural Geology,* 23**,** 619-638.

FINNESAND, S. 2013. *Analysis of Structural Control in Fault Interactions and their Sediment accumulation in the Gulf of Corinth rift, Greece.* M.Sc, University of Stavanger.

FLOTTÉ, N., SOREL, D., MÜLLER, C. & TENSI, J. 2005. Along strike changes in the structural evolution over a brittle detachment fault: Example of the Pleistocene Corinth-Patras rift (Greece). *Tectonophysics,* 403**,** 77-94.

FORD, M., HEMELSDAEL, R., MARCO, M. & PALYVOS, N. 2016. Rift migration and lateral propagation: evolution of normal faults and sediment-routing systems of the western Corinth rift (Greece). *Geological Society London Special Publications*.

FORD, M., ROHAIS, S., WILLIAMS, E. A., BOURLANGE, S., JOUSSELIN, D., BACKERT, N. & MALARTRE, F. 2013. Tectono-sedimentary evolution of the western Corinth rift (Central Greece). *Basin Research,* 25**,** 3-25.

FORD, M., WILLIAMS, E. A., MALARTRE, F. & POPESCU, S. M. 2007. Stratigraphic Architecture, Sedimentology and Structure of the Vouraikos Gilbert-Type Fan Delta, Gulf of Corinth, Greece. *Sedimentary processes, environments and basins: a tribute to Peter Friend***,** 49-90.

FOSSEN, H. 2010. *Structural geology,* United Kingdom, Cambridge, Cambridge university Press.

FOSSEN, H. 2016. *Structural Geology*, Cambridge University Press.

GAUTIER, P., BRUN, J. P., MORICEAU, R., SOKOUTIS, D., MARTINOD, J. & JOLIVET, L. 1999. Timing, kinematics and causes of Aegean extension: a scenario based on a comparison with simple analogue experiments. *Tectonophysics,* 315**,** 31-72.

GAWTHORPE, R. L., HARDY, S. & RITCHIE, B. 2003. Numerical modelling of depositional sequences in half-graben rift basins. *Sedimentology,* 50**,** 169-185.

GAWTHORPE, R. L. & HURST, J. M. 1993. Transfer zones in extensional basins: their structural style and influence on drainage development and stratigraphy. *Journal of the Geological Society,* 150**,** 1137.

GAWTHORPE, R. L. & LEEDER, M. R. 2000. Tectono-sedimentary evolution of active extensional basins. *Basin Research,* 12**,** 195-218.

GHISETTI, F. & VEZZANI, L. 2005. Inherited structural controls on normal fault architecture in the Gulf of Corinth (Greece). *Tectonics,* 24**,** 1-17.
GIBBS, A. D. 1984. Structural evolution of extensional basin margins. *Geological Society of London,* 141**,** 609-620.
GILLESPIE, P., WALSH, J. T. & WATTERSON, J. 1992. Limitations of dimension and displacement data from single faults and the consequences for data analysis and interpretation. *Journal of Structural Geology,* 14**,** 1157-1172.
HADLAND, S. 2016. *Geological Mapping and Investigation into a Proposed Syn-rift Alluvial Fan Deposit in the Kerpini Fault Block, Greece.* M.Sc, University of Stavanger.
HILLS, E. S. 1972. *Elements of structural geology,* London, Chapman and Hall.
JOLIVET, L., BRUN, J. P., GAUTIER, P., LALLEMANT, S. & PATRIAT, M. 1994. 3D-kinematics of extension in the Aegean region from the early Miocene to the Present, insight from the ductile crust. *Bulletin de la Societe Geologique de France,* 165**,** 195-209.
LE PICHON, X. & ANGELIER, J. 1979. The Hellenic Arc and Trench System: A key to the neotectonic evolution of the Eastern Mediterranean Area. *Tectonophysics,* 60**,** 1-42.
LEEDER, M. R., MACK, G. H., BRASIER, A. T., PARRISH, R. R., MCINTOSH, W. C., ANDREWS, J. E. & DUERMEIJER, C. E. 2008. Late-Pliocene timing of Corinth (Greece) rift-margin fault migration. *Earth and Planetary Science Letters,* 274**,** 132-141.
LISTER, G. S., ETHERIDGE, M. A. & SYMONDS, P. A. 1986. Detachment faulting and the evolution of passive continental margins. *Geology,* 14**,** 246-250.
LOPES, G. C. 2015. *Geological Mapping of the South-central Gulf of Corinth Coastal Fault System - Greece.* M.Sc, University of Stavanger.
MARRETT, R. & ALLMENDINGER, R. W. 1991. Estimates of strain due to brittle faulting: sampling of fault populations. *Journal of Structural Geology,* 13**,** 735-738.
MCKENZIE, D. 1972. Active Tectonics of the Mediterranean Region. *Geophysical Journal International,* 30**,** 109-185.
MCNEILL, L. C. & COLLIER, R. E. L. 2004. Uplift and slip rates of the eastern Eliki fault segment, Gulf of Corinth, Greece, inferred from Holocene and Pleistocene terraces. *Journal of the Geological Society,* 161**,** 81-92.
MORETTI, I., SAKELLARIOU, D., LYKOUSIS, V. & MICARELLI, L. 2003. The Gulf of Corinth: An active half graben? *Journal of Geodynamics,* 36**,** 323-340.
OPPEDAL, E. 2017. *Rift Segmentation: Structural mapping in the Kerpini-Tsivlos and the Dhoumena Fault Blocks, Greece.* M.Sc, University of Stavanger.
ORI, G. G. 1989. Geological history of the extensional basin of the Gulf of Corinth (?Miocene-Pleistocene), Greece. *Geology,* 17**,** 918-921.
RHODES, P. E. 2015. *Interaction of Extensional Tectonics on Synrift Deposition: Using Field Analogues from Greece and a North Viking Graben Dataset.* M.Sc, University of Stavanger.
RIETBROCK, A., TIBERI, C., SCHERBAUM, F. & LYON-CAEN, H. 1996. Seismic slip on a low angle normal fault in the Gulf of Corinth: Evidence from a high-resolution cluster analysis of microearthquakes. *Geophysical Research letters,* 23**,** 1817-1820.

ROGNMO, T. 2015. *Sedimentary infill in the Kalavrita faulted block, south-central Gulf of Corinth, Greece.* M.Sc, University of Stavanger.
ROHAIS, S., ESCHARD, R., FORD, M., GUILLOCHEAU, F. & MORETTI, I. 2007. Stratigraphic architecture of the Plio-Pleistocene infill of the Corinth Rift: Implications for its structural evolution. *Tectonophysics,* 440**,** 5-28.
SIGMUNDSTAD, E. 2016. *Detailed Structural Mapping and Correlation of a Thick Syn-Rift Sequence in the Kerpini Fault Block, Greece.* M.Sc, University of Stavanger.
SOREL, D. 2000. A Pleistocene and still-active detachment fault and the origin of the Corinth-Patras rift, Greece. *Geology,* 28**,** 83-86.
STUVLAND, M. E. 2015. *Kalavryta and Kerpini Fault Block: Investigation into correlation and nature of sub-horizontal layers; Corinth Graben, Greece.* M.Sc, University of Stavanger.
SYAHRUL, R. 2014. *Fault Controlled Sedimentation: A case study of the Kerpini Fault, Greece.* M.Sc, University of Stavanger.
VEITEBERG, A. 2017. *Geological Mapping and Investigation into tectonic control on deposition. A case study of the Doumena Fault Block, Greece.* M.Sc, University of Stavanger.
WALSH, J. J., BAILEY, W. R., CHILDS, C., NICOL, A. & BONSON, C. G. 2003. Formation of segmented normal faults: a 3-D perspective. *Journal of Structural Geology,* 25**,** 1251-1262.
WALSH, J. J. & WATTERSON, J. 1988. Analysis of the relationship between displacements and dimensions of faults. *Journal of Structural geology,* 10**,** 239-247.
WATTERSON, J. 1986. Fault dimensions, displacements and growth. *Pure and Applied Geophysics,* 124**,** 365-373.
WESTAWAY, R. 2002. The Quaternary evolution of the Gulf of Corinth, central Greece: coupling between surface processes and flow in the lower continental crust. *Tectonophysics,* 348**,** 269-318.
WOOD, A. M. 2013. *The influence of fault geometric uncertainty on hydrocarbon reservoir and simulation models.* Ph.D. Doctoral thesis, University of Leeds.
ZHONG, X., ESCALONA, A., SVERDRUP, E. & BUKTA, K. E. 2018. Impact of fault evolution in Gilbert-type fan deltas in the Evrostini area, south-central Gulf of Corinth, Greece. *Marine and Petroleum Geology,* 95**,** 82-99.